CZECH TECHNICAL
UNIVERSITY
IN PRAGUE

FACULTY
OF ELECTRICAL
ENGINEERING

DOCTORAL
THESIS

2018

PETR
PICHLÍK

CZECH TECHNICAL UNIVERSITY IN PRAGUE

FACULTY OF ELECTRICAL ENGINEERING
DEPARTMENT OF ELECTRIC DRIVES AND TRACTION

Strategy of Railway Traction Vehicles Wheel Slip Control

Doctoral Thesis

Petr Pichlík

Prague, February 2018

Ph.D. Programme: Electrical Engineering and Information Technology (P2612)
Branch of study: Electric Machines, Apparatus and Drives (2642V004)

Supervisor: Ing. Jiří Zděnek, CSc.

Declaration

I hereby declare that I have written my doctoral thesis on my own and I have used only the literature listed at the end of the doctoral thesis in the references.

Petr Pichlík

Abstract

The doctoral thesis deals with a novel slip controller for electric locomotives design that is based on adhesion-slip characteristic slope detection. The purpose of the slip controller is to transfer the maximum possible force between wheels and rails if it is required and at the same time keep a wheel slip velocity at the acceptable value. The slip controllers are developed for many decades, and a large number of slip control methods were developed. However, the problematics of the slip control is currently unresolved, and development of the slip controllers is very current till now. The proposed slip controller is designed to cope with the main drawbacks of the current slip control methods. The main drawbacks of the current slip control methods are that they, typically, do not consider a nonlinearity of the adhesion-slip characteristic and noise that occurs in the system for simplification. These simplifications can cause the existing methods fail. The second problem of the existing slip control methods is that the train velocity must be typically known which is difficult to determine. The proposed slip controller takes into account the problems mentioned above, and it does not need to know the train velocity and only one wheelset velocity is only required. The slip controller is designed as modular, and it consists of the adhesion-slip characteristic slope detection part and a controller part. The detection part is based on an unscented Kalman filter that is used as the estimator. The unscented Kalman filter is intended for nonlinear systems and can cope with the nonlinear adhesion-slip characteristic and provides the stable and appropriate results. The slip controller modularity enables to replace the unscented Kalman filter by another estimator. Therefore, a comparison of the proposed slip controller with the unscented Kalman filter with other selected estimation techniques to verify the correctness of the unscented Kalman filter use is made. The proposed slip controller functionality is verified by comparisons of the measured data and simulation model in Matlab software. The measured data were obtained on an electric locomotive Skoda 93E that hauls a freight train.

Keywords: adhesion, unscented Kalman filter, rail transportation, slip control, tractive force control.

Abstrakt

Disertační práce se zabývá návrhem skluzového regulátoru pro elektrické lokomotivy, který je založený na detekci sklonu adhezní charakteristiky. Úkolem skluzového regulátoru je přenést maximální sílu mezi koly a kolejnicemi, pokud je požadována a současně držet skluzovou rychlost kol na přijatelné hodnotě. Skluzové regulátory jsou vyvíjeny po desetiletí a velké množství skluzových regulátorů bylo během této doby vyvinuto. Nicméně, problematika skluzové regulace není stále dořešena a vývoj skluzových regulátorů je stále aktuální. Navržený skluzový regulátor nemá nedostatky známých skluzových regulátorů. Mezi hlavní nedostatky současných skluzových regulátorů patří to, že obvykle neuvažují nelinearitu adhezní charakteristiky a šum, který se vyskytuje v systému. Ignorování těchto jevů může způsobit selhání těchto skluzových regulátorů. Další problém, se kterým se musí současné skluzové regulátory vypořádat je určení rychlosti vlaku. Navržený skluzový regulátor bere v úvahu výše uvedené problémy a nepotřebuje znát rychlost vlaku a využívá pouze rychlost jedné nápravy. Skluzový regulátor je nevržený jako modulární a skládá se z detekční části, která určuje sklon adhezní charakteristiky a regulační části. Detekční část je založena na unscented Kalmanově filtru, který je určený pro nelineární systém a umí se tedy vypořádat s nelineární adhezní charakteristikou a poskytuje stabilní a odpovídající výsledky. Modularita navrženého skluzového regulátoru umožňuje nehradit unscented Kalmanův filtr jinou metodou stavového odhadu. Proto je také provedeno porovnání, aby byla ověřena správnost použití unscented Kalmanova filtru. Funkčnost navrženého skluzového regulátoru je ověřena na naměřených datech a na matematickém modelu za použití programu Matlab. Naměřená data byla naměřena na nákladním vlaku taženém elektrickou lokomotivou Škoda 93E.

Klíčová slova: adheze, skluzová regulace, regulace trakční síly, unscented Kalmanův filtr, železniční doprava.

Table of Contents

List of Figures

List of Tables

Nomenclature

$\mathbf{A}$	system matrix in continuous time
a_a, b_a, c_a, d_a, a_b, b_b, a_c, b_c,	adhesion-slip characteristic parameters
$\mathbf{A}_{mechanical}$	system matrix that describes the mechanical subsystem
a	acceleration
a_C	wheel circumference acceleration
a_{SM}	slip acceleration reference value
$\mathbf{A}_{velocity}$	system matrix that describes the velocity estimation
$\mathbf{B}$	system input matrix
$\mathbf{C}$	system output matrix
c	stiffness
$\mathbf{C}_m$	matrix of stiffness
$\mathbf{D}$	system feedforward matrix
d	damming
$\mathbf{D}_m$	matrix of damming
e	regulatory error
$\mathbf{e}$	dynamic error of LO
f	nonlinear function
F_A	adhesion force
$\hat{F}_A$	estimated adhesion force
F_{AMax}	maximum value of the adhesion force
F_N	normal force
F_R	resistance force
F_{SDrop}	force drop
F_T	tractive force
F_T^*.	required value of the tractive force
g	nonlinear function
i	current
$i_{FAdhesion}$	relative adhesion force
$i_{FAdhesionMAX}$	maximum value of the relative adhesion force
$i_{FAdhesion}^*$	required value of a relative adhesion force
I_S	impulse (during a controller action)
J	moment of inertia
J_D	directly driven wheel moment of inertia
J_I	indirectly driven wheel moment of inertia
J_M	motor moment of inertia
$\mathbf{J}_m$	matrix of moments of inertia
$\mathbf{K}$	Kalman gain matrix
k	coefficient
k_{mech}	mechanical constant of an electric motor
K_S	adhesion-slip characteristic parameter
K_p, K_i, K_c	PI controller constants
L	inductance
$\mathbf{L}$	observer gain
L_M	magnetizing inductance
M	mass
n_W	number of wheelsets
n, m, r	sizes of matrices for system description
o_P	poles of the observer
$\mathbf{O}$	observability matrix

p	complex frequency
p_p	number of pole pairs
$\mathbf{P}$	error covariance matrix
P_SLoss	loss power
$\mathbf{P}_\mathrm{xx}$	predicted error covariance matrix
$\mathbf{P}_\mathrm{yy}$	prediction output error covariance matrix
$\mathbf{P}_\mathrm{xy}$	output error covariance matrix
$\mathbf{P}_\mathrm{zz}$	predicted output error covariance matrix
$\mathbf{Q}$	process noise covariance matrix in discrete time
$\mathbf{Q}_\mathrm{t}$	process noise covariance matrix in continuous time
R	resistance
$\mathbf{R}$	measurement uncertainty covariance matrix in discrete time
$\mathbf{R}_\mathrm{t}$	measurement uncertainty covariance matrix in continues time
R_G	gear ratio
r_w	wheel radius
r_J	ratio of moments of inertia J_M and J_D
s	slip
S	threshold coefficient
T	motor torque
T^*	required motor torque
$\hat{T}_\mathrm{L}$	estimated load torque
$t_\mathrm{iOutDelay}$	estimator output detection time delay
T_L	load torque
t_S	slip velocity time duration
$\mathbf{u}$	system input vector
v	random sensor noise
v_0	initial velocity
v_C	wheel or wheelset circumference velocity
v_C^*	required wheel or wheelset circumference velocity
v_Cmin	velocity of the slowest wheel or wheelset
v_L	wheel or wheelset longitudinal velocity or train velocity
v_S	slip velocity
v_SEst	estimated value of the slip velocity
v_SM	slip velocity threshold or reference value
v_Smax	slip velocity at maximum point
v_SPeak	maximum value of a slip velocity
v_ST	slip velocity threshold for the estimator evaluation purpose
$\mathbf{W}$	weights of sigma points
w	random dynamic disturbances
$\mathbf{x}$	system state vector
$\mathbf{y}$	system output vector
$\mathbf{Y}_\mathrm{err}$	UKF output error matrix
ΔF_T	tractive force change
Δi	currents difference
ΔT	difference torque
ΔT_D	disturbance torque
ΔT_T	difference of torsional torque
Δv_S	slip velocity change
$\Delta\varphi$	shaft torsion
$\Delta\omega_\mathrm{M}$	motor angular velocity change
ϵ	angular acceleration

η	transformed sigma points through nonlinear function f
λ, α, β, κ	scaling parameters
γ	coefficient
μ	adhesion coefficient actual value
μ_{max}	adhesion coefficient maximum value
ξ	transformed sigma points through nonlinear function g
ρ_k, ρ_0	correcting factors
Φ	system matrix in discrete time
φ	angle
φ_s	phase shift
φ_s^*	required value of a phase shift
ϕ_{rd}^*	reference value of rotor flux linkage
$\mathbf{X}$	sigma points matrix
ω	angular velocity
ω_1	motor synchronous angular velocity
ω_D	directly driven wheel angular velocity
ω_f	angular modulation frequency
ω_I	indirectly driven wheel angular velocity
ω_L	train velocity recalculated to an angular velocity
ω_M	motor angular velocity
ω_{Mf}	motor angular modulation frequency

Abbreviations

DO	Disturbance Observer
DSP	Digital Signal Processor
EKF	Extended Kalman Filter
ELO	Extended Luenberger Observer
EMU	Electric Multiple Unit
GPS	Global Positioning System
HHT	Hilbert-Huang Transformation
HIL	Hardware In the Loop (simulation)
KF	Kalman Filter
LKF	Linearized Kalman Filter
LO	Luenberger Observer
P&O	Perturb and Observe
PID	Proportional–Integral–Derivative controller
SISO	Single-Input-Single-Output system
UKF	Unscented Kalman Filter

1 INTRODUCTION

Modern railway traction vehicles reach high-speed and high tractive effort. The whole vehicle tractive effort is achieved by forces transfer between individual wheels and rails in small contact areas. The contact area features causes the railway transport advantage that is in its lower power loss due to the low friction in the wheel-rail contact. However, the force that can be transferred between wheels and rails is limited by the actual adhesion conditions that mainly depends on the rails surface conditions [1]. Therefore, the effective maximum adhesion utilisation is required to achieve high tractive effort [2]. The typical conditions are dry rails and wet rails. However, the rails can be covered with leaves, moisture, ice, oil, dust, or by some dirt. Moreover, the rails can be even contaminated by mud on road crossings [3]. The situation becomes worse when the dirt and dust are wet [4]. All of these contaminations decrease the adhesion, and consequently, the maximum force that can be transferred is decreased too. When the tractive force applied to the wheels exceeds the maximum force that can be transferred between wheels and rails, the wheels velocity starts to increase while a train velocity increases slowly or even decreases. This case will increase wear of wheels and rails [5], and some mechanical vehicle parts can be damaged if the wheel circumference velocity is significantly higher than the train velocity. A force applied to the wheel has to be decreased to slow down the wheel velocity to an acceptable value in this case. The force decrease causes the whole vehicle tractive effort decrease. When the force is inappropriately decreased, a train delay can occur [6], or under very adverse conditions, the train can jamming on the track, or the train can be separated into two parts. To avoid of all of these problems the modern railway vehicles are equipped with a slip controller or older ones are equipped with a re-adhesion controller. The slip controller has to avoid the rise of the wheel slip velocity and the wheel slippage emergence by decreasing the applied force to maximum transferable value if the required vehicle tractive force is higher than the maximum transferable force. The traction vehicles can be sorted into locomotives and multiple units. The most significant problems with the force transfer have locomotives that haul freight train because they have to fully utilise the available adhesion. Therefore, the applied force is near the maximum transferable force [7]. Generally, all types of railway tractive vehicle can have the same problem. Therefore, the railway vehicles are equipped with sanders that enable to improve the adhesion conditions. However, the sanding increases 10 to 100 times wheels and rails wear, and can cause the damage to the track [3]. Therefore, a good slip controller is better than the use of the sanding.

The slip controllers have been developed for decades [8], and many slip control methods were developed. However, the slip control method development continues [9]. The slip control method can be sorted into methods that eliminate the occurred slippage and methods that try to find the maximum adhesion and prevent the slippage occurrence [10]. The methods that eliminate the slippage are re-adhesion controllers. The re-adhesion controllers were developed and used before the slip controllers occurred. The re-adhesion controllers only limit high slip velocity value to the acceptable value but they cannot prevent the slippage emergence and cannot optimally utilise available adhesion. The re-adhesion controllers are not primarily used nowadays, but they are used on locomotives that are in service and sometimes they are used as additional protection to some types of the slip controllers. The maximum transferable force depends on the actual adhesion-slip characteristic parameters. The adhesion-slip characteristic describes a dependence of an adhesion coefficient on a slip. The characteristic is nonlinear and has a maximum [11]. The characteristic shape changes while a train runs [9] and [12]. The modern slip controllers try to find the maximum point on the adhesion-slip characteristic or

determine the characteristic slope. The efficient slip controllers determine the characteristic slope and try to work near the characteristic maximum point with the acceptable slip velocity. The controllers for the force transfer between the wheels and surfaces are also solved in the automotive industry, e.g. [13] [14], [15] and [16] or mobile robots [17]. However, the automotive has to consider other types of the forces that are applied to the car like side forces or a tire cornering stiffness coefficient [18]. However, the principles of the controllers are similar.

1.1 Motivation

The doctoral thesis focuses on the slip controller for electric locomotives that are intended for freight trains hauling. The current slip controllers typically have problems that are not solved, or the existing slip controllers can be improved. Therefore, there are wide possibilities in the research of the slip controllers. The slip control of the locomotives closely relates to the electric drive control. The electric drive should have high dynamics to fulfil the slip controller requirements. Moreover, the slip controller has to be implemented to the electric drive controller structure. The members of the Department of electric drives and traction participated in an electric locomotive computer design [19], [20] and [21], and currently participate in a slip controller development. Therefore, there are experiences with the slip controllers design in the department. Moreover, measurements on Skoda 93E locomotive are also available. The proposed slip controller is designed to be possible its implementation into a locomotive computer where the slip controller has to cooperate with an electric drive controller.

1.2 Current State of Art

The slip control methods try to solve a problem with a nonlinear adhesion-slip characteristic and the characteristic changes. An example of the adhesion-slip characteristic is depicted in Figure 1.1. The characteristic describes the dependence of the adhesion coefficient μ on the slip s. The slip is a ratio between a slip velocity and train velocity. The slip velocity is a difference between a wheel circumference velocity and its longitudinal velocity or a train velocity. The typical characteristic has a maximum point. A stable area is a part of the characteristic before the maximum point, and an unstable area is the part of the characteristic behind the maximum point. The slip velocity in the stable area is called as an efficient slip velocity or a slip, and the slip velocity in the unstable area is called as a slippage. The characteristic shape mainly changes according to the conditions of a rail surface and the train velocity. The re-adhesion controllers have to turn back the operating point to the stable area of the adhesion-slip characteristic when it gets to the unstable area. On the other hand, the slip controllers have to keep the operating point around the maximum value of the adhesion-slip characteristic [2].

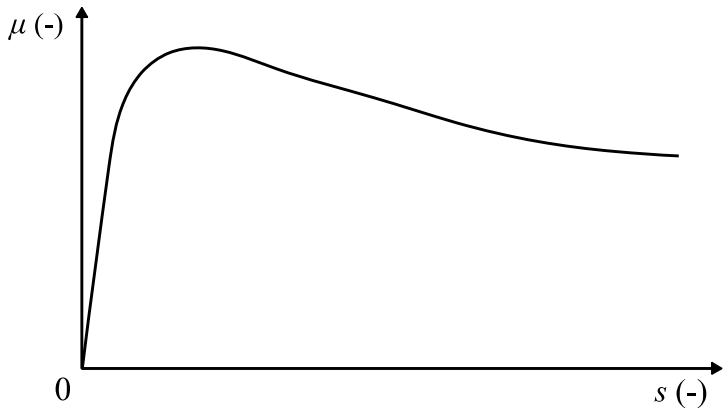

Figure 1.1 Example of an adhesion-slip characteristic

The slip control methods can be sorted into many groups and no exactly given slip control methods classification is presented in the literature. Generally, the methods can be sorted into the re-adhesion controllers and the slip controllers [10]. Proposed method classification is depicted in Figure 1.2. The re-adhesion controllers are the forerunners of the slip controllers, and they work as a protection against the slippage. The re-adhesion controllers can be sorted into direct methods that use wheel circumference velocity or acceleration and compare it with a threshold, and indirect methods that use voltage or current difference between serially or in parallel connected motors. On the other hand, the slip controllers try to prevent the slippage formation by continues regulatory interventions. The slip controllers can be sorted into methods that determine the actual adhesion-slip characteristic parameters, and the methods that are based on other principles. The method that uses the adhesion-slip characteristic parameters can determine the position of the maximum point of the actual characteristic, or determine a slope of the actual characteristic. The methods can be further sorted according to the adhesion or slip detection mechanism. The method based on the slope determination of the adhesion-slip characteristic requires knowledge of the adhesion coefficient value or the adhesion force value. These values cannot be directly measured during a train runs. Therefore, the methods use some estimation techniques to determine the value. The estimators can be, e.g. observer [22], [23], [24], [25], [26], [27], [28] and [29], Kalman filter [30] or it's some nonlinear variant [31] and [32]. Another way how to determine the slope is based on a mechanical phenomenon that occurs in the torque transfer chain between electric drive and wheels, e.g. determination of a phase shift between motor torque and its velocity [33] and [34]. The adhesion-slip characteristic slope can be also detected according to torsional vibrations [35] and [36]. The second group of methods detects the maximum point position [37] and [38]. Methods that detect a maximum point must work in the unstable area of the adhesion-slip characteristic. Therefore, the methods require a dynamic electric drive. However, the methods disadvantage is that they can cause some undesirable mechanical effects that are connected with stick-slip oscillations that occur when the operating point moves from the stable area to the unstable area and back [39]. Methods that evaluate noise [40] and [41], or use a Hilbert-Huang transformation (HHT) [42] or methods that control a slip velocity on a constant value or limit the wheel acceleration [43] are included in other methods although the methods can be included among other.

The method sortation according to Figure 1.2 was made according to the methods principle presented in the available literature. However, different classification can be used by different authors. The slip control method classification can be done according to the target railway traction vehicles. There are differences between an Electric Multiple Unit (EMU) and locomotive in applied control method. The differences are in the overall train weight and amount of driven axes. The EMUs are lighter and can have more driven wheelset distributed under the whole EMU in contrast of train hauled by a locomotive. The EMUs typical tractive force is not as high as the locomotives. The operating point of the EMUs is typically placed in the stable area of the adhesion-slip characteristic [7], and the slip velocity is lower during the normal operation than the slip velocity of the locomotives. The locomotives must produce high tractive effort when hauls a freight train. In this case, the tractive forces are high, and the operating point is placed near the maximum point of the adhesion-slip characteristic. The operating point can simply overstep the maximum point and get to the unstable part of the adhesion-slip characteristic even in good conditions of rail surfaces. The [44] supposes division to conventional methods, intelligent methods and model control methods. The conventional methods are basically the re-adhesion controller, and the model control methods are methods that estimate an adhesion coefficient are methods that estimate adhesion-slip characteristic slope

from Figure 1.2. The intelligent methods use fuzzy logic and wavelet denoising. Another slip control method sortation is presented [45]. The paper proposes division into a speed difference, pattern control, fuzzy logic, model-based, current and voltage difference, and neural networks.

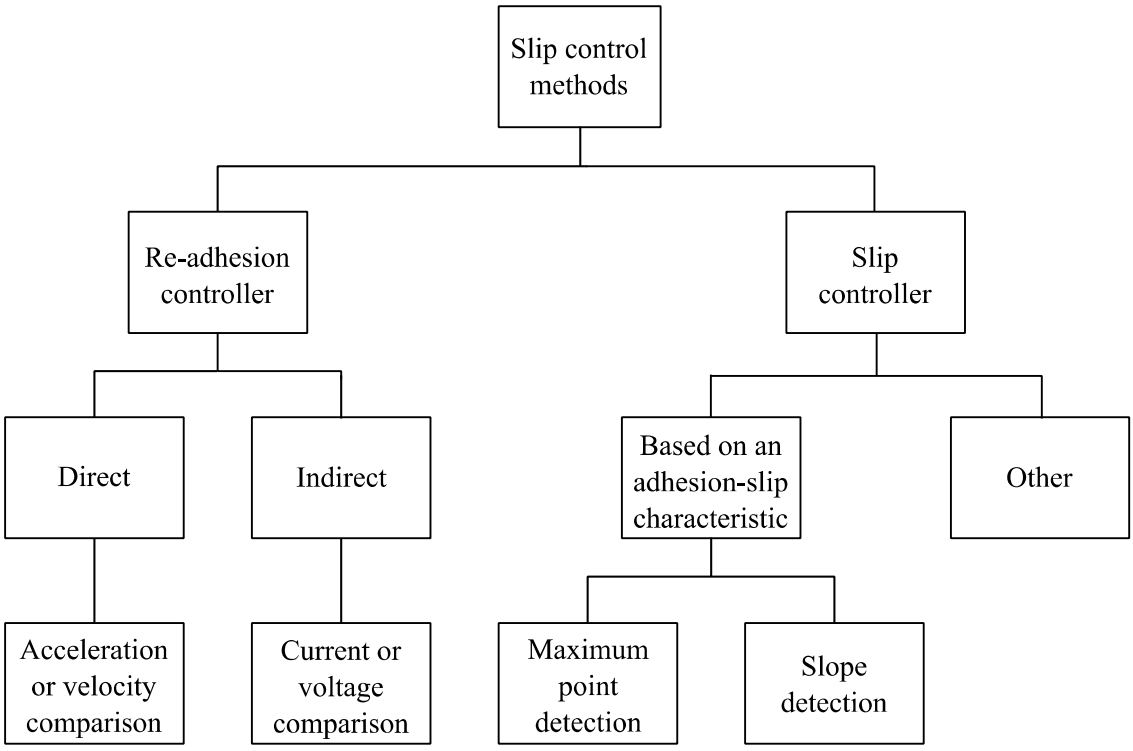

Figure 1.2 Classification of the slip control methods

The slip controller basically consists of adhesion conditions or a slip detection part and controller part. Both parts can be designed separately in some types of methods, and some methods require both part design together. Methods that are based on a characteristic slope can be designed separately because the output of the detection part is a characteristic slope and the controller only control the value of the detection part on a required value. The methods that control the operating point to the maximum value are typically designed with a controller because they need to implement a speed controller to the slip controller structure. The speed controller is needed because the methods have to work in the characteristic unstable area.

Many requirements are placed to the slip controllers, and the description of the most important of them is described next. The proper slip control method should prevent a slippage creation, should work from the train low velocity to the maximum velocity, cope with situations when the maximum point is not significant, and damp torsional vibrations if it is possible. The slip control methods typically have a problem when the wheel velocity is low. This problem is connected with a wheel velocity measurement that is done by an incremental encoder with a low number of pulses per revolution. Therefore, when the wheel velocity is low, the encoder has a long response time. The second problem can occur if the method requires a train velocity for its proper work. The train velocity is difficult to measure when all wheels are driven because all wheels have non zero slip velocity. Another problem can occur when the conditions of a rail surface are very bad, and the adhesion-slip characteristic has a maximum point placed in high slip velocity value that is undesirably high. Moreover, the peak is typically flat in this case. Therefore, some types of a used slip control method can fail in this case. Because they try to achieve the maximum point and the method create the high slip velocity. The slip controller

should not excite torsional vibrations in mechanical parts, and the proper slip controller should damp the vibrations.

1.3 Objectives Formulation

The doctoral thesis objectives are:

1. **Summarize the pieces of knowledge about slip control method principles and evaluate their requirements and effectivity**. The summarization of the knowledge is the first step in the slip controller design. The slip control methods have been developed for decades and experiences at the Department of electric drives and traction and in the literature are available. Every method has its strengths and weaknesses. Knowledge about the strengths and weaknesses of the methods will be used in the new slip controller design. The possible method use is also limited by a locomotive computer computational performance. Therefore, the methods are also evaluated from the computational complexity. Some methods require knowledge of the slip velocity for its proper work. Therefore, the slip velocity determination is also described.
2. **Summarize appropriate state estimators that can be used in the proposed slip controller and evaluate their possible using in the proposed slip controller and select a proper estimator for the slip controller.** The designed slip controller is based on the adhesion estimation by an estimator. The summarization of the possible used estimators are made because they features have to be known for the decision.
3. **Design a slip controller that can be used for a locomotive.** The slip controller design is based on the existing slip control methods study and the summarization of the state estimators. The slip controller is based on an estimator that uses a nonlinear function of the adhesion-slip characteristic. The nonlinear function depends on the actual adhesion conditions. Therefore, the point also consists of the adhesion description.
4. **Design a proper mathematical simulation model of a locomotive part that can be used for the slip controller design and evaluation. Design a proper mathematical model for the slip controller.** The slip controller will be evaluated according to simulation results and the available measured data. A proper mathematical simulation model is designed for the purpose. The mathematical model design is based on measured data, to get a match between the real locomotive and model. The model is needed because the measured data do not enable to evaluate the slip controller performance because the slip controller with a controller part can be evaluated only in the model. The mathematical model for simulations is too complex for usage in the slip controller. Therefore, the second mode for the slip controller is also designed.
5. **Verify the designed slip controller performance with the help of a mathematical model and measured data as well as the slip controller execution time in a digital signal processor.** The designed slip controller is based on the unscented Kalman filter. However, the slip controller structure can be modified. Therefore, comparisons with other estimators and some conventional slip control methods are also made. The possible slip controller implementation in a DSP is done to verify the possibility of the slip controller implementation in a locomotive computer.

2 INTRODUCTION TO THE SLIP CONTROL METHODS

During the decades, various types of the slip control methods were developed, and their development still continues. Therefore, the basic principles of known methods are summarized in the chapter. Correct work of some methods depends on the actual adhesion function. Therefore, the adhesion phenomenon is firstly described in the chapter.

2.1 Adhesion Phenomenon

The adhesion coefficient enables to transfer force between wheels and rails. The adhesion is the fundamental phenomenon that influences the locomotive tractive and brake performance. Therefore, the adhesion phenomenon and related terms are briefly described in the subchapter. The adhesion phenomenon is also described because the proposed slip controller is based on the nonlinearity of the adhesion-slip characteristic. The adhesion coefficient changes its value during the train runs, and its value can be considered as random value. The value of the adhesion coefficient changes every few metres. Maximally it can be constant up to 11 metres [46]. Moreover, the situation is more complicated because contaminations can be only on one rail and the second rail can be clear and if the adhesion coefficient changes due to the contaminations on rail surface, the contaminations are partially removed by the first wheelset. Therefore, the next wheelset has better adhesion coefficient than the first wheelset. This effect is called as cleaning effect [11]. The maximum value of the transferable force changes if the value of the adhesion coefficient changes. If the adhesion coefficient decreases, the maximum transferable force can decrease below an actual applied force. A wheel circumference velocity starts to increase in this case.

The adhesion coefficient is typically expressed as a function of a slip velocity. The dependence is called as an adhesion-slip characteristic. The adhesion-slip characteristic is a nonlinear function. The nonlinearity can cause the incorrect function of some existing slip control methods. Therefore, the adhesion phenomenon fundamental principles are essential for a slip control method design. An adhesion coefficient, adhesion-slip characteristic, slip velocity, and force transfer are described in the subchapter. Finally, the adhesion models are described. The model is required for next simulations and the nonlinearity description for the estimator.

2.1.1 Slip Velocity

The slip velocity is defined as a difference between a wheel circumference velocity v_C and the wheel longitudinal velocity v_L. The wheel longitudinal velocity can be considered as a train velocity. The slip velocity is essential because without the slip velocity a force between wheel and rail cannot be transferred [9]. Therefore, every driven wheel has a higher circumference velocity than the longitudinal velocity, and the braked wheel has a lower circumference velocity than the longitudinal velocity. An example of the driven wheel is schematically depicted in Figure 2.1. The adhesion force and normal force are applied to the wheel in the figure. The maximum possible value of an adhesion force F_A depends on the current adhesion-slip characteristic shape. The adhesion-slip characteristic shape changes at any moment and depends on many parameters. The value of a normal forces F_N is constant only in the static case. However, the normal force value changes during the vehicle dynamic motions.

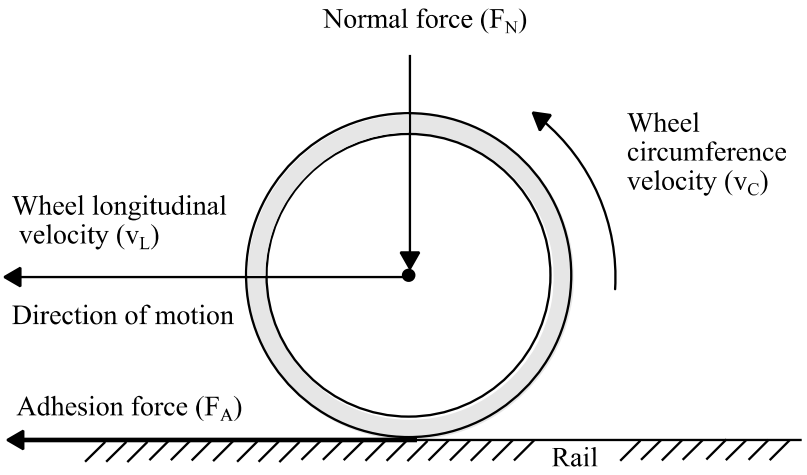

Figure 2.1 Applied forces and velocities to a driven wheel

The slip velocity v_S can be calculated as:

$$v_S = v_C - v_L \tag{2.1}$$

The common value of the slip velocity is typically under 2 km·h^{-1} [9]. However, when the adhesion conditions are adverse, the value can be higher. The value of the slip velocity continuously changes during the train run. The high value of the slip velocity causes higher wear of the wheels and rails, can damage some mechanical part that transfers torque from a motor to the wheels and power losses increase.

A slip is often used instead of the slip velocity. The slip s is defined as a ratio of the slip velocity and the wheel longitudinal velocity:

$$s = \frac{v_S}{v_L} \tag{2.2}$$

The slip velocity is used for any difference between the wheel longitudinal velocity and wheel circumference velocity higher than zero. The slip velocity is sometimes used for small difference in the stable area of the adhesion-slip characteristic and spinning, slippage or wheelspin for high slip velocity that corresponds with the operating point position in the adhesion-slip characteristic unstable area. Next, in the thesis is used the slip or the slip velocity for a low slip velocity that corresponds to the operating point position in the stable area of the adhesion-slip characteristic and the slippage for the slip velocity that corresponds to the operating point position in the unstable part of the adhesion-slip characteristic.

2.1.2 Adhesion-Slip Characteristic

The value of the adhesion coefficient is typically depicted as a dependence of the slip velocity or the slip. The adhesion-slip characteristic is nonlinear, and a general characteristic is depicted in Figure 2.2. The adhesion-slip characteristic has a stable area and an unstable area. The stable area and the unstable area are assessed from the electric drive point of view. The electric drive can stably work in the characteristic stable area without any controller reaction. However, in the unstable area, the electric drive will increase speed without a proper controller reaction. The characteristic has a maximum point between the areas with the maximum value of the adhesion coefficient μ_{max}. The slip controller goal is to keep the operating point in the working area that is also depicted in the figure. The working area is limited to the stable area or the unstable area

near the maximum point. When the operating point moves from the stable area to the unstable area and back, stick-slip oscillations can occur. Therefore, it is better to avoid the operating point movement through the maximum point if it is possible during the slip controller normal operation. However, some slip control methods require this movement, and the stick-slip oscillations are the side effect of the method.

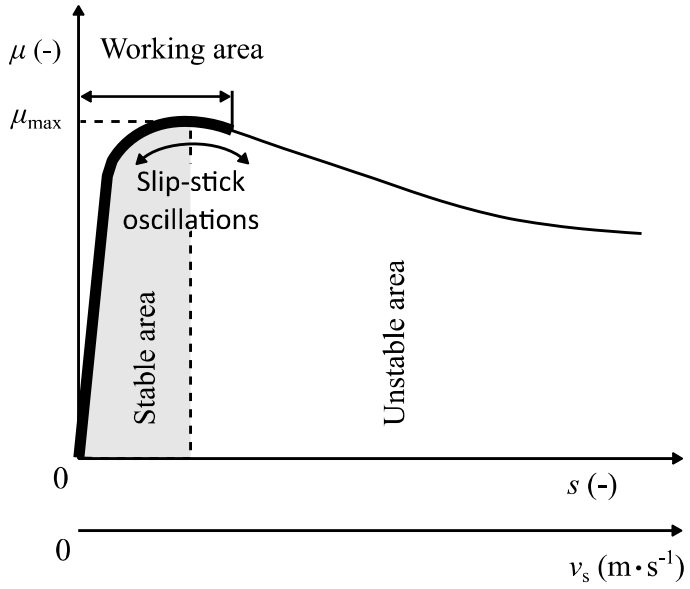

Figure 2.2 Example of an adhesion-slip characteristic

The adhesion-slip characteristic depicted in Figure 2.2 is valid for the static case. An example of a measured adhesion-slip characteristic from [47] is depicted in Figure 2.3.

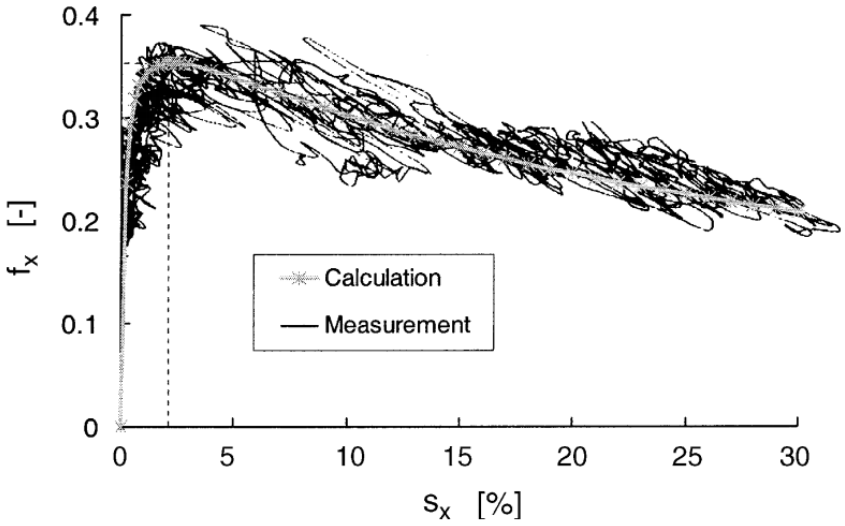

Figure 2.3 Example of a measured adhesion-slip characteristic [47]

The maximum value and shape of the adhesion-slip characteristic depend on several parameters. The most important are the conditions of the rail surface and the train velocity. The rail surface can be, e.g. dry or wet, sand, snow, leaves or oil can be on a rail surface. These parameters influence the adhesion-slip characteristic shape, and the slip velocity determines a position of an operating point on the current characteristic. The characteristic changes shape, when the

maximum value of adhesion-slip characteristic changes its position. An example of the dependence of adhesion-slip characteristic shape on the rail surface conditions is depicted in Figure 2.4. The conditions are random and unpredictable, and the conditions change even when the weather does not change. The value of adhesion coefficient varies from 0.05 up to 0.4 [9]. The lower value is for damp leaves and the upper for dry sand on the rail. The dry and clean rail has value around 0.33. Some characteristic depicted in Figure 2.4 has a peak, and some characteristics have a plateau instead of the peak. The plateau can cause fail of some methods. A similar adhesion-slip characteristic as characteristics depicted in Figure 2.4 can be found in [48] and [49].

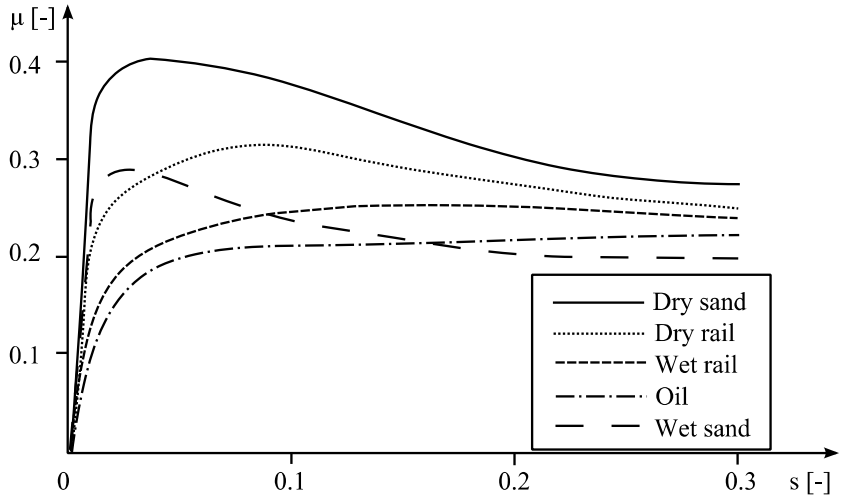

Figure 2.4 Example of the adhesion-slip characteristic for different conditions of a rail surface [50]

The maximum value of the adhesion coefficient decreases with the increasing train velocity v_L. The dependence can be described by known functions according to Curtius and Kniffler or Kother. The functions give similar results for a dry rail. Japan railway uses its functions for normal rails and wet rails [9]. The dependence of the adhesion coefficient maximum value on the train velocity is depicted in Figure 2.5.

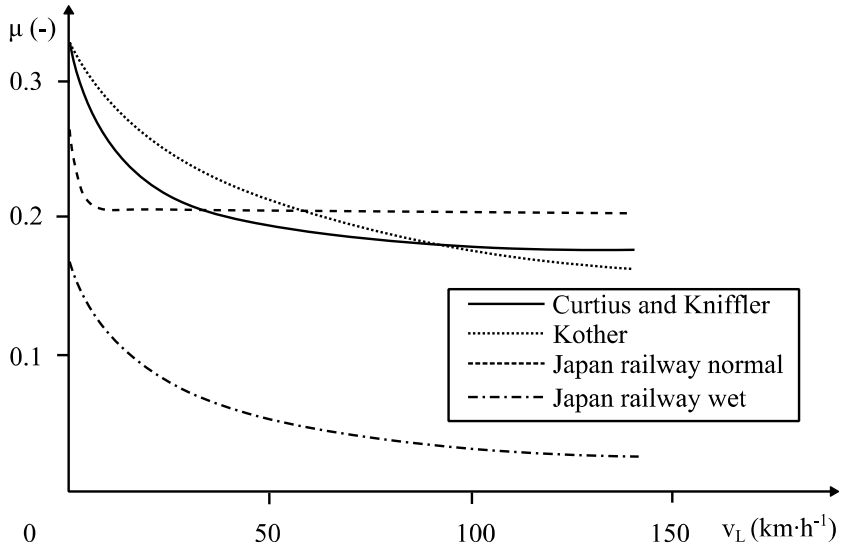

Figure 2.5 Adhesion coefficient value as the train velocity function

The description of the functions for Curtius and Kniffler, and Kother formulas follows. The (2.3) and (2.4) are valid for dry rail only.

$$\mu_{\max} = \frac{7.5}{v_{\mathrm{L}} + 44} + 0.161 \tag{2.3}$$

$$\mu_{\max} = \frac{9}{v_{\mathrm{L}} + 42} + 0.116 \tag{2.4}$$

2.1.3 Force Transferred between Wheel and Rail

The maximum value of the adhesion force F_{AMax} depends on the adhesion coefficient value and the normal force. Both values change during the train runs. The maximum value of the adhesion force depends on the value of the maximum adhesion coefficient $\mu_{\max}$:

$$F_{\mathrm{AMax}} = \mu_{\max} \cdot F_N \tag{2.5}$$

An actual value of the adhesion force F_{A}:

$$F_{\mathrm{A}} = \mu \cdot F_N \tag{2.6}$$

The maximum adhesion force can be transferred only if the maximum value of the adhesion coefficient is achieved. A slip controller has to find the maximum value of the adhesion coefficient. The task is a difficult due to the coefficient changes. Moreover, every wheel has a different actual value of the adhesion coefficient. Therefore, the adhesion force of the whole locomotive is given by a sum of partial wheelsets forces:

$$F_{\mathrm{A}} = \sum_{\mathrm{i}=1}^{n_W} \mu_{\mathrm{i}} \cdot \mathrm{F}_{\mathrm{Ni}} \tag{2.7}$$

(2.8)

2.1.4 Wheel-Rail Contact Area

The wheels and rails are made of steel, and its reciprocal contact area has only a few square centimetres. The wheel and railhead have cylindrical shapes. Therefore, according to the Hertz theory [9] and [51] the contact area has an elliptical shape. The position of the wheels and rail influences the contact area shape. The dependence of the ideal contact area on wheel and rail reciprocal position is depicted in Figure 2.6. The train moves from side to side during the train runs even if the train runs on a straight railway. The moving is caused by a lateral displacement of the train that is caused by a wheels and rails shape. The movement is well known as a hunting movement. The ellipse shape depends on an applied normal force. The force causes wheel and rail deformation in the contact area. The deformation is small due to the material of wheels and rails. When the wheel is shifted to one side, two contact areas between wheel and rail can occur. This two contact area makes the situation more complicated. For calculation simplicity, the elliptical shape can be approximated by a rectangle [52].

The force in the wheel-rail contract is only transferred by a part of the contact area. Therefore, the contact area can be divided into two areas. The first area is called as a stick area, and there is no reciprocal movement between wheel and rail. The area is located in leading part of the contact area. The second area is called a slip area and a reciprocal movement between wheel and rail occurs in the area. The force is only transferred by a slip area [9]. The slip area size and the adhesion force value depend on a slip velocity. The whole contact area example is shown in

Figure 2.7. The maximum force can be transferred when the slip area is expanded over the entire contact area [9]. The shape of the adhesion area can be different according to different theories [51].

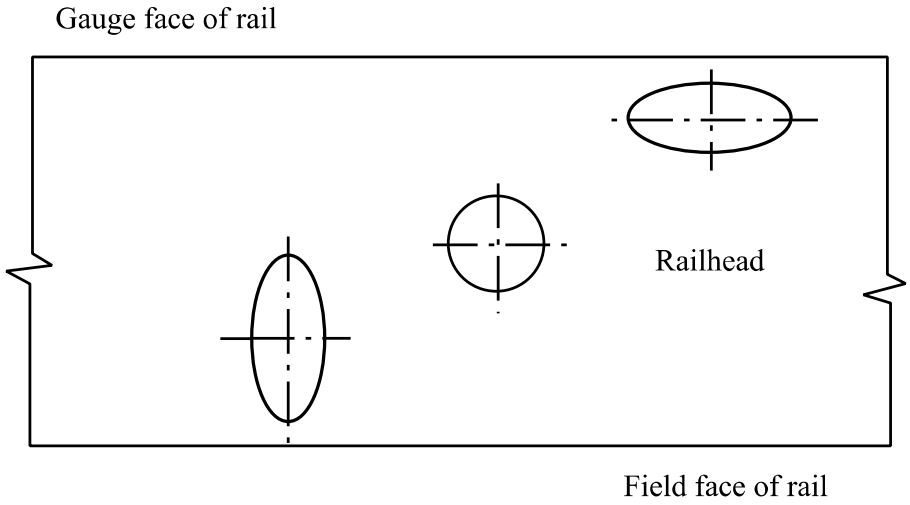

Figure 2.6 Example of the wheel-rail contact areas shapes [53]

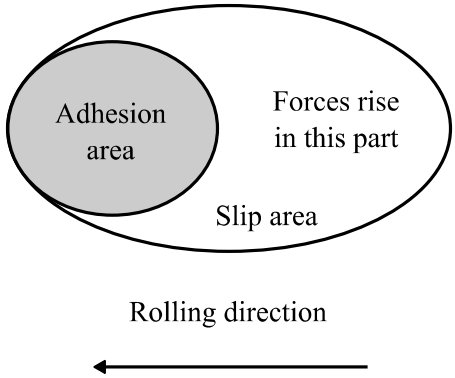

Figure 2.7 Example of adhesion and slip area in the wheel-rail contract area

Because the wheels and rails are made of steel, it is difficult to deform them. However, some deformation it the wheel-rail contact occurs. The wheel deformation is depicted in Figure 2.8. The wheel leading part is contracted, and the rail is expanded under the rolling wheel. The adhesion area occurs in this part of the wheel-rail contact. The deformation is balanced in the wheel rear part, where the wheel is expanded, and rail is contracted. These deformations cause the reciprocal movements the wheel-rail contact, and a slip area occurs in this part. The rail is bent in the contact area. Figure 2.8 explain the adhesion area and slip area creation depicted in Figure 2.7.

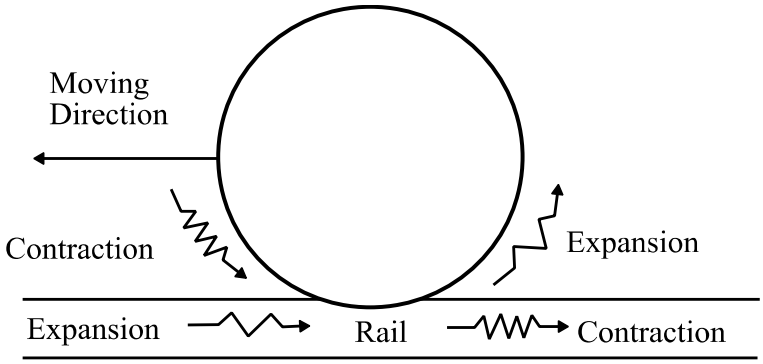

Figure 2.8 Schematic presentation of the wheel and rail deformations in the wheel-rail contact area [54]

2.1.5 Modelling of the Adhesion-slip Characteristic

The adhesion-slip characteristic can be modelled in different ways. The models can be roughly sorted into the methods that use wheel-rail contact parameters and contact theories, and the methods that try to approximate the characteristic by a curve. The first type of the methods requires understanding how the force is transferred between wheels and rails. The second methods type use measured characteristics that approximate by proper function. Both principal methods description follows.

The models that use the contact area parameters are widely used. Static model based on a beam model and a dynamic model based on a bristle model is described in [52]. Both models are verified on a test bench and the models can provide similar results as the experimental results [52]. Another model is described by Polach in [55]. The model described in [55] is one of the most used model type in the literature [11]. The two-dimensional theory of Carter, the linear Kalker theory, and other contact theory of rolling contact are an overview in [56]. However, the equations of all models require plenty of parameters that can be difficult to determine especially during the train run. The equations require, e.g. a normal force value and the contact area geometry. These values are not possible to determine during the train runs. Because of the normal force changes, e.g. due to the track irregularity [57], that can cause the bouncing and pitching of a locomotive or the train normal force change due to the change of applied force [58] and the wheel-rail contact area geometry also change as it is depicted in Figure 2.6. Therefore, the usage of the models during on-line calculation is very complicated.

The models that approximate the adhesion-slip characteristics are more straightforward than previous models type. However, the approximation is not exact. The equations contain parameters that describe the actual conditions of the rail surface. The adhesion-slip characteristic approximation by a curve can be described as follows [26] and [31]:

$$\mu = c_{\mathrm{a}} \cdot e^{-a_{\mathrm{a}} \cdot v_{\mathrm{S}}} - d_{\mathrm{a}} \cdot e^{-b_{\mathrm{a}} \cdot v_{\mathrm{S}}} \tag{2.9}$$

Where a_{a}, b_{a}, c_{a} and d_{a} are coefficients that are given in Table 2.1.

Table 2.1 Adhesion-slip characteristics coefficients values for (2.9) [31]

Rail surface conditions	a_{a}	b_{a}	c_{a}	d_{a}
Dry	0.54	1.2	1.0	1.0
Wet rail	0.54	1.2	0.1	0.1
Wet dew	0.05	0.5	0.08	0.08

Another similar characteristic representation can be written [59]:

$$\mu = a_b \cdot e^{-b_b \cdot v_s} \tag{2.10}$$

Where a_b and b_b are coefficients that are different from coefficients given in Table 2.1. The coefficients are described in [59] in detail.

Another adhesion-slip characteristic description is published in [60]:

$$\mu = a_c \cdot \left(1 - e^{-b_c \cdot v_S}\right) - \frac{v_S}{10} \tag{2.11}$$

The coefficients a_c and b_c are given in Table 2.2.

Table 2.2 Adhesion-slip characteristics coefficients values for (2.11)

Rail surface conditions	a_c	b_c
Dry	0.265	40
Intermediate	0.2013	45
Wet	0.1302	55

The equations (2.9), (2.10) and (2.11) use coefficients to describe the adhesion-slip characteristic according to the actual rail surface conditions. It is difficult to determine the coefficients meaning. Therefore, another description of the characteristic can be used [61]:

$$\mu = \frac{2 \cdot K_S \cdot \mu_{max}^2 \cdot v_S}{\mu_{max}^2 \cdot v_S^2 + K_S^2} \tag{2.12}$$

Where K_s is a multiplication of μ_{max} and v_{SPeak} that occur at μ_{max}.

The coefficients for (2.12) to get a similar result as according (2.9) and Table 2.1 are given in Table 2.3.

Table 2.3 Adhesion-slip characteristics coefficients values for (2.12) to get match with (2.9)

Rail surface conditions	μ_{max}	v_s	K_s
Dry	0.289	1.3	0.375
Wet rail	0.029	1.2	0.034
Wet dew	0.056	5.1	0.284

The adhesion-slip characteristics according (2.9) and corresponding Table 2.1 and according (2.12) and corresponding Table 2.3 are depicted in Figure 2.9. The depicted characteristics are for dry, wet-rail and wet-dew rail surface conditions. The depicted characteristics are similar. Therefore, (2.12) can give similar results as the (2.9), when proper parameters are used. The dry characteristics according (2.9) are sharp, and the unstable area of the characteristic decreases too low. The characteristic does not match with the measured characteristic depicted in Figure 2.3 and the theoretical characteristic depicted in Figure 2.4 that does not have so steep the unstable area. More similar characteristic to the measured characteristic according (2.12), are depicted in Figure 2.10. The corresponding coefficients are given in Table 2.4.

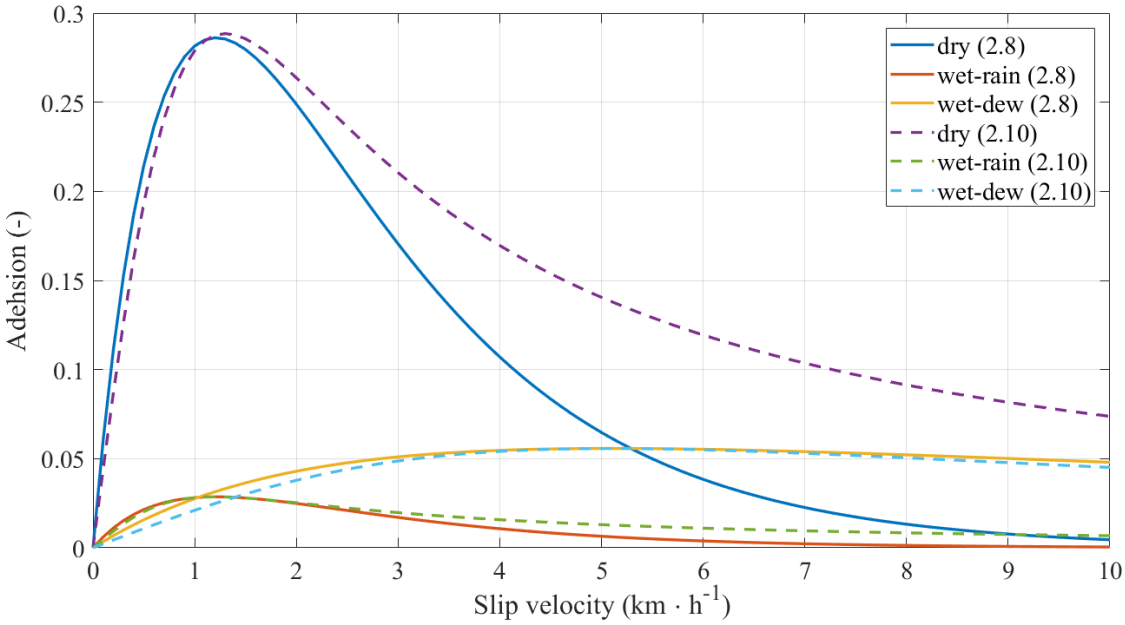

Figure 2.9 Adhesion-slip characteristics according (2.9) and Table 2.1 and according (2.12) and Table 2.3

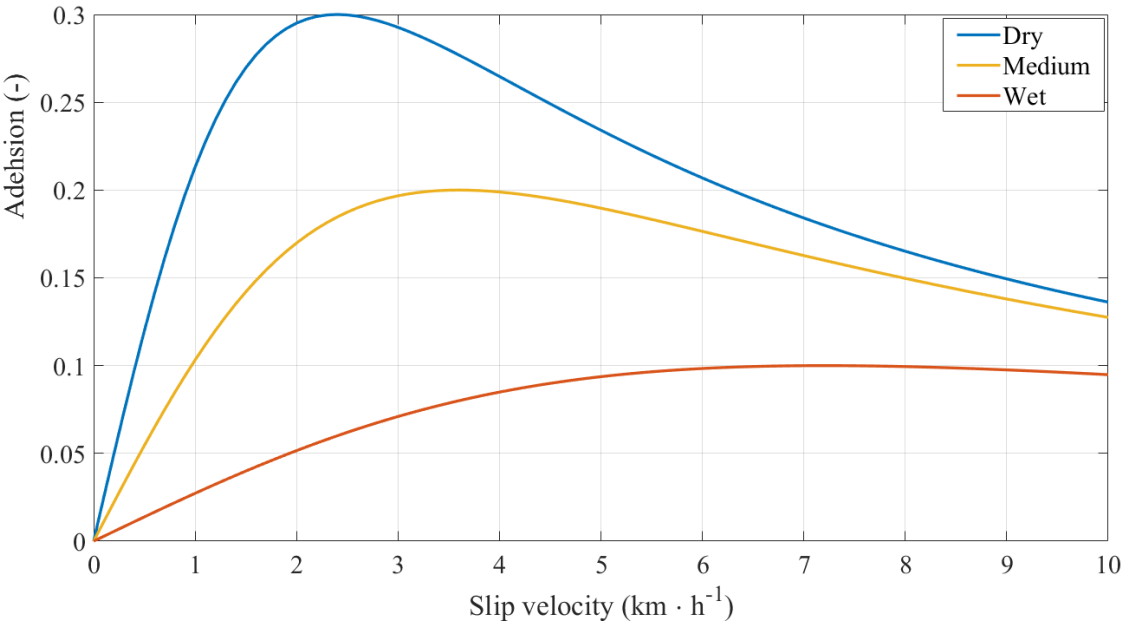

Figure 2.10 Adhesion-slip characteristics according (2.12) to get match with measured characteristic

Table 2.4 Adhesion-slip characteristics coefficients values for (2.12) to get match with measured characteristic

Rail surface conditions	μ_{max}	v_s	K_s
Dry	0.3	2.4	0.72
Medium	0.2	3.6	0.72
Wet	0.1	7.2	0.72

2.2 Slip Controllers

The principles of the conventional slip controllers are described in this subchapter. The main part of the subchapter is dedicated to the principles of the adhesion or slip detection part of the slip controllers. The re-adhesion controllers and the control part of the slip controller are also briefly described.

The first thing is to propose requirements to the slip controller. The mentioned requirements here are based on requirements presented in [61] and [62]:

1. Permanent work in the stable area of the adhesion-slip characteristic, or in the unstable area of the characteristic near the maximum value for necessary time.
2. The proper reaction to fast adhesion condition change when the adhesion change or slippage is detected.
3. The proper work during the train start. To fulfil the requirement is problematic because most of the methods are based on a wheel velocity measurement that has long response.
4. The proper work with any adhesion-slip characteristic shape. The requirement is simple to fulfil in characteristic with a peak. However, when the characteristic has a plateau, the slow increase of the slip velocity can occur.
5. Continuous and fast tractive force change according to the actual adhesion conditions, and eliminating a subsequent slippage by improper tractive force increasing.
6. Resistance against synchronous slippage. In this case, an actual train velocity cannot be determined from the measured velocity by simple measurement.
7. Damping of torsional vibrations, or at least not generating the torsional vibrations.

The slip control methods have to provide a transfer of the highest possible tractive force by the wheel-rail contact and keep the slip velocity in the acceptable value by decreasing the tractive force if the required tractive force is higher than the maximum transferable force. The slip controller has to cope with the adhesion-slip characteristic nonlinearity when the controller task can be fulfilled. Basically, there are two different conditions in which the slip controller has to work correctly. In the first case, an adhesion-slip characteristic is almost stable, and the maximum point position changes in a small range. In the case, the controller has to find the maximum point and keep the operating point near the maximum point during the adhesion-slip characteristic changes. This situation can occur, e.g. due to the train velocity increasing. In the second case, the adhesion-slip characteristic can change its shape abruptly. When the maximum point decreases, the operating point that was near the characteristic maximum point in the stable area gets to the characteristic unstable area, and the wheel slip velocity starts to increase. The slip controller has to react fast in this case and decrease the tractive force. This situation can occur when the rail surface conditions change. The difference between the small change of the adhesion-slip characteristic and the significant change is shown in Figure 2.11 and Figure 2.12 respectively. The depicted characteristic in the figures represents a dependence of an adhesion force F_A on the slip. The adhesion force is equal to the adhesion coefficient multiplied by a normal force applied to the wheel. If the normal force is constant, then the dependence of the adhesion force on the slip has the same shape as the adhesion-slip characteristic. The scale is only different. The operating point A is set below the maximum point of the characteristic 1 depicted in Figure 2.11 at the beginning. This position is typical for methods that determine the characteristic slope. The position of the point A is given by the actual characteristic shape and the applied tractive force. The value of the applied tractive force at point A is F_{TA}. When the small change of the adhesion-slip characteristic occurs and the characteristic changes to characteristic 2, the operating point spontaneously moves to the point B, and then by controller

intervention to the point C. The applied force F_{TA} is changed by the controller to F_{TC}. If the characteristic movement is small and fast, the operating point movement from point A to point B can occur without a controller reaction. Otherwise, the controller reacts and decreases the force during the movement, and the operating point moves from the point A to the point C without crossing through the point B, or the position of the point B can be different. The second case, when the significant characteristic change is depicted in Figure 2.12. If the characteristic 1 changes to characteristic 2 the operating point has to move from the point A to point C if the adhesion should be fully utilised. The movement from the point A to point C requires the slip controller reaction. If there is no reaction, the operating point moves to high slip velocity and the slippage occur because the wheels are accelerated by an acceleration force. The acceleration force is a difference in applied motor force and an actual adhesion force. The operating point moves to the high slip velocity value through a point D in this case. Therefore, a controller has to react and decreases the applied tractive force. The operating point moves from point A to point C through point B. The position of the point B depends on a slip controller reaction. If the controller is fast the direct transfer from the point A to point C is possible.

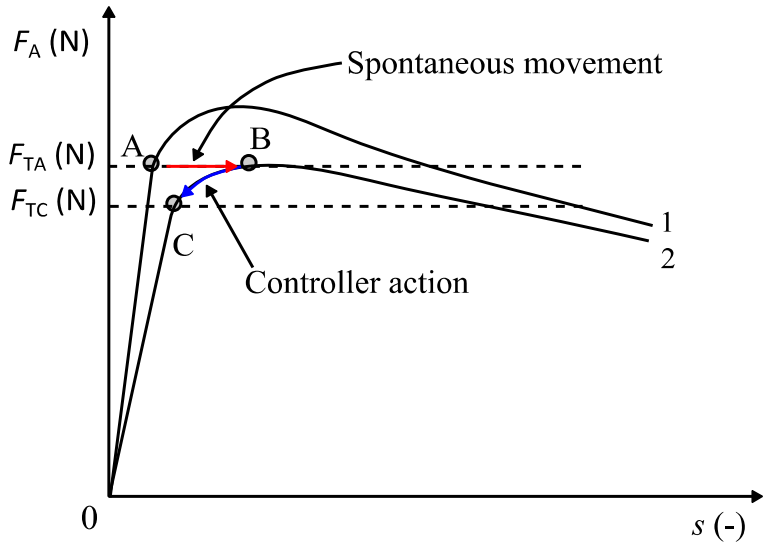

Figure 2.11 Controller work under a small change of an adhesion-slip characteristic

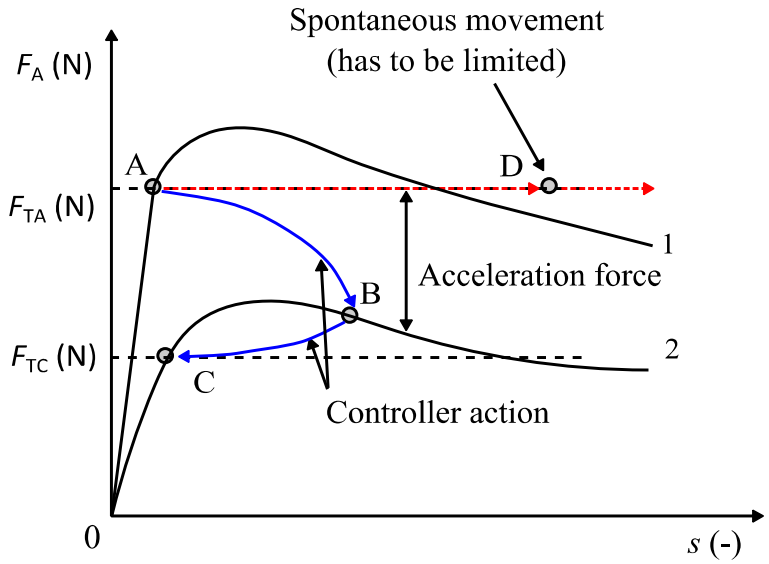

Figure 2.12 Controller work under a significant change of an adhesion-slip characteristic

The chapter focuses on a slip control method, but antiskid methods also exist. The antiskid method has to prevent a wheel skid during braking. If the wheels are braked by the electric drive during electrodynamic braking, the antiskid control method works on a similar principle as the slip control method. The slip velocity and the adhesion signs are only changed. Therefore, there is no principal difference between slip control method and antiskid control method. Another situation can occur if the wheels are braked mechanically, the method is designed to control dump valves instead an electric drive. However, the method principle can be used as a slip controller basis if the method is modified because the method has to detect the beginning of the skid.

2.2.1 Re-adhesion Controllers

The doctoral thesis does not focus on re-adhesion controllers. However, the re-adhesion controllers are a developmental precursor of the slip controllers, and the re-adhesion controllers are sometimes used as supplementary protection in some slip controllers. Therefore, a brief description is only mentioned in the subchapter. The re-adhesion controller cannot prevent the slippage formation. The re-adhesion controller limits the slippage to acceptable value when the slippage is detected by decreasing the applied force to the wheelset. When the slippage is suppressed, the applied force is increased to the original value. This approach can create another slippage when the conditions on rail surfaces become permanently bad. Therefore, a train driver has to decrease the required tractive effort to prevent the next rise of the slippage. The re-adhesion controller has to decrease the force steeply to suppress the slippage because the operating point is far in the unstable area of the adhesion-slip characteristic when the re-adhesion controller starts to work.

The simple re-adhesion method compares velocity of the slowest wheelset with other wheelsets. When the difference exceeds a threshold, a regulatory reaction is done. Therefore, the proper threshold has to be set to the method proper work. The assumption is that the slowest wheelset is the slowest because it has the best adhesion. The method can simply fail when a synchronous slippage occurs. The method can be resistant to the slow slip rising of one wheelset. However, when the situation occurs, all wheelset probably will have a similar slip velocity, and the method will fail. The problem can be solved by independent train velocity measurement, e.g. by GPS or Doppler radar. Similarly, acceleration can be used because a difference between an operating acceleration and acceleration during high slip velocity increasing is high. Another simple method compares voltage or current of the two motors that are connected in series or parallel to one converter. The method was developed for locomotives with DC motors. The regulatory intervention is done when the voltage or current difference exceeds a threshold. The method with a current difference can be modified for induction motors [63] and [64]. The methods were improved, and some slip controllers are based on the principles as it is shown in the next subchapters.

2.2.2 Slip Controllers Based on the Slip Velocity or Acceleration

A simple slip controller maintains a slip velocity at a constant value. The slip velocity is maintained at the maximum acceptable value that corresponds to a velocity in which a maximum adhesion coefficient occurs. The slip controller cannot provide accurate slip control because the threshold value is only one and no adaptation on the actual adhesion-slip characteristic is made. Therefore, the slip controller can only optimally work for one characteristic. The slip controller was created by a re-adhesion controller improvement, and its block diagram is depicted in Figure 2.13. A measured wheelset velocity of an actual wheelset v_C is compared with the slowest wheelset velocity v_{Cmin}. The calculated slip velocity v_S is compared

with a threshold velocity v_{SM}, which represents the maximum acceptable slip velocity. The value can be approximatively set to value 2 km·h^{-1} [43], [61] and [65]. A difference torque ΔT is generated according to the velocity difference value and difference torque is decreased proportionally to velocity difference value when it exceeds the threshold. The difference torque decreases the required motor torque. The slip controller is equipped with a re-adhesion controller that also modifies the difference torque ΔT according to the actual slip velocity value, but the threshold is set higher than the slip controller threshold, and it works as a protection to the slip controller. The final difference torque ΔT is given by a sum of both ΔT from the slip controller and form the re-adhesion controller. The slip controller disadvantage is that it cannot optimally work with every adhesion-slip characteristic and it can simply fail when a synchronous slippage occurs.

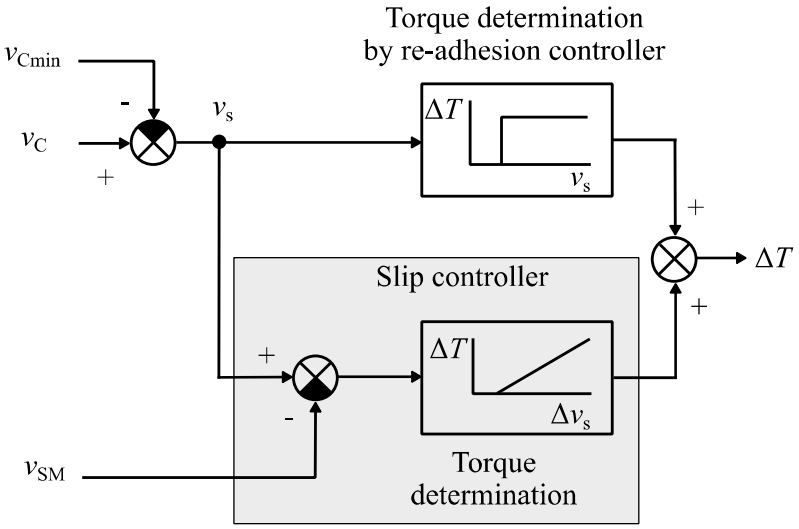

Figure 2.13 Block diagram of the slip controller that controls the slip velocity at a constant value [61]

Another similar simple slip controller is based on the wheelset acceleration comparison with the threshold. The wheelset acceleration, during the normal operation without a slippage, is significantly lower than acceleration when the slippage occurs. The freight train acceleration is below 0.3 m·s^{-2}, and the threshold can be set up to 1.4 m·s^{-2} [66] because the wheelset acceleration is higher than 2.8 m·s^{-2} when the slippage occurs. The slip controller requires calculation of the wheelset acceleration from a measured wheelset velocity. The calculation can be problematic due to the noise in the measured velocity. The torque is limited according to the difference between the actual acceleration and the threshold. The slip controller advantage is that the slip controller does not require the train velocity. The slip controller can be improved by comparing the wheelset acceleration with the train acceleration. However, the train acceleration has to be calculated. The slip controller can fail when the slip velocity increases gradually during the adverse conditions of a rail surface.

A hybrid slip controller is presented in [43]. The slip controller combines the slip velocity control and the slip controller that uses acceleration. The slip controller block diagram for a vehicle with 4 wheelsets is depicted in Figure 2.14. The slip controller combines the two principles described above, and the slip controller does not require a re-adhesion controller. A similar approach is presented in [48] and [67].

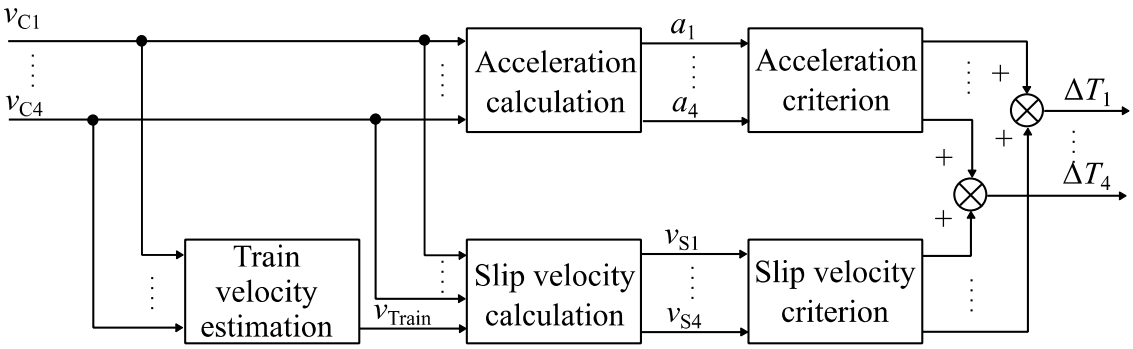

Figure 2.14 Hybrid slip controller proposed by [43]

The presented slip controller can be improved by using fuzzy logic as it is described in [68] and [69]. The [69] is designed for brake, but the principle can be used for slip control too. The slip controller uses a wheelset slip velocity and accelerations. These values are not evaluated by a simple controller as in previous cases, but they are evaluated by fuzzy logic, and the control action is done according to the fuzzy controller rules. The slip controller is depicted in Figure 2.15.

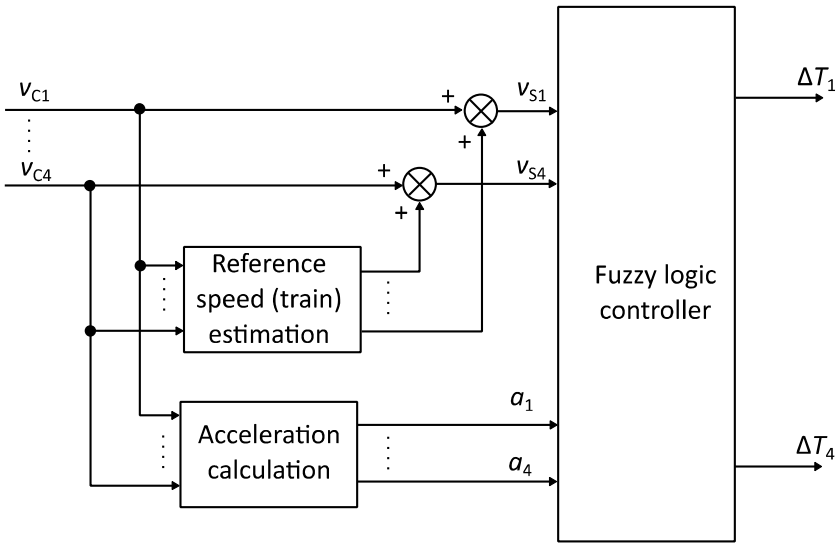

Figure 2.15 Velocity difference and acceleration slip controller with a fuzzy logic [69]

The described slip controllers are based on simple principles and have a small requirement for the calculation power. If the train velocity is not determined by the driven wheelsets, the slip controller can be reliable and resistant to the synchronous slippage. However, the slip controller cannot optimally utilise the adhesion in all rail surface conditions.

2.2.3 Slip Controller Based on the Evaluation of the Current Difference between Two Parallel Motors

The slip controller is based on a current difference comparison of two motors. The motors have to be connected to one inverter in parallel. When one wheelset has higher velocity, the current difference between the motors occurs. The slip controller principle is presented in [63], [64], [70] and [71]. The slip controller is designed for sensorless motor vector control method. Therefore, the slip controller can simpler cope with a problem with the low wheelset velocity. The slip controller basic idea is depicted in Figure 2.16. The motors currents i_1 and i_2 are the same if the motors have the same angular velocity. The situation is depicted in Figure 2.16 a.

When one motor has a higher angular velocity than the second motor, the motor currents are different. If the inverter does not operate with constant current control, the currents change, as it is depicted in Figure 2.16 b. The case for the constant current control is depicted in Figure 2.16 c. However, the current difference Δi is almost the same in both cases.

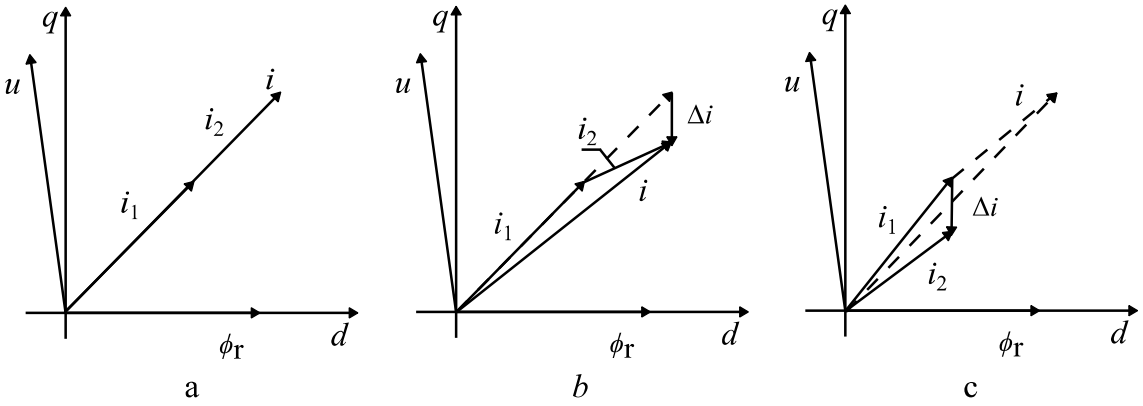

Figure 2.16 Vector diagrams for case without slippage and with slippage [63]

The slip velocity can be calculated as follows:

$$v_{\mathrm{S}} = k_{\mathrm{mech}} \cdot \frac{R_2}{L_2} \cdot \frac{i_{\mathrm{q1}} - i_{\mathrm{q2}}}{i_{\mathrm{d}}} \tag{2.13}$$

Where k_{mech} is a mechanical constant that includes a wheel diameter, a number of motor pole pairs, and a gear ratio, R_2 is a rotor resistance, L_2 is a rotor inductance, i_{q1} and i_{q2} are motor torque current and i_{d} is a motor flux current.

The motor torque T_{x} can be calculated as follows:

$$T_{\mathrm{x}} = \frac{p_{\mathrm{p}} \cdot L_{\mathrm{M}}}{L_2} \cdot \phi^*_{\mathrm{rd}} \cdot i_{\mathrm{qx}} \tag{2.14}$$

Where L_{M} is a magnetizing inductance, ϕ^*_{rd} is a reference value of rotor flux linkage p_{p} is a number of pole pairs, and subscript x identifies a motor number.

The load torque T_{Lx} can be calculated as follows:

$$T_{\mathrm{Lx}} = T_{\mathrm{x}} - J_{\mathrm{M}} \frac{\mathrm{d}\omega_{\mathrm{Mx}}}{\mathrm{d}t} \tag{2.15}$$

Where J_{M} is a moment of inertia of electric drive system, i.e. rotor, gearbox and wheelset, and ω_{Mx} is a rotor angular velocity.

The motor angular velocity can be calculated as follows:

$$\frac{\mathrm{d}\omega_{\mathrm{x}}}{\mathrm{d}t} = \frac{\mathrm{d}\omega_1}{\mathrm{d}t} - \frac{\mathrm{d}}{\mathrm{d}t}\left(\frac{R_2 \cdot L_{\mathrm{M}}}{L_2} \cdot \frac{i_{\mathrm{qx}}}{\phi^*_{\mathrm{2dx}}}\right) \tag{2.16}$$

Where ω_1 is a motor synchronous angular velocity, and ϕ^*_{2dx} is a reference value of a rotor flux.

The slip can be detected by comparison of the current difference or according to the estimated load torque. The method is classified as a slip controller and according to [63] works well.

However, according to the [40] is more suitable as a re-adhesion controller. The described slip controller can detect smaller slippages than methods with speed sensors.

2.2.4 Slip Controllers Based on the Characteristic Slope Detection

This group of slip controllers try to determine a slope of the adhesion-slip characteristic, and they are based on several different principles. This group of the slip controllers is preferable, and some authors consider this type of slip controllers as the most accurate and efficient slip controllers [61]. The adhesion-slip characteristic slope can be detected by a derivative of an adhesion force according to a slip velocity, or by measuring a phase shift between motor torque and its speed, or by evaluation of torsional vibrations that occur between wheels and electric drive. The slip controller that uses the adhesion force has to estimate the force by some estimator. The slip controllers that determine the phase shift require the addition of some disturbing torque to the required torque or evaluate the torsional vibrations that occur spontaneously in the mechanical parts.

2.2.4.1 Slip Controllers based on an Adhesion Force Derivative

The slip controllers that calculate a derivative of the adhesion force F_A needs to know the adhesion force value and the slip velocity v_s. However, the adhesion force value is unknown. Therefore, the value has to be estimated by some estimator. When the adhesion force is known, its derivative can be calculated:

$$\frac{\mathrm{d}F_A}{\mathrm{d}v_S} = 0 \tag{2.17}$$

When (2.17) is met, the operating point is located in the maximum point of the adhesion-slip characteristic. If the derivative is positive, the operating point is located in the stable area of the characteristic, and if the derivative is negative, the operating point is located in the unstable area of the characteristic. The slip velocity determination is difficult in locomotives, and the possible determination ways are discussed in subchapter 2.3. However, the derivative can be simplified by removing the slip velocity [22]:

$$\frac{\mathrm{d}F_A}{\mathrm{d}t} = 0 \tag{2.18}$$

The slip controllers based on the principle are presented in [22], [23], [24], [25], [26], [27] and [28]. The authors use disturbance observers to estimate the adhesion force. The typically used disturbance observers are zero order, first order or full order. The difference between the observer orders lays in its complexity and accuracy. The simple ones can sometimes have problems with proper function [22]. The zero-order observer is based on an equation of motion. The disturbance observer is typically defined as follows [29]:

$$J_M \frac{\mathrm{d}}{\mathrm{d}t}\omega_M = T - T_L \tag{2.19}$$

$$T_L = \frac{\mu \cdot F_N \cdot r_w}{R_g} \tag{2.20}$$

$$\hat{T}_L = \frac{o_P}{p + o_P}(T - J_M \cdot p \cdot \omega_M) \tag{2.21}$$

$$\hat{F}_{\mathrm{A}} = \frac{R_{\mathrm{g}}}{r_{\mathrm{w}}} \hat{T}_{\mathrm{L}} \tag{2.22}$$

Where J_{M} is a motor moment of inertia, ω_{M} is the motor angular velocity, T is the motor torque, T_{L} is the motor load torque, $\hat{T}_{\mathrm{L}}$ is estimated load torque, $\hat{F}_{\mathrm{A}}$ is an estimated adhesion force, R_{G} is a gear ratio, r_{w} is a wheel radius, p a complex frequency, and o_{P} is the observer pole.

The general description of the slip controllers based on the disturbance observer is depicted in Figure 2.17. The slip controller input is a required torque T^* that is set by a train driver. The required torque is multiplied by a slip controller limiting value that is in a range from zero to one. The modified required torque is led to a torque controller block, and then to an electric drive block. The electric drive block output is measured motor angular velocity ω_{M} and calculated motor torque T. The motor torque is calculated by a motor controller. Instead of the motor angular velocity, a wheel angular velocity can be used. The velocity type depends on a placement of the speed measurement sensor position. Both values, the torque and the velocity, are led to a disturbance observer that estimates a load torque or load force according (2.21) or (2.22) respectively. Then, a derivative according (2.17) or (2.18) is calculated. The PI controller output maintains the required torque value to be the PI controller input equal zero or positive. The positive value is used more often to avoid the operating point oscillates around the maximum point. When the PI controller input is maintained at a positive value, the operating point is located in the stable area of the adhesion-slip characteristic.

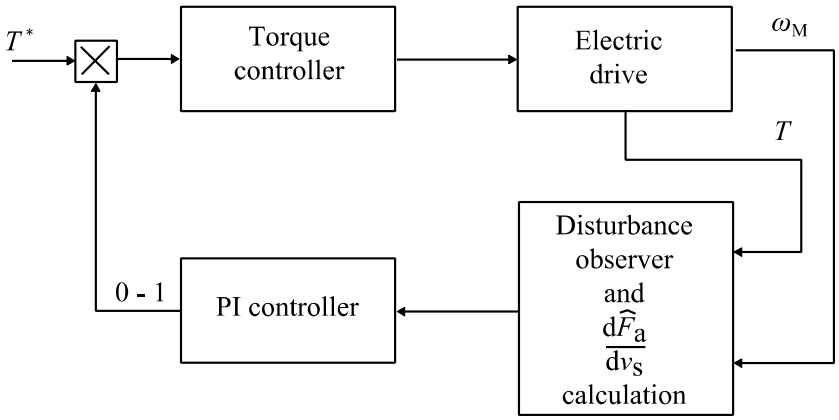

Figure 2.17 Slip controller based on an adhesion-slip characteristic slope with an observer

The estimated adhesion coefficient creates only a part of the adhesion force described by (2.6). The second part of the adhesion force is a normal force that changes during the train run. Therefore, the estimation of the adhesion coefficient provides less accurate results than that the estimation of the adhesion force if the dynamic motions that influence the normal force are taken into account. The disadvantage of the slip controllers based on observes is that a sensor noise, which is ignored by the observer cannot be suppressed [72]. The slip controllers are, therefore, affected and disturbed by the noise [42] and [73]. Therefore, the method described in [74] estimates the adhesion-slip characteristic slope by an observer and control the output by a sliding mode controller. To eliminate the noise, which is ignored by the disturbance observer, a forgetting factor is used. The slip is calculated from the estimated adhesion-slip characteristic slope. When the estimated slope is higher or lower than a threshold, the slip is increased or decreased about a constant value. The method is controlled by a modified sliding mode controller that eliminates the high-frequency chattering phenomenon that occurs when the

system states get near the sliding mode surface. The slip controller with observer also exists with the Kalman filter that can eliminate some observer based slip controller disadvantages [60], [75] and [76].

The adhesion coefficient can also be estimated according to a wheel-rail contact area. The approach is described in [52] and [77]. The slip controllers are based on a model of the contact area. A beam model and a bristle model are used for the purpose, and the slip controllers use a sliding mode observer. An adaptive sliding mode controller is used for the control. Basically, the slip controller is a variant of the slip controller that uses an observer for the adhesion force estimation. However, a different approach is used in this case.

2.2.4.2 Slip controllers Based on the Evaluation of a Phase Shift between Motor Torque and Speed

Another approach of detecting the adhesion-slip characteristic slope is to detect a phase shift between motor torque and the corresponding angular speed. The slip controller was presented in papers [33], [34] and patents [78], [79]. The slip controller requires adding a small periodic disturbance torque ΔT_D to the motor torque T. The disturbance torque causes oscillations of the motor torque and angular speed. Between the motor torque oscillations and motor angular speed, a phase shift occurs. The phase shift φ_S is proportional to the actual adhesion-slip characteristic slope. The phase shift dependence on a motor angular velocity is demonstrated in Figure 2.18. The figure shows an uncontrolled slippage. The required motor torque T^* increases the motor torque T until an operating point exceeds the maximum point, then the motor torque decreases. The motor angular velocity ω_M and angular velocity that corresponds to its longitudinal velocity ω_L are also depicted in the figure. When the slip velocity is small, and operating point is in a stable area, the phase shift value is about -0.5 rad. When the operating point, goes to the maximum point the phase shift starts decreasing.

The slope of the adhesion-slip characteristic is calculated as follows. The electric drive torque is calculated first:

$$T = T^* + \Delta T_D \cdot \sin \omega_f t \tag{2.1}$$

Where ω_f is an angular modulation frequency.

Measured motor angular velocity ω_M is filtered by a filter to get back the modulated motor angular velocity ω_{Mf}:

$$\omega_{Mf} = \Delta\omega_M \cdot \sin(\omega_f t - \varphi_s) \tag{2.2}$$

Where $\Delta\omega_M$ is a motor angular velocity change

The modulated velocity is multiplied by a sine wave and a cosine wave with a modulation frequency. The outputs of the low pass filters are:

$$a_f = \frac{\omega_f}{2\pi} \int_0^{\frac{2\pi}{\omega}} (\omega_{Mf} \cdot \sin(\omega_f t))\, dt \tag{2.3}$$

$$b_\mathrm{f} = \frac{\omega_\mathrm{f}}{2\pi} \int_0^{\frac{2\pi}{\omega}} (\omega_\mathrm{Mf} \cdot \cos(\omega_\mathrm{f} t)) dt \tag{2.4}$$

The phase shift φ_S is calculated as follows:

$$\varphi_\mathrm{s} = \operatorname{atan} \frac{b_\mathrm{f}}{a_\mathrm{f}} \tag{2.5}$$

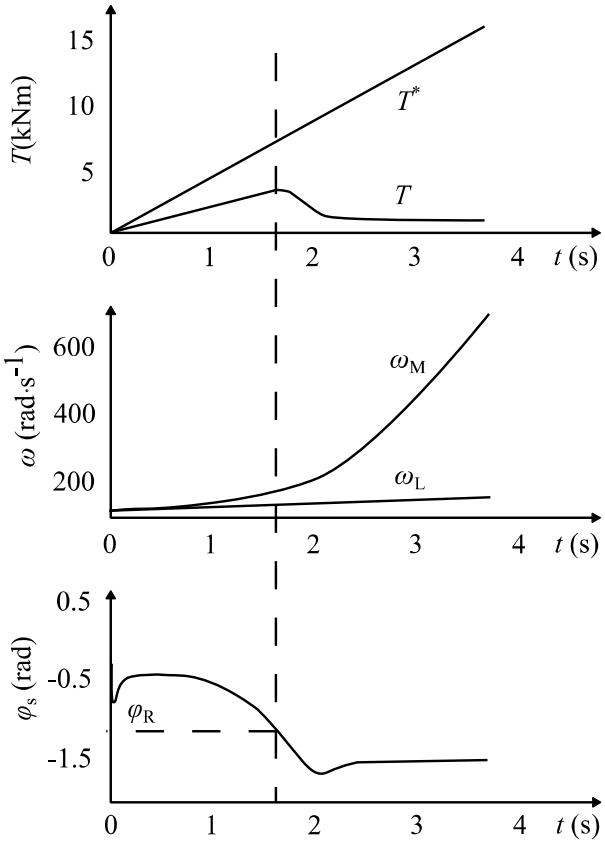

Figure 2.18 Example of the dependence of phase shift φ_S on wheel velocity [33]

The block diagram of the slip controller is depicted in Figure 2.19. The input of the slip controller is the limit value of the phase shift φ_S^*. The limit value determines the position of the operating point on the adhesion-slip characteristic. The second parameter is a required velocity v_C^* that is compared with an actual wheel velocity v_C. The required wheel velocity is used because the slip controller uses a speed controller if the slip controller does not use the speed controller, the value is not needed. The angle φ_S is calculated from the measured wheel velocity, and the angle is used as a reference input to an angle controller.

The phase shift shape depends on used modulation frequency. The modulation frequency has to be lower than the lowest mechanical eigenfrequency. On the other hand, a low modulation frequency increases the detection time delay. The disturbance torque can be sinus which frequency is proposed from 5 to 12 Hz. Similar slip controller based on the phase shift is described by [73]. The phase shift is evaluated in the same way, and proposed frequency is from 7 to 10 Hz, and amplitude is from 2 to 4 %. The slip controller can cause undesirable

mechanical oscillations. However, the slip controller is one of the more perspective slip controller [61].

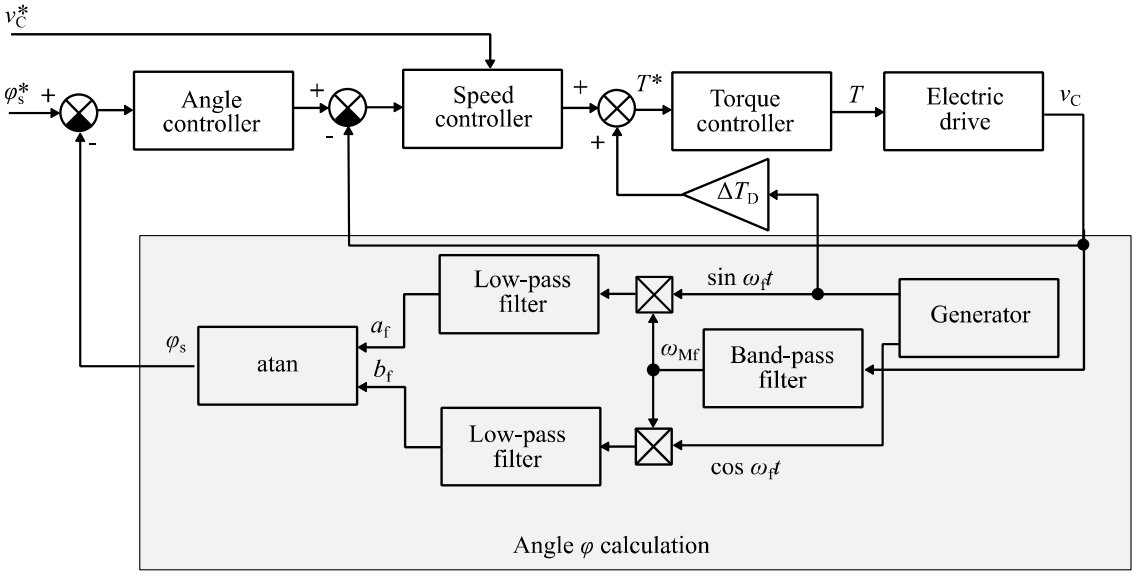

Figure 2.19 Block diagram of the slip controller that determines a phase shift between motor torque and speed [61]

2.2.4.3 Slip controllers Based on the Evaluation of Torsional Vibrations

The adhesion-slip characteristic slope can be determined from torsional vibrations that occur between a motor and gearbox and between the wheels. This principle uses slip controllers developed in [35] and [36]. The torsional vibrations occur due to the non-rigid shafts between the rotating masses. The torsional vibrations sources are demonstrated in Figure 2.20. The slip controller is based on the assumption that adhesion coefficient damps dynamic motions. The torsional vibrations are self-excited. When the operating point is in the stable area of the adhesion-slip characteristic, the torsion vibrations are damped. When the operating point is at the maximum point, the damping is zero, and when the operating point is in the unstable area the damping is negative [35] and [80].

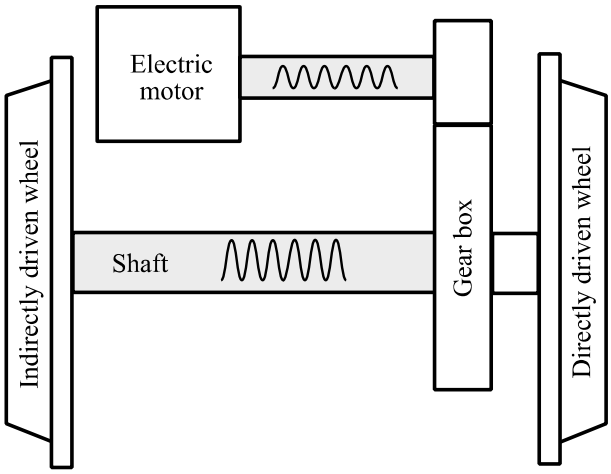

Figure 2.20 Wheelset configuration with torsional vibrations

The slip controller from [35] uses a Kalman filter with a system model to detect the vibrations. The state equations are:

$$\frac{\mathrm{d}}{\mathrm{d}t}\begin{bmatrix}\Delta\omega_\mathrm{D}\\ \Delta\omega_\mathrm{I}\\ \Delta T_\mathrm{T}\end{bmatrix}=\begin{bmatrix}-\frac{k_1}{J_\mathrm{D}} & 0 & -\frac{1}{J_\mathrm{D}}\\ 0 & -\frac{k_2}{J_\mathrm{I}} & \frac{1}{J_\mathrm{I}}\\ k_\mathrm{s} & -k_\mathrm{s} & 0\end{bmatrix}\cdot\begin{bmatrix}\Delta\omega_\mathrm{D}\\ \Delta\omega_\mathrm{I}\\ \Delta T_\mathrm{S}\end{bmatrix}+\begin{bmatrix}\frac{1}{J_\mathrm{D}}\\ 0\\ 0\end{bmatrix}\cdot\Delta T \tag{2.6}$$

$$y=\begin{bmatrix}1 & 0 & 0\end{bmatrix}\cdot\begin{bmatrix}\Delta\omega_\mathrm{D}\\ \Delta\omega_\mathrm{I}\\ \Delta T_\mathrm{T}\end{bmatrix} \tag{2.7}$$

Where ω_D and ω_I are directly driven and indirectly driven wheel angular velocities, ΔT_T is a difference of torsional torque, J_D and J_I are directly driven and indirectly driven wheel moments of inertia, and k_1, k_2 and k_s are coefficients that depend on the system mechanical parameters.

The (2.6) is valid in a case when speed measurement sensor is placed on a wheelset, and torsional vibrations between the wheels are detected. If the sensor is located on the motor, the torsional vibration between the motor and directly drive wheel can be detected. In this case, parameters in (2.6) have to be modified. The speed sensor is placed on a directly driven wheel according (2.7). An example of the presented result is depicted in Figure 2.21. The magnitude starts to increase when the slip velocity starts to increase. The slip controller can detect the adhesion-slip characteristic slope.

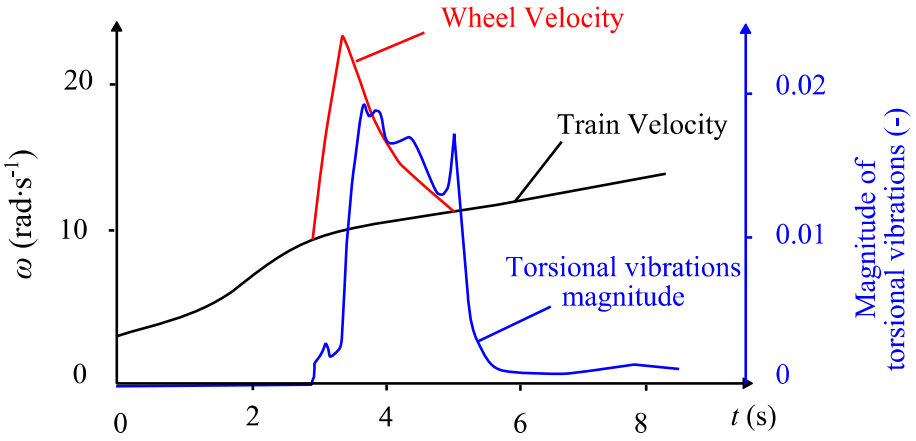

Figure 2.21 Example of the magnitude of the torsional vibrations [35]

2.2.5 Slip Controllers Based on the Maximum Point Detection

The slip controllers in this group try to determine a position of the maximum point on the adhesion-slip characteristic. The slip controllers based on this principle are presented in [37] and [38]. Generally, the slip controllers increase the required force while the maximum point on the characteristic is overstepped. Then, the required force is decreased to get the operation point back to the stable area. The slip controllers have to permanently work in the unstable part of the characteristic and can cause a problem with stick-slip oscillations. When the slip velocity change is positive or negative, and the corresponding force change is positive or negative, respectively, the operating point is in the stable area of the characteristic. When the slip velocity change is positive or negative, and the corresponding force change is negative or positive respectively, the operating point is in the unstable part of the characteristic. The slip controller principle is demonstrated in Figure 2.22. When the slip velocity is increased about the slip velocity value Δv_S, the tractive force is increased about the force ΔF_T1 when the operating point

is in the stable area. If the operating point is in the unstable area, the force decreases about the force ΔF_{T2} when the slip velocity is increased again about the slip velocity Δv_S. The operating point is in the stable area if the following condition is met:

$$\mathrm{sgn}(\Delta F_T) = \mathrm{sgn}(\Delta v_S) \tag{2.8}$$

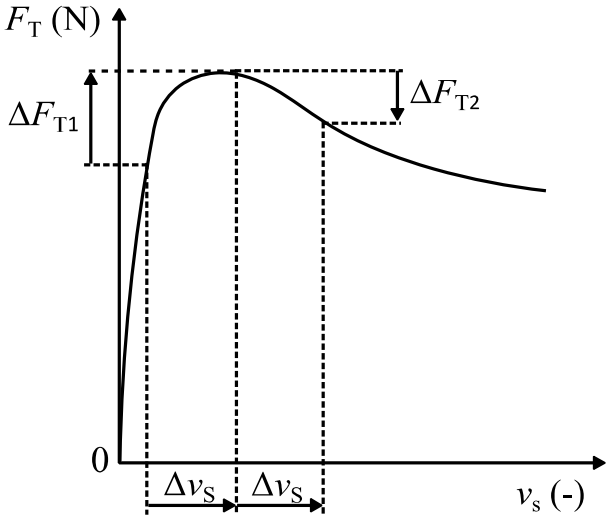

Figure 2.22 Maximum point detection of the adhesion-slip characteristic

The slip controller principle is based on a speed controller that enables stable work in the unstable area of the adhesion-slip characteristic, i.e. the motor velocity cannot spontaneously increase in the unstable area. The speed controller can only prevent an uncontrollable speed increase, but the required wheel velocity has to be set by the slip controller logic. The slip controller logic increases or decreases the required wheel velocity according to the operating point position. The slip controller block diagram is depicted in Figure 2.23. The slip controller contains logic that determines the position of the operating point on the actual adhesion-slip characteristic. The decision is not as straight as described by (2.8) because the operating point returns to the stable area from the unstable area on a different characteristic that is lower [81]. The logic consists of a torque memory to determine the maximum point position. When the decision is made, a required acceleration a is added or subtracted to actual wheel acceleration a_C. The slip controller requires a wheel acceleration calculation and then acceleration integration.

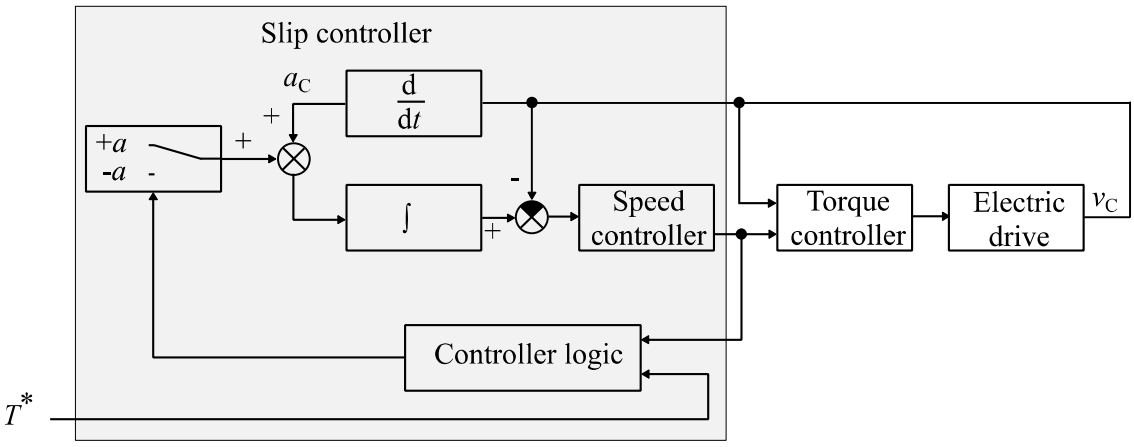

Figure 2.23 Block diagram of the slip controller based on the maximum point detection

The slip controller advantage is that the available adhesion can be entirely used and the slip controller can work as near as possible to the maximum point. However, a high dynamic electric drive is required, and slip controller can cause stick-slip oscillations. The slip controller can fail when the characteristic has no maximum point, in this case, the slip controller tries to find the maximum point by increasing the slip velocity, and the velocity can increase above the acceptable value. Therefore, the slip controller has to be equipped with protection that limits the slip velocity to the acceptable value. The slip controller can work without the speed controller. However, an electric drive with a high dynamics and the fast slip controller is required. Because, when the operating point exceeds the maximum point of the adhesion-slip characteristic, the slip velocity starts to increase.

The methods described above are the typical representative of the group. However, some modification also exists. The slip controller described in [82] uses a similar principle as Perturb and Observe method (P&O) used by converters for photovoltaic panels for the maximum power point tracking. The slip controller changes applied force, and according to the estimated force and velocity change tries to find the maximum point. The slip controller was tested on Hardware in the Loop (HIL). Another slip controller based on a disturbance observer is described in [10]. The slip controller estimates an adhesion force, and according to the rules that compare a value of the estimated force and a tractive force change, the slip controller evaluates a position of an operating point on the adhesion-slip characteristic. The method based on the similar principle with different rules is described in [83]. However, the problem with working in the unstable area and stick-slip oscillations remains.

2.2.6 Slip Controllers Based on Other Principles

The adhesion coefficient can be estimated by an acoustic diagnostic of a wheel-rail contact. The slip controller based on the principle is described in [40] and [41]. The slip controller uses microphones mounted on bogies for the adhesion coefficient determination. The noise is analysed and compared with a spectrum that depends on a current position on the track. The position is determined by a GPS. The slip controller can work only on the track on which the spectrum was measured previously. The slip controller was evaluated by simulation.

The slip controller proposed in [42] uses a Hilbert-Huang Transformation (HHT) for the slip control. The HHT is an empirical data analysis method for the obtaining the frequency data [42]. If the operating point gets to an unstable part of the adhesion-slip characteristic, torsional vibrations are excited. The Hilbert energy spectrum of the wheel velocity signal can be used for the slippage determination. The Hilbert energy spectrum is calculated from the signal amplitude. The method compares the actual energy with an average spectrum. The slip controller was tested on a locomotive. However, the results were not presented. The slip controller is based on a similar principle as the slip controller for the adhesion-slip characteristic slope detection based on torsional vibrations. The slip controller can be included between methods that determine an adhesion-slip characteristic slope because of a similarity of the mentioned slip controller. However, according to the slip controller working description, the slip controller can be classified as a slip controller that lies between a re-adhesion controller and a slip controller.

2.2.7 Controller Part of the Slip Controller

The previously described methods, with exceptions, describe the adhesion or slip detection part of the slip controller and the controller is represented by a block named controller without further explanation. The detection part detects the maximum point overstep, the characteristic

slope, or some threshold exceedance. This information has to be further processed by a controller. Some slip controllers are designed with a controller part. However, the controller can be replaced by any type of a controller, without the method change in the most cases. The detection part of the slip controller output is a ratio of the derivative of the adhesion force, the required slip velocity, angle, or the maximum torque. The output has some range and when some threshold is exceeded the controller has to work and limit the value. For the purpose, different types of the controller can be used. Therefore, the controller part of the slip control method is briefly overviewed in the subchapter.

The controller has to set the operating point to the required position, has to work correctly during quick characteristic change and even slow the characteristic change and change the motor torque fast and continuously. The slow controller cannot fulfil the requirements, but the fast controller can cause oscillations of the detection part of the slip controller or mechanical parts. The detection part oscillations cause the method fails. The mechanical oscillations can be caused by the operating point exceedance of the maximum point, but the same oscillations can be excited by a fast controller.

A PID controller is a known and widely used controller type. The controller exists in many implementations. The controller advantages are its simple implementation and description. The controller structure does not depend on the controlled system structure. The controller disadvantage is the controller constants settings. Fuzzy controllers are used in some described methods. The fuzzy logic uses a linguistic approach and commonly is based on an expert knowledge [69] and can be used for nonlinear systems with advantage. The fuzzy logic principle is simple. However, its tuning requires more parameters than the PID controller. The fuzzy controllers are described in many papers from different disciplines, and papers that are related to the slip control are, e.g. [1], [37], [68] and [69]. State space controllers can be used for the slip control. The controller requires a system model for the proper controller work. Sliding mode controllers [60], [76] and [84] can also be used. There are comparisons of the controllers in the literature. The comparison between a PID and a fuzzy controller is made in [69] where the fuzzy controller is a little better. A comparison presented in [85] compares a fuzzy controller with a state controller from the point of view of two mass model lifetime extensions, where the state controller provides better results.

The slip controller has to cooperate with the electric drive controller and has to be implemented into the vehicle control structure. The slip controller typical connections into a control system are depicted in Figure 2.24. The first possible slip controller connection is parallel to the electric drive control structure. This variant is depicted in Figure 2.24 a). The structure contains a *Control panel* block that is located in a driver's cabin. The output of the *Control panel* is a required torque that is multiplied by a torque correction value from the slip controller that decreases the required torque according to actual adhesion conditions. The torque settings by a driver cannot change abruptly. Therefore, a rate of the torque change is limited by a ramp function. The corrected torque is a *Torque controller* block input. The *Slip controller* block input is typically wheel velocity and torque. The torque can be a corrected torque or an actual motor torque that has to be calculated by a motor controller in the *Electric drive* block. The required values depend on the slip controller type. In the second variant the *Slip controller* block is connected in series to the vehicle control structure as it is shown in Figure 2.24 b). A corrected torque is directly produced by the *Slip controller* block in this case. A control structure with a speed controller is depicted in Figure 2.24 c). The speed controller is not typically implemented in the electric drive control scheme of the freight locomotives. This

structure type is required by some slip control methods that need to stable work in an unstable part of an adhesion-slip characteristic. A slip controller generates a required wheel speed in this case.

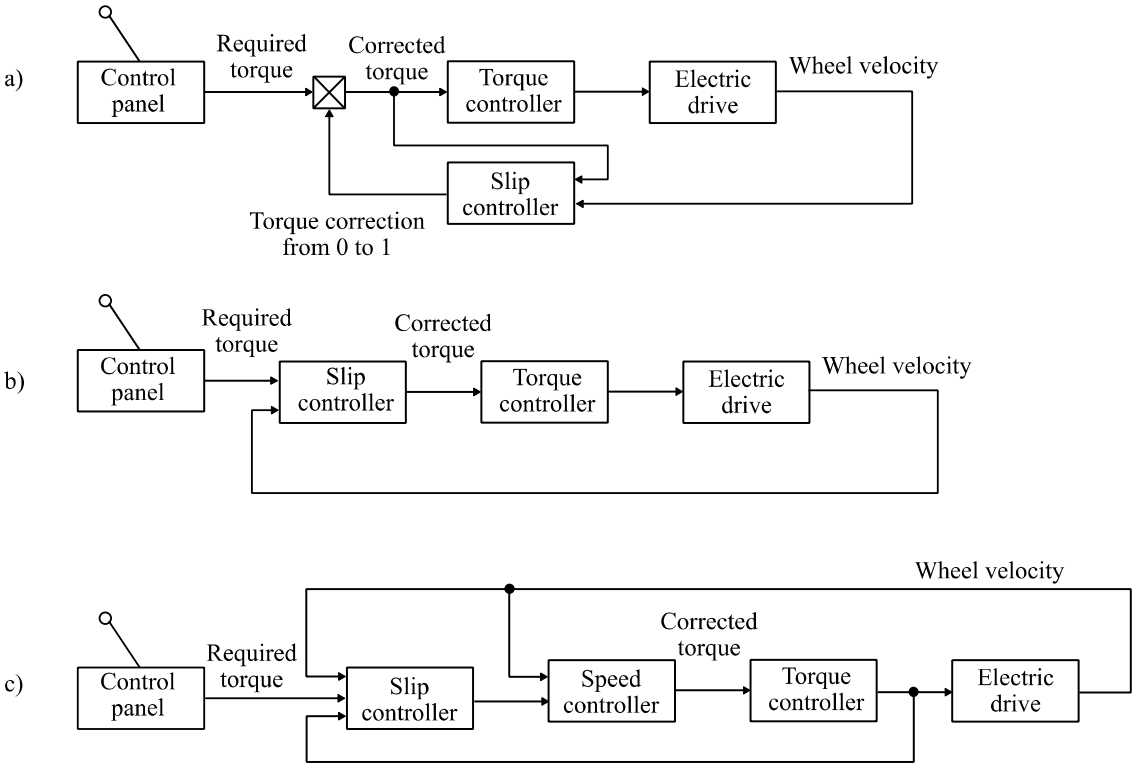

Figure 2.24 Slip controller possible connections to the vehicle control structure of the electric drive

2.3 Slip Velocity Determination

The slip velocity is calculated from the wheel longitudinal velocity and wheel circumference velocity. The wheel circumference velocity is typically measured by incremental encoders that are mounted on wheelsets or motors. The wheel longitudinal velocity determination is not as straightforward as the wheel circumference velocity. The wheel longitudinal velocity can be measured as the velocity of the non-driven wheels. However, this approach is typically possible only in EMU, and the method cannot optimally work in adhesion control [2]. Locomotives have typically every wheelset driven. A velocity of the slowest wheelset can be considered as a longitudinal velocity. The slip velocity calculated from the slowest wheelset velocity and the actual wheelset velocity is not the correct slip velocity, but it is higher than the actual slip velocity. The similar results can be achieved by some averaging of all driven wheelsets. The velocity can be miscalculated when all wheelsets have the same high slip velocity. This situation is called as a synchronous slippage. Another method problem can be caused by a vehicle computer. Every driven wheelset has a computer that besides calculates the wheelset velocity, i.e. wheel circumference velocity. The calculated velocity is sent to the locomotive computer that is a master computer for all wheelsets computers via a communication bus. The information is sent from the wheelsets computers one after another. Then the locomotive computer calculates the train velocity and sends it back to the wheelset computers. Therefore, the velocity data can be measured at a different time because the newest available data are sent to the locomotive computer. When the locomotive accelerates, the oldest data can have the lowest value while they may have the highest value [86].

Another approach to determine the wheel longitudinal velocity value is the wheel longitudinal velocity estimation. The estimation can be based on an observer or fuzzy logic. The method described in [87], [88] and [89] uses an adaptive filter for the longitudinal velocity. The method can cope with the problem of the synchronous slippage. The method estimates velocity that is close to the slowest wheelset velocity. The method described [90] uses an adaptive filter with fuzzy logic to determine the wheel longitudinal velocity. The estimated velocity is close to velocity measured by a GPS. Therefore, the calculated slip velocity is close to the actual slip velocity. The proposed method requires an acceleration and jerk calculation to its proper work. In [86], [91], [92] and [93] a KF, EKF and UKF respectively are used to estimate the wheel longitudinal velocity. The methods estimate the velocity that is close to the wheel circumference velocity when the slip velocity is low, and an operating point is in the stable area of the adhesion-slip characteristic. When the slip velocity starts to increase, the estimated velocity does not copy the increase. The estimated velocity has the same time course as the actual wheel longitudinal velocity, but there is an offset between these velocities. These methods can be used for the velocity estimation only or in cooperation with the estimation of, e.g. adhesion force. An example of the longitudinal velocity estimation and estimation of some mechanical parameters by the estimator is described by (2.9). This method requires extending the system matrix **A** about velocity submatrix $\mathbf{A}_{\text{velocity}}$. The matrix $\mathbf{A}_{\text{mechanical}}$ describes a mechanical system. This approach causes increasing of the computational power. However, usage of the method has to be thoroughly considered because the real-time calculation can be complicated.

$$\mathbf{A} = \begin{bmatrix} \mathbf{A}_{\text{mechanical}} & 0 \\ 0 & \mathbf{A}_{\text{velocity}} \end{bmatrix} \tag{2.9}$$

An example of the submatrix $\mathbf{A}_{\text{velocitiy}}$ is in [86]. The submatrix size is 3x3:

$$\mathbf{A}_{\text{velocity}} = \begin{bmatrix} 1 & dt & 0 \\ 0 & 1 & dt \\ 0 & 0 & 1 \end{bmatrix} \tag{2.10}$$

The longitudinal velocity can be directly measured by a GPS or Doppler radar. The methods require additional installation of the GPS or radars if they are not installed. The GPS proper operation is not guaranteed in every area, e.g. in tunnels or urban canyons. Therefore, the GPS is used in connection with other sensors fusion to get sufficient accuracy and reliability [94], [95] and [96]. Doppler radars are used for the velocity measurement [97] and [98]. The method can be inaccurate due to the dynamic locomotive motions when the car body is inclined, and the distance between the Doppler radar and ground is changed [99] and [100]. Therefore, two radars are required for the proper method work [99]. Moreover, the method can fail when the surface is very smooth due to the loss of the reflected signal [99]. The train velocity can be obtained from the train acceleration. The train acceleration can be measured by accelerometers. However, the offset and integral error accumulation occurs in this case.

A principle proposed by [60] and [62] can also be used for the slip velocity estimation. The method estimates the train velocity from estimated adhesion force by using a simple equation (2.11). Moreover, the resistance force is considered in [62].

$$v = v_0 + \int_0^t \sum_{i=1}^{n_{\text{W}}} \frac{F_{\text{Ai}}}{M} dt \tag{2.11}$$

Where v_0 is initial velocity and M is the vehicle mass.

2.4 Slip Controller and a Locomotive Computer

The slip controller, electric drive controller, velocity measurement and other programs run on a locomotive computer. The locomotive computer is a distributed one and consists of a master computer and wheelset computers and auxiliary computers. The computers communicate among themselves through communication buses. The vehicle computer is schematically depicted in Figure 2.25. The computer structure influences the slip controller design and limits the slip controller field of application to the wheelset that is controlled by the computer because the wheelsets computers typically are not directly connected and communication between the computers is made through the master computer. This communication type produces a time delay in the communication. Therefore, slip controller that uses information from other wheelsets is problematic to design. The problem occurs in the train velocity calculation as it is outlined in subchapter 2.3. The wheelset computer drives corresponding electric drive according to the force command from the master computer, and when the slip controller reacts, the force is decreased for the intervention time. The wheelset computer is typically a DSP with limited computing power. The dynamic electric drive requires fast control with a short control period. The period can be from tenths of microseconds to milliseconds. The modern electric drives with induction motors are driven by a field-oriented control that can be complicated and consume the significant time of the control period. For the slip controller calculation can remain tenths of microseconds. This time strongly limits the slip controller complexity.

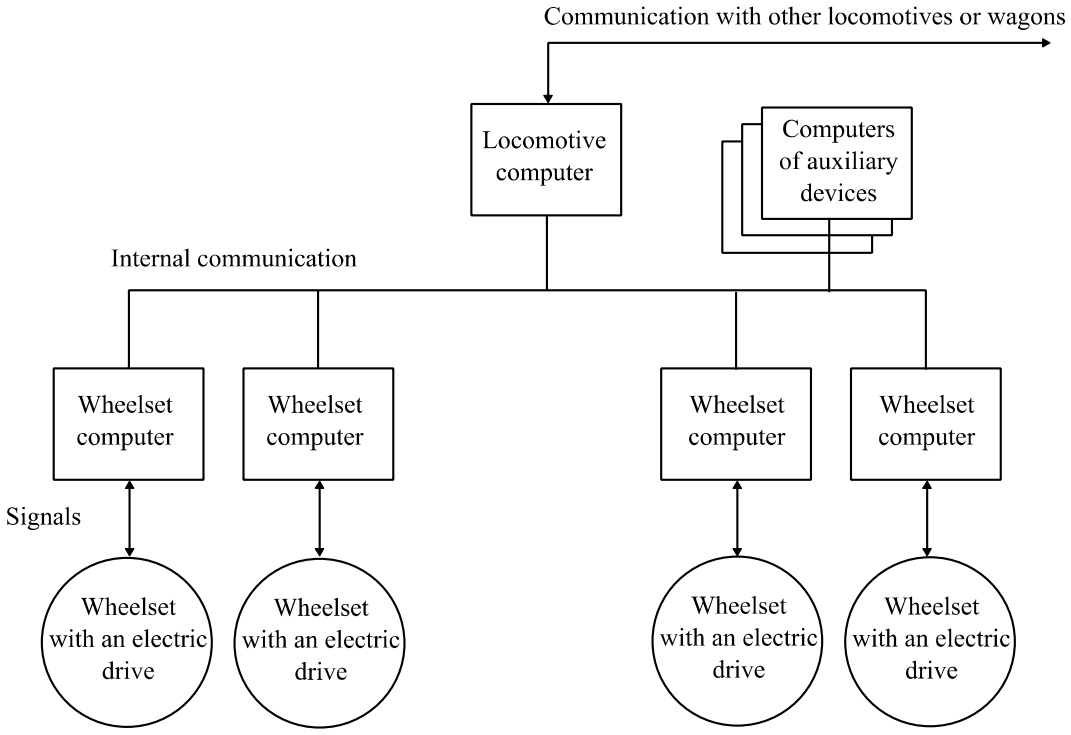

Figure 2.25 Locomotive distributed computer

Some slip control methods supposed to preventively reduce the tractive effort applied to wheelsets when a slippage is detected on another wheelset [11] and [101]. In this case, a probability of the slippage creation of other wheelsets increases and the information about slippage of one wheelset can be sent to other computers to prepare for the possible slippage as the method improvement. On the other hand, the cleaning effect is employed in the case. The contaminations are gradually removed from the rails when the train moves. The worst conditions have the first wheelset, and it removes the contaminations. Thus, the next wheelset

has better conditions. Therefore, the probability of the slippage creation on the other wheelsets decreases and the efficiency of the preventive actions are questionable. Moreover, these preventive actions are not common due to the computer structure that produces time delay, and because the information time delay is not typically known. Using information from other vehicles or wagons is even more difficult because the communication is made through slowest bus than the communication between computers in one vehicle.

2.5 Summary of Slip Control Methods

The adhesion phenomenon and used slip control methods are described in the chapter. The force that can be transferred between wheels and rails depends on an adhesion coefficient value. The adhesion coefficient value depends on an adhesion-slip characteristic shape, and current value depends on a slip velocity or slip. The adhesion-slip characteristic shape changes during a train run every few meters. The characteristic change can be small and gradual or significant and abrupt. The characteristic shape mainly depends on conditions of rails surface and the train velocity. The standard slip control methods principles are described in the chapter. The methods are sorted into a re-adhesion controller and slip controllers. The re-adhesion controllers are older one and cannot fulfil the requirements that are required from the slip controllers. The slip controllers are more sophisticated and can stably work near the maximum point of any adhesion-slip characteristic. The two main groups of slip controllers create methods that determine the characteristic slope or find the characteristic maximum. There are used many slip control methods on the locomotives, but not every method was presented in paper or patent. The described re-adhesion controllers methods are summarized in Table 2.5 and described slip controllers are summarized in Table 2.6.The summarizations describe the basic methods without modifications and improvement.

Table 2.5 Summary of the re-adhesion controllers

Method name	Required parameters	Strengths of the method	Weaknesses of the Method
Speed difference	Wheel velocity, train velocity, slip velocity threshold	Simple, can be used as an additional method for more sophisticated methods	Cannot optimally work, one threshold for all characteristics, can fail during synchronous slippage
Acceleration	Wheel velocity, acceleration threshold	Simple, can cope with the synchronous slippage, can be used as an additional method for more sophisticated methods	Cannot optimally work, is not suitable as a stand-alone method, can fail when a high slip velocity forms gradually
Voltage or current difference	Voltage or current, motors connected in series or parallel	Simple	Cannot optimally work, requires specific configuration of electric drive

The function of the slip controllers and the operating point comparison are demonstrated in Figure 2.26. Adhesion-slip characteristics and position of operating points for different slip controller types are depicted in the figure. A position of the maximum point is depicted by circles and ellipses in the figure. The slip controllers that try to detect the position of the maximum point will work around the point, i.e. in the circles and ellipses. The adhesion-slip characteristic shape is sharp around the maximum point for good adhesion conditions, but for

worse adhesion conditions, the point becomes more extensive and determines its location to be more difficult. The slip controllers can cause slippage when the adhesion conditions are bad as it is shown in the lowest characteristic. Slip controllers that estimate the adhesion-slip characteristic slope is demonstrated by tangents to the characteristics and the operating points are located to the points of contacts of the tangents and the adhesion-slip characteristics. The operating point is near the maximum point when the adhesion is good. The operating point moves away from the maximum point when the adhesion is worse. The slip controller cannot keep the maximum point for the bad adhesion conditions, but the slip velocity is not high as in the previous slip controller. Finally, the slip controller that keeps the slip velocity at a constant value is depicted in the figure as a dashed line. The slip controller can optimally work only for a narrow range of the adhesion-slip characteristics.

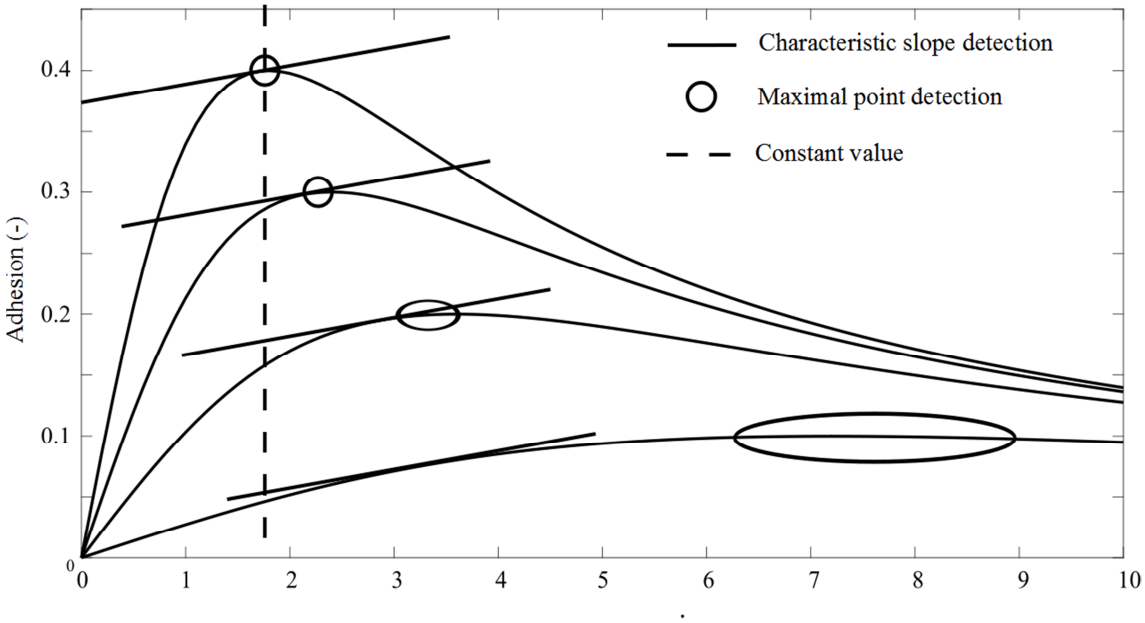

Figure 2.26 Slip control method principle comparison

Some slip control methods were tested or implemented on locomotives or EMUs, and some methods were tested on HIL. The methods that were implemented and tested on the locomotives and EMUs are summarized next. The method described in [102] is based on an acceleration criterion with an axle weight transfer. The method was tested on electric freight EH200-type DC locomotive from Toshiba. The method is improved in [66] by early detection of the slip elimination. The improved method was tested on a shunting locomotive HD-300. A method presented in [24] that is based on disturbance observer that determines the adhesion-slip characteristic slope was tested on an EMU Series 205-5000. A method presented in [65], was tested on an E2 Series Shinkansen. The described method is based on a speed difference method that changes the slip velocity threshold according to the train velocity. The method based on HHT was tested on an HXD2C-type electric locomotive. The test is described in [42]. A method based on the parallel motors current comparison was tested on a Shinkansen train in [70]. However, the type is not mentioned. The method for braking based on a slip velocity and acceleration with fuzzy logic, described in [69], is used on vehicles from Mitsubishi Electric Company.

Table 2.6 Slip controllers summary

Method name	Required parameters	Method strengths	Method weaknesses
Slip velocity control to a constant value	Wheel velocity, train velocity, threshold slip velocity	Simple, low computational requirements, can be used as an additional method for more sophisticated methods	Cannot optimally work, one threshold for all characteristics, can fail during synchronous slippage
Current difference	Motor parameters, values from vector control	Simple, low computational requirements	Can fail during synchronous slippage, requires specific configuration of electric drive
Characteristic slope detection based on the estimator	Wheel velocity, train velocity, motor torque, system model	Can optimally work near the maximum point at any type of characteristic, can be resistant against the synchronous slippage, does not causes the stick-slip oscillations during normal operation	Computational complexity depends on the used estimator complexity and can be very high
Characteristic slope detection based phase shift	Wheel velocity, torque		High computational requirements, a disturbance signal is required, motor input torque has to contain a disturbance component
Characteristic slope detection based torsional vibrations	Wheel velocity, system model		High wheel measurement resolution, can have a problem with the operation during low speed, high computational requirements
Characteristic maximum point detection	Wheel velocity, motor torque	Can optimally work at the maximum point at some characteristics, resistant against the synchronous slippage	Oscillates around the maximum point, can cause stick-slip oscillations, requires an electric drive with high dynamic and speed controller, can cause slippage when the characteristic has no peak
Method based on noise detection	Noise measurement, track noise spectrum, train position on the track	Can theoretically optimally work	Track noise spectrum is required
Method based on HHT	Wheel velocity, thresholds for control logic	Can theoretically optimally work	Complicated decisions have to be made, complicated tuning

3 PROPOSED SLIP CONTROLLER

The proposed slip controller is based on a detection of the adhesion-slip characteristic slope, and the slip controller uses a state estimator as the essential part. To eliminate the problem of the observers with the noise that is not taken into account by the observer, the state estimators for stochastic systems are considered as possible estimators.

The possible state estimators are firstly described in the chapter. Then, the proposed novel slip controller background, principle, and performance are described. The estimators require a system model for their proper work. The models are derived in chapter 4.1 because the concrete model is not necessary for the slip controller design although it influences the slip controller performance.

3.1 Estimators

When the system contains some state variables that cannot be measured, or the variables measurement is difficult, an estimator can be used for the variables value estimation. The estimators use the system model, and according to input values that are the same as the system input values, the estimator calculates the system states. The estimated states do not correspond to the actual states of the system because the actual system is disturbed. Therefore, at least one estimated state should be compared with a measurement, and according to the difference is modified the current or next state estimation to get a better match with the system. Many types of the state estimators are described in the literature. The [103] sorts the estimators into an early estimator, modern estimators and disturbance estimators. Early estimators are estimators like Luenberger Observer (LO) or nonlinear observer or simple observers without input or output. The common feature of the early estimators is that they do not consider disturbances. Therefore, modern estimators are presented. The Kalman Filter (KF), Extended Kalman Filter (EKF), Unscented Kalman Filter (UKF) is included in the modern estimators. The disturbance estimators also take disturbances into account, and the disturbance observer (DO), unknown input observer, or extended state observer is included in the group. The list of estimators above is not exhaustive, but it contains the possible state estimators that are often mentioned in the literature and can be used in real-time slip control in a DSP. The principles of the estimators are different, and their fields of application are also different. Some estimators can be unsuitable for use in some applications. The estimators are widely used in many applications. The comparison of the mentioned estimators is made in [104], [105], [106] and [107]. This subchapter focuses on the appropriate estimators, their basic description and their possible usage in the proposed slip controller. The comparison of selected state estimators is mentioned in Table 3.1.

Table 3.1 Comparison of the estimators

Estimator name	Basic model	Computational cost
Luenberger observer	Linear	Low
Disturbance observer	Linear	Low
Kalman filter	Linear	Low
Extended Kalman filter	Locally linear	Low or Medium
Unscented Kalman filter	Nonlinear	Medium

The general equations for a linear continuous-time dynamic system model are:

$$\frac{d}{dt}\mathbf{x}(t) = \mathbf{A}\mathbf{x}(t) + \mathbf{B}\mathbf{u}(t) + \mathbf{w}(t) \tag{3.1}$$

$$\mathbf{y}(t) = \mathbf{C}\mathbf{x}(t) + \mathbf{D}\mathbf{u}(t) + \mathbf{v}(t) \tag{3.2}$$

where **A** is a system matrix in continuous time, **B** is a system input matrix, **C** is an output matrix, **D** a system feedforward matrix, **x** is a system state vector, **u** is an input vector, **y** is an output vector, **w** is random dynamic disturbance, and **v** is random sensor noise.

The general state estimator principle is shown in Figure 3.1. The real system and the state estimator have the same input. The system output is compared with the estimator output, and the difference is led to the state estimator as its input. The state estimator requires the system model that has different complexity. The model complexity depends on the estimation purpose.

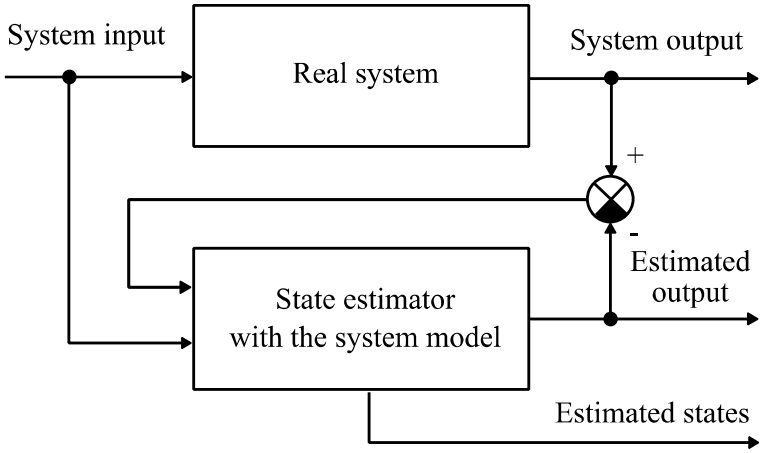

Figure 3.1 State estimator principle

The LO is widely used as the estimator. However, the LO is intended for deterministic systems and the LO does not take into account disturbances and sensor noise. On the other hand, the KF, EKF and UKF are intended for a stochastic system, and they take into account disturbances and sensor noise. The LO and KF are intended for linear systems, but when the nonlinear system is linearized at an operating point, the LO and KF can be used too [108]. The EKF and UKF are intended for nonlinear systems. For the nonlinear case (3.1) and (3.2) changes to form:

$$\frac{d}{dt}\mathbf{x}(t) = f\big(\mathbf{x}(t), \mathbf{u}(t)\big) + \mathbf{w}(t) \tag{3.3}$$

$$\mathbf{y}(t) = g\big(\mathbf{x}(t), \mathbf{u}(t)\big) + \mathbf{v}(t) \tag{3.4}$$

where *f* and *g* are nonlinear functions.

For better orientation in the subchapter, the dimensions and meaning of the most important variables that are used in the chapter are summarized in Table 3.2.

Table 3.2 Variables dimension

Variable	Dimension	Description
x	$n \times 1$	System state vector
y	$m \times 1$	Output vector
u	$r \times 1$	Input vector
A	$n \times n$	System matrix in continues time
Φ	$n \times n$	System matrix in discrete time
B	$n \times r$	System input matrix
C	$m \times n$	System output matrix
L	$n \times m$	Observer gain
Q	$n \times n$	Process noise covariance matrix
R	$m \times m$	Measurement uncertainty covariance matrix
K	$n \times m$	Kalman gain matrix
P	$n \times n$	Error covariance matrix, the UKF contains more **P** matrices with different sizes.
f, *g*	-	Nonlinear functions, used in EKF and UKF only
X	$n \times 2n+1$	Sigma points matrix, for scaled transformation, used in the UKF only
W	$2n+1 \times 1$	Weights of sigma points. For scaled transformation, used in the UKF only

The state system dimension is *n*, *r* is a number of inputs and *m* is a number of outputs. For SISO systems are *r* and *m* equal to 1. The estimated value is indicated by the symbol ^.

3.1.1 Disturbance Observer and Luenberger Observer

The DO and LO cannot be directly used in the proposed slip control method, but many slip control methods are based on their principles. The observers estimate an adhesion force that required derivate calculation to get the adhesion-slip characteristic slope. These observers are briefly described because the conventional slip controllers based on the observers are compared with the proposed slip controller in chapter 5. The DO algorithm is described in part 2.2.4.1. The LO uses the structure as mentioned in the previous subchapter and the LO with a real system is depicted in Figure 3.2. The system output $\mathbf{y}(t)$ is compared with the observer output $\hat{\mathbf{y}}_k$. The system output is a continuous analogue value and has to be discretised. The discretisation is typically made during measurement.

The equations of the LO in discrete time are:

$$\hat{\mathbf{x}}_k = \mathbf{\Phi} \cdot \hat{\mathbf{x}}_{k-1} + \mathbf{B} \cdot \mathbf{u}_{k-1} + \mathbf{L} \cdot (\mathbf{y}_{k-1} - \hat{\mathbf{y}}_{k-1}) \tag{3.1}$$

$$\hat{\mathbf{y}}_k = \mathbf{C} \cdot \hat{\mathbf{x}}_k \tag{3.2}$$

The observer gain **L** is set according to the system eigenvalues. The value of **L** can be determined from an error dynamic **e** that is defined as:

$$\mathbf{e}_k = \mathbf{x}_k - \hat{\mathbf{x}}_k = (\mathbf{\Phi} - \mathbf{L} \cdot \mathbf{C})\mathbf{e}_{k-1} \tag{3.3}$$

The value of **L** determines the observer dynamic. When **L** is selected so that eigenvalues of matrix (**A**-**LC**) have negative real parts, the $\hat{\mathbf{x}}$ will converge to **x**.

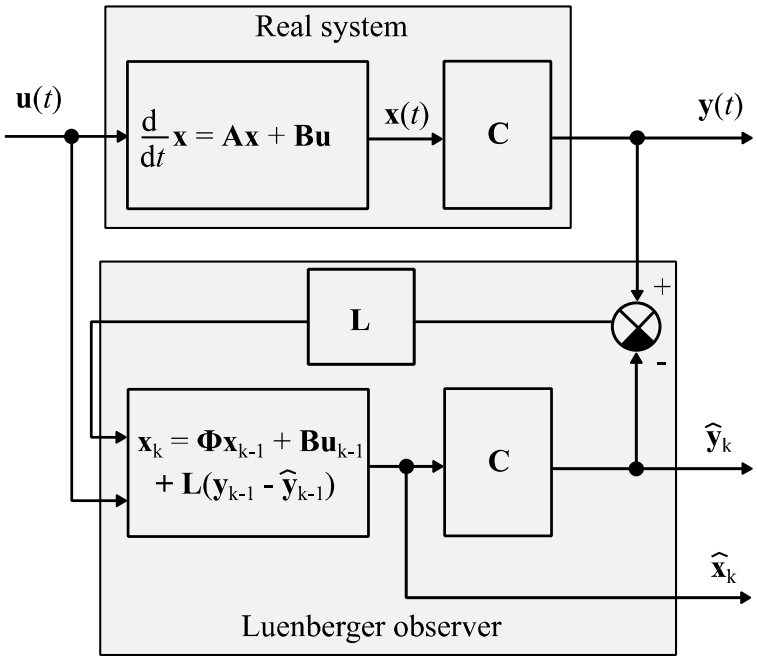

Figure 3.2 Luenberger observer principle

The LO is intended for linear systems. However, an Extended Luenberger Observer (ELO) can be used for nonlinear systems. The ELO uses a linearization, and it is not a true nonlinear observer, thus its applications are limited [108].

3.1.2 Kalman Filter, Extended Kalman Filter and Unscented Kalman Filter

The KF was described in papers in 1960 for the first time. The KF is an optimal estimation algorithm that combines measurement and a prediction to find the optional states estimation. Therefore, the KF is often used for optimal estimation of a system internal states that cannot be directly measured. The KF is typically used in navigation and guidance systems, especially in GPS, computer vision systems, and signal processing. The KF is used in applications when variables cannot be directly measured, or there are various sensors with noise, i.e. for data fusion [109]. The EKF is a nonlinear version of the KF. The EKF linearizes the model equations about the current estimate. The UKF was introduced in series of papers [110], [111] and [112]. The UKF is alternative to EKF with equivalent computational cost [113]. The UKF can be more accurate and can be easier to implement than the EKF [110].

3.1.2.1 Kalman Filter

The KF algorithm is defined for a linear system only. The KF performance depends on the system model. Therefore, the appropriate model is required. The KF goal is to make an estimation of system state vector $\mathbf{x}$ if it works as an estimator. The KF algorithm can be described as follows [114]:

1. Make a prediction of a state vector $\hat{\mathbf{x}}_k^-$ and an error covariance matrix $\mathbf{P}_k^-$.
2. Make a compensation of the difference between a measurement and a prediction for an estimation calculation. The estimation result is a system state vector $\hat{\mathbf{x}}_k$ and an error covariance matrix $\mathbf{P}_k$.
3. Continue to the step one.

The estimated value is marked as $\hat{\mathbf{x}}$. A superscript "-" means a prediction of the value. The equations (3.4) to (3.8) describe the KF algorithm.

$$\hat{\mathbf{x}}_{\mathrm{k}}^{-} = \boldsymbol{\Phi} \cdot \hat{\boldsymbol{x}}_{\mathrm{k-1}} \tag{3.4}$$

$$\mathbf{P}_{\mathrm{k}}^{-} = \boldsymbol{\Phi} \cdot \mathbf{P}_{\mathrm{k-1}} \cdot \boldsymbol{\Phi}^{T} + \mathbf{Q} \tag{3.5}$$

$$\mathbf{K}_{\mathrm{k}} = \frac{\mathbf{P}_{\mathrm{k}}^{-} \cdot \mathbf{C}^{T}}{\mathbf{C} \cdot \mathbf{P}_{\mathrm{k}}^{-} \cdot \mathbf{C}^{\mathrm{T}} + \mathbf{R}} \tag{3.6}$$

$$\hat{\mathbf{x}}_{\mathrm{k}} = \hat{\mathbf{x}}_{\mathrm{k}}^{-} + \mathbf{K}_{\mathrm{k}} \cdot (\mathbf{y}_{\mathrm{k}} - \mathbf{C} \cdot \hat{\mathbf{x}}_{\mathrm{k}}^{-}) \tag{3.7}$$

$$\mathbf{P}_{\mathrm{k}} = \mathbf{P}_{\mathrm{k}}^{-} - \mathbf{K}_{\mathrm{k}} \cdot \mathbf{C} \cdot \mathbf{P}_{\mathrm{k}}^{-} \tag{3.8}$$

The algorithm can be divided into a prediction and estimation part. Equations (3.4) and (3.5) represent the prediction part of the algorithm. This part depends on the state matrix **Φ**, and the system noise covariance matrix **Q**. Equations (3.6), (3.7) and (3.8) represent the estimation part of the algorithm. The system output matrix **C** and measurement noise covariance matrix **R** influence the estimation. The Kalman gain **K**, which adjusts the filter weighting, is calculated by (3.6). The difference between the KF estimation and the actual value is represented by an error covariance matrix $\mathbf{P}_{\mathrm{k}}$. The actual value is unknown. If $\mathbf{P}_{\mathrm{k}}$ has a large value, the error of the estimate is also large, and if $\mathbf{P}_{\mathrm{k}}$ value is small, the error of estimate is small too. The prediction is sometimes called as a priory estimate, and estimation is called as a posteriori estimate.

The sequence of the two steps is depicted in Figure 3.3. At time k-1 the state value is around $\hat{\mathbf{x}}_{\mathrm{k-1}}$. The uncertainty is represented by a probability density function. The predicted value in the next step $\hat{\mathbf{x}}_{\mathrm{k}}^{-}$ has higher uncertainty that is represented by a higher variance of the probability function. The measurement is represented by its own probability function. The final optimal state estimate is given by multiplication of predicted state estimation and measurement. The optimal state estimation is given by the two probability functions. The optimal state estimation has a smaller variance than predicted state estimation.

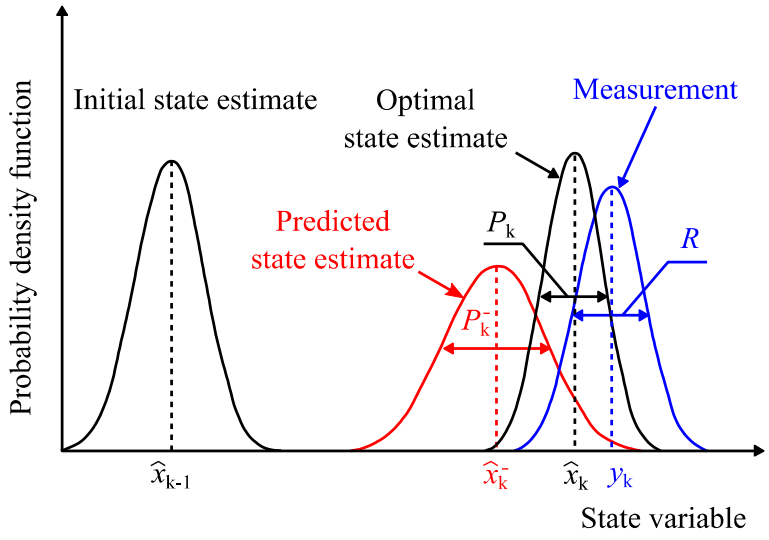

Figure 3.3 Demonstration of the KF probability density functions

The KF is intended for linear systems only. If it is used for a nonlinear system, the algorithm may not converge. However, the KF algorithm can be used for nonlinear systems if a system model is linearized. Then a Linearized Kalman Filter (LKF) is created. However, the LKF can reliably work only near the point of linearization [114].

3.1.2.2 Extended Kalman Filter

The EKF algorithm is similar to KF. The algorithm is described by equations (3.9) to (3.13).

$$\hat{\mathbf{x}}_{\mathrm{k}}^{-} = f(\hat{\mathbf{x}}_{\mathrm{k}-1}) \tag{3.9}$$

$$\mathbf{P}_{\mathrm{k}}^{-} = \boldsymbol{\Phi} \cdot \mathbf{P}_{\mathrm{k}-1} \cdot \boldsymbol{\Phi}^{\mathrm{T}} + \mathbf{Q} \tag{3.10}$$

$$\mathbf{K}_{\mathrm{k}} = \frac{\mathbf{P}_{\mathrm{k}}^{-} \cdot \mathbf{C}^{\mathrm{T}}}{\mathbf{C} \cdot \mathbf{P}_{\mathrm{k}}^{-} \cdot \mathbf{C}^{\mathrm{T}} + \mathbf{R}} \tag{3.11}$$

$$\hat{\mathbf{x}}_{\mathrm{k}} = \hat{\mathbf{x}}_{\mathrm{k}}^{-} + \mathbf{K}_{\mathrm{k}} \cdot \left(\mathbf{y}_{\mathrm{k}} - g(\hat{\mathbf{x}}_{\mathrm{k}}^{-})\right) \tag{3.12}$$

$$\mathbf{P}_{\mathrm{k}} = \mathbf{P}_{\mathrm{k}}^{-} - \mathbf{K}_{\mathrm{k}} \cdot \mathbf{C} \cdot \mathbf{P}_{\mathrm{k}}^{-} \tag{3.13}$$

The EKF considers a nonlinear system model. The nonlinearity can occur in the system model or measurement model. These nonlinearities are represented by functions $f(\hat{\mathbf{x}}_{\mathrm{k}-1})$ and $g(\hat{\mathbf{x}}_{\mathrm{k}}^{-})$, and the model is represented by these functions. The functions are used in (3.9) and (3.12) instead of a system matrix $\boldsymbol{\Phi}$, and a measurement matrix $\mathbf{C}$. Since the matrices are required in (3.10), (3.11) and (3.13) the Jacobians have to be calculated to get the matrixes:

$$\boldsymbol{\Phi} \equiv \left.\frac{\partial f}{\partial \mathbf{x}}\right|_{\hat{\mathbf{x}}_{\mathrm{k}}} \tag{3.14}$$

$$\mathbf{C} \equiv \left.\frac{\partial g}{\partial \mathbf{x}}\right|_{\hat{\mathbf{x}}_{\mathrm{k}}} \tag{3.15}$$

The Jacobians may be difficult to calculate. If the Jacobians cannot be determined analytically, the numerical calculations take the high computational cost. The EKF can be used with systems that have a differentiable model only. Therefore, the EKF cannot be used for systems with a discontinuous model. The EKF can work with systems that can be approximated by a linear function. Thus, the EKF is not suitable for highly nonlinear systems. If the system model is linear, the EKF is identical to the KF. However, the EKF is not an optimal estimator because it provides only an approximation to optimal nonlinear estimation [113] and the EKF output can diverge due to the linearization [115].

3.1.2.3 Unscented Kalman Filter

The UKF algorithm is described by (3.16) – (3.27), and the algorithm is different from previous filters. The difference is in the UKF principle that models a probability distribution of nonlinear function instead of the function modelling. The UKF does not find an approximation of the nonlinear function as the EKF. However, it calculates the mean and covariance of the function.

$$\mathbf{U}^{\mathrm{T}} \cdot \mathbf{U} = (n + \kappa) \cdot \mathbf{P}_{\mathrm{k}} \tag{3.16}$$

$$\begin{gathered} \boldsymbol{\chi}_0 = \hat{\mathbf{x}}_{\mathrm{k}} \\ \boldsymbol{\chi}_{\mathrm{i}} = \hat{\mathbf{x}}_{\mathrm{k}} + \mathbf{U}_i \cdot \sqrt{n + \lambda}, \;\; i = 1, 2, \dots, n \\ \boldsymbol{\chi}_{\mathrm{i+n}} = \hat{\mathbf{x}}_{\mathrm{k}} - \mathbf{U}_i \cdot \sqrt{n + \lambda}, \;\; i = 1, 2, \dots, n \end{gathered} \tag{3.17}$$

$$\begin{gathered} \mathbf{W}_0 = \frac{\lambda}{n + \lambda} \\ \mathbf{W}_0^{(\hat{\mathrm{z}})} = \frac{\lambda}{n + \lambda} \\ \mathbf{W}_0^{(\mathrm{P_{zz}})} = \frac{\lambda}{n + \lambda} + 1 + \alpha^2 + \beta \\ \mathbf{W}_{\mathrm{i}} = \frac{1}{2(n + \kappa)}, \;\; i = 1, 2, \dots, n \\ \mathbf{W}_{\mathrm{i+n}} = \frac{1}{2(n + \kappa)}, \;\; i = 1, 2, \dots, n \end{gathered} \tag{3.18}$$

$$\hat{\mathbf{x}}_{\mathrm{k}}^{-} = \sum_{i=0}^{2n} \mathbf{W}_{\mathrm{i}} \cdot \eta_{\mathrm{i}} \tag{3.19}$$

$$\mathbf{P}_{\mathrm{xx}} = \sum_{i=0}^{2n} \mathbf{W}_{\mathrm{i}} \cdot (\boldsymbol{\eta}_{\mathrm{i}} - \hat{\mathbf{x}}) \cdot (\boldsymbol{\eta}_{\mathrm{i}} - \hat{\mathbf{x}})^{\mathrm{T}} \tag{3.20}$$

$$\hat{\mathbf{y}}_{\mathrm{k}} = \mathbf{W}_0^{(\hat{\mathrm{z}})} \cdot \boldsymbol{\xi}_0 + \sum_{i=1}^{2n} \mathbf{W}_{\mathrm{i}} \cdot \boldsymbol{\xi}_{\mathrm{i}} \tag{3.21}$$

$$\begin{aligned} \mathrm{P_{yy}} = \mathbf{W}_0^{(\mathrm{P_{zz}})} \cdot (\boldsymbol{\xi}_0 - \hat{\mathbf{y}}) \cdot (\boldsymbol{\xi}_0 - \hat{\mathbf{y}})^{\mathrm{T}} \\ + \sum_{i=1}^{2n} \mathbf{W}_{\mathrm{i}} \cdot (\boldsymbol{\xi}_{\mathrm{i}} - \hat{\mathbf{y}}) \cdot (\boldsymbol{\xi}_{\mathrm{i}} - \hat{\mathbf{y}})^{\mathrm{T}} \end{aligned} \tag{3.22}$$

$$\mathbf{P}_{\mathrm{xy}} = \sum_{i=0}^{2n} \mathbf{W}_{\mathrm{i}} \cdot (\boldsymbol{\eta}_{\mathrm{i}} - \hat{\mathbf{x}}_{\mathrm{k}}^{-}) \cdot (\boldsymbol{\xi}_{\mathrm{i}} - \hat{\mathbf{y}}_{\mathrm{k}})^{\mathrm{T}} \tag{3.23}$$

$$\mathbf{K}_{\mathrm{k}} = \frac{\mathbf{P}_{\mathrm{xy}}}{\mathbf{P}_{\mathrm{yy}} - \mathbf{R}} \tag{3.24}$$

$$\hat{\mathbf{x}}_{\mathrm{k}} = \hat{\mathbf{x}}_{\mathrm{k}}^{-} + \mathbf{K}_k \cdot (\mathbf{y}_{\mathrm{k}} - \hat{\mathbf{y}}_{\mathrm{k}}) \tag{3.25}$$

$$\mathbf{P}_{\mathrm{k}}^{-} = \mathbf{P}_{\mathrm{xx}} + \mathbf{Q} \tag{3.26}$$

$$\mathbf{P}_{\mathrm{k}} = \mathbf{P}_{\mathrm{k}}^{-} + \mathbf{K}_{\mathrm{k}} \cdot \mathbf{P}_{\mathrm{yz}}^{\mathrm{T}} \tag{3.27}$$

where $\boldsymbol{\chi}$ is a sigma point matrix, $\mathbf{P}_{\mathrm{k}}$ is an error covariance matrix, λ, α, β and κ are scaling parameters, $\mathbf{W}_{\mathrm{i}}$ are weights of $\boldsymbol{\chi}_{\mathrm{i}}$, $\hat{\mathbf{y}}$ is an output estimation $\mathbf{P}_{\mathrm{yy}}$ is prediction output error covariance matrix, $\mathbf{P}_{\mathrm{xy}}$ is an output error covariance matrix, $\mathbf{P}_{\mathrm{xx}}$ is prediction error covariance

matrix, $\mathbf{K}_k$ is the Kalman gain, $\mathbf{y}_k$ is a measured system output, ξ is transformed sigma points through nonlinear function g and η is transformed sigma points through nonlinear function f.

The scaling parameter λ that is defined as:

$$\lambda = \alpha^2 \cdot \kappa + n(1 + \alpha^2) \tag{3.28}$$

Where a range of sigma points around $\hat{\mathbf{x}}$ is described by a scaling parameter α that contains information on the distribution of $\mathbf{x}$, its value is 2 [115], and κ is a scaling parameter, and it is usually set to zero, or its value can be negative [116].

The UKF algorithm can be divided into the tasks:

1. Select sigma points and its weights (3.16), (3.17) and (3.18).
2. Predict state and error covariance (3.19) and (3.20).
3. Predict measurement and covariance (3.21) and (3.22).
4. Kalman gain computation (3.23) and (3.24).
5. Compute the state estimation (3.25).
6. Compute the covariance error (3.26) and (3.27).

The UKF algorithm requires calculation of the Cholesky factorization of the matrix $\mathbf{P}_k$. Therefore, the matrix has to be positive-definite, but the matrix changes during the UKF execution and the matrix can become not positive-definite. In this case, the UKF algorithm fails. The improvement is presented in [117]. The improvement is based on a divergence criterion and an adaptive correcting factor. The divergence criterion is:

$$\mathbf{Y}_{\mathrm{err}}^{\mathrm{T}} \cdot \mathbf{Y}_{\mathrm{err}} \leq S \cdot \mathrm{tr}\left(E\left(\mathbf{Y}_{\mathrm{err}} \cdot \mathbf{Y}_{\mathrm{err}}^{\mathrm{T}}\right)\right) \tag{3.29}$$

$$\mathbf{Y}_{\mathrm{err}} = \mathbf{y} - \hat{\mathbf{y}} \tag{3.30}$$

Where S is a threshold coefficient and tr means a trace.

If (3.29) is met, the correcting factor ρ_k that limits the value of $\mathbf{P}_{XX}$ in (3.20) is calculated:

$$\rho_k = \begin{cases} \rho_0, & \rho_0 \geq 1 \\ 1, & \rho_0 < 1 \end{cases} \tag{3.31}$$

$$\rho_0 = \frac{\mathrm{tr}(\mathbf{C}_0 - \mathbf{R})^T}{\mathrm{tr}\left(\sum_{i=1}^{2n} \mathbf{W}_i \cdot (\boldsymbol{\xi}_i - \hat{\mathbf{y}}) \cdot (\boldsymbol{\xi}_i - \hat{\mathbf{y}})^{\mathrm{T}}\right)} \tag{3.32}$$

$$\mathbf{C}_0 = \begin{cases} \mathbf{Y}_{\mathrm{err}} \cdot \mathbf{Y}_{\mathrm{err}}^{\mathrm{T}}, & k = 1 \\ \dfrac{\gamma \cdot \mathbf{C}_0 + \mathbf{Y}_{\mathrm{err}} \cdot \mathbf{Y}_{\mathrm{err}}^{\mathrm{T}}}{1 + \gamma}, & k > 1 \end{cases} \tag{3.33}$$

Where γ is a coefficient.

3.1.2.4 Covariance Matrices

All types of Kalman filters described above uses a covariance matrix of a measurement uncertainty $\mathbf{R}_t$ and process noise covariance matrix $\mathbf{Q}_t$. The covariance matrices **Q** and **R,** used in the Kalman filters equation, are transformed to discrete time, while matrices $\mathbf{Q}_t$ and $\mathbf{R}_t$ are expressed in continues time. The matrices are connected with a random dynamic disturbances **w**

(3.34) and random sensor noise **v** (3.35). The matrices influence the filter performance. Therefore, their setting is essential for the filter work.

$$\mathbf{w} \sim N(0, \mathbf{Q}_t) \tag{3.34}$$

$$\mathbf{v} \sim N(0, \mathbf{R}_t) \tag{3.35}$$

Both matrices are diagonal. For the system with n states and m inputs, the matrix $\mathbf{Q}_t$ size is $(n \times n)$, and it is the same as the system matrices **A** or **Φ**. The **R** matrix size is $(m \times m)$, and its value depends on the output matrix **C** size.

$$\mathbf{Q}_t = \begin{bmatrix} \sigma_{q1} & & & \\ & \sigma_{q2} & & \\ & & \ddots & \\ & & & \sigma_{qn} \end{bmatrix} \tag{3.36}$$

$$\mathbf{R}_t = \begin{bmatrix} \sigma_{r1} & & & \\ & \sigma_{r2} & & \\ & & \ddots & \\ & & & \sigma_{rm} \end{bmatrix} \tag{3.37}$$

Every element σ_{qx} of $\mathbf{Q}_t$ matrix influences different filter feature. The σ_{rx} elements of matrix $\mathbf{R}_t$ influence the corresponding measurement input and set its filtration level. The $\mathbf{Q}_t$ matrix is connected to the $\mathbf{R}_t$ matrix. The dependence is shown in (3.5) and (3.6) in the KF. The values of the matrices influence the Kalman gain. The $\mathbf{Q}_t$ matrix influences a numerator in (3.6) through (3.5). The $\mathbf{R}_t$ matrix influences a denominator in (3.6) directly. Therefore, if both matrices increase or decrease their influence to the (3.6) can be partially disrupted. The same dependence can also be found in EKF and UKF.

The measurement uncertainty covariance matrix $\mathbf{R}_t$ can be determined from measured values [30] and [118]. The process noise covariance matrix $\mathbf{Q}_t$ setting is more difficult than matrix $\mathbf{R}_t$. The analytical solution is complicated. Therefore, some authors determine the matrix experimentally [119] or based on simulations [30]. The matrixes settings are described in [30] and [120] in more detail.

3.1.3 Matrices Discretisation

System models are typically designed as differential equations in continuous time, and after their verification, the systems are converted to discrete time. This way is more natural and it is considered as more reliable [116]. The continuous model can be simulated, e.g. in Matlab software by using a function for solving differential equations. On the other hand, a discrete time form is needed to be possible implement it to a DSP.

In previous chapters are described the algorithms of the filters that are in discrete time. Therefore, the system matrix **Φ**, process noise covariance matrix **Q**, and measurement uncertainty covariance matrix **R** must be transformed from continues time form to discrete time form. The transformation could be made as follows:

$$\mathbf{\Phi}_{k-1} = \exp\left(\int_{t_{k-1}}^{t_k} \mathbf{A}(s) \cdot ds \right) \tag{3.38}$$

$$\mathbf{Q}_{k-1} = \mathbf{A}(t_k, t_{k-1}) \cdot \left(\int_{t_{k-1}}^{t_k} \mathbf{A}^{-1}(s, t_{k-1}) \cdot \mathbf{Q}_t(s) \cdot \mathbf{A}^{-T}(s, t_{k-1}) \cdot ds \right) \cdot \mathbf{A}^T(t_k, t_{k-1}) \tag{3.39}$$

$$\mathbf{R}_k = \frac{1}{t_k - t_{k-1}} \int_{t_{k-1}}^{t_k} \mathbf{R}_t(t) \cdot dt \tag{3.40}$$

The discretisation can be calculated by the method described in [116] and [121]. The matrixes $\mathbf{\Phi}$ and $\mathbf{Q}_k$ can be calculated as follows:

$$\mathbf{M} = \Delta t \cdot \begin{bmatrix} -\mathbf{A} & \mathbf{B} \cdot \mathbf{Q} \cdot \mathbf{B}^T \\ 0 & \mathbf{A}^T \end{bmatrix} \tag{3.41}$$

$$e^{\mathbf{M}} = \begin{bmatrix} \mathbf{\Psi} & \mathbf{\Phi}_k \cdot \mathbf{Q}_k \\ 0 & \mathbf{\Phi}^T \end{bmatrix} \tag{3.42}$$

3.1.4 System Observability and Controllability

The described estimators require the system model that is represented by the system matrix. The matrix can have any complexity. The more complex models describe the system more precisely, but the model can contain some parts that are unobservable or uncontrollable. The complex models can be used, e.g. in Matlab software for the system behaviour study. When a real-time calculation is required, the model should be as simple as possible due to the calculation requirements. The system model for the estimators has to be observable for their proper work. The system model decomposition is depicted in Figure 3.4. The system can contain observable, controllable, unobservable or uncontrollable subsystems and its combinations. The model for observer should contain the observable and controllable subsystem only.

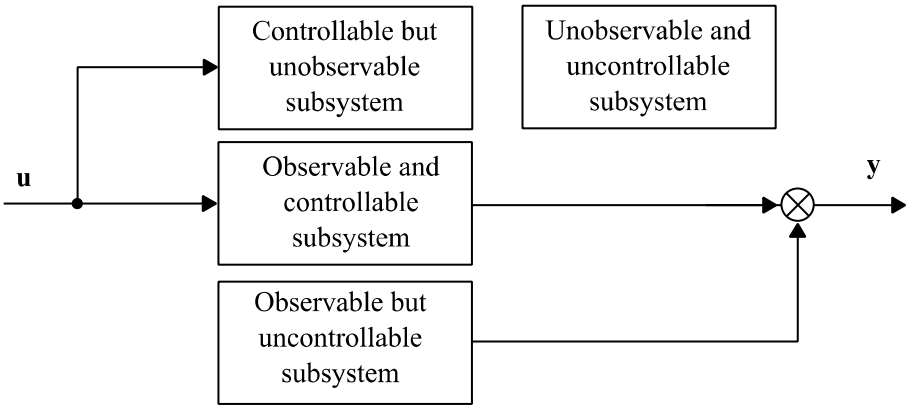

Figure 3.4 System decomposition

The system observability can be evaluated according to observability matrix **O** rank. The system is observable when an observability matrix rank is equal to system matrix size. Observability matrix is:

$$\mathbf{O} = \begin{bmatrix} \mathbf{C} \\ \mathbf{CA} \\ \mathbf{CA}^2 \\ \vdots \\ \mathbf{CA}^{n-1} \end{bmatrix} \tag{3.43}$$

3.1.5 Estimators Comparison Summary

The proposed slip controller contains the description of the adhesion that is nonlinear. Therefore, the nonlinear estimator should be used for the solving. However, if the linearization is made, the linear estimator can also be used. Therefore, the estimators that can be used for the task solution are described in the chapter. The LO, KF, EKF and UKF are described in the chapter. The covariance matrices settings are discussed, and matrices discretisation is also described in the chapter too. The estimators require a system model that has to be observable. Therefore, system observability is also described in this part.

The LO is the only one estimator that is intended for a deterministic system. Therefore, the LO does not take into account disturbances, but the LO has the most straightforward algorithm. The LO is described in the chapter because of its simple algorithm and low computational cost.

The KF is described in detail because the EKF is based on the algorithm. The KF can be used only for linear systems, but an LKF can be used when the system model is nonlinear. This filter is described for its simple implementation and low computation requirements although the KF or LKF cannot perform the best results in the proposed slip control method.

The EKF is often used in nonlinear applications. The EKF does not calculate with a nonlinear function, but it uses its linearization. The EKF implementation can be simple, and the computational requirements are low if the nonlinearity can be described analytically. However, when the nonlinearity cannot be described analytically, a Jacobian has to be calculated. The computational cost increases when the Jacobian cannot be analytically described and the calculation is nontrivial and often lead to implementation difficulties [110]. The EKF disadvantage is that the filter can diverge in some cases. The filter can have unstable performance when the time step intervals are not small [110]. However, the small time step increases computational requirements.

The UKF is intended for nonlinear systems and has the most complicated algorithm, and its computational requirements are the highest from the described estimators. However, the UKF is more accurate than the EKF. The UKF does not have a problem with a divergence that can occur in EKF when the initial conditions are far away from the actual value. However, the calculation can fail when the error covariance matrix is not positive-definite. Therefore, the algorithm improvement is presented.

The comparison of an LO, DO, KF, EKF and UKF are made in Table 3.1. It is clear that the UKF can calculate with a nonlinear model at the cost of higher computational cost. The slip controller with the KF is presented in [30]. The presented slip controller works with a system linearized model. The optimal slip controller requires the nonlinear estimator. The EKF can diverge when the initial EKF conditions are far from the system conditions. This situation can occur, e.g. if the locomotive transfers from coasting to traction. Therefore, the UKF was chosen as the most appropriate estimator.

3.2 Proposed Slip Controller

The proposed slip controller and the development stages are presented by the author in [30], [32], [120], [122], [123] and [124]. The proposed slip controller is based on the slip controller described in [30], and the final version of the proposed slip controller is presented in [124]. The slip controller from [30] uses a KF as the state estimator, and the slip controller in [124] uses the UKF as the estimator. The slip controller based on the EKF was also designed and it is described in [32]. The difference of the estimators leads to the system nonlinearity approach. The UKF does not require the linearization, and the nonlinear function is included in the algorithm. Therefore, the slip controller with the UKF provides the same performance in all possible states that are not guaranteed in the KF and EKF. The proposed slip controller with a KF, EKF and UKF as the estimator was compared in [122] and [123]. From the papers, it is obvious that the UKF provides better results than other estimators. The UKF is considered in the proposed slip controller description, but the UKF can be directly replaced by the EKF and after linearization by the KF.

3.2.1 Background of the Proposed Slip Controller

Slip controllers described in chapter 2 are based on different principles. Many of them are based on the adhesion-slip characteristic slope determination. The methods require the state estimations that estimate an adhesion coefficient or an adhesion force. Then, a derivative of the estimated adhesion coefficient or the adhesion force is derived according to a slip velocity or time to get the adhesion-slip characteristic slope. The derivatives are defined as:

$$\frac{\mathrm{d}\mu}{\mathrm{d}v_\mathrm{s}} = 0 \tag{3.44}$$

For calculation of (3.44), an actual value of an adhesion coefficient has to be known. The actual value of the adhesion coefficient is estimated because a direct measurement of the adhesion coefficient during the train runs is not possible. Observers or a variant of Kalman filters is used for this purpose. The method principle is based on the derivative sign changes during the operating point movement on the adhesion-slip characteristic. The derivative is positive in the stable area, and negative in the unstable area of the adhesion-slip characteristic. At the top of the characteristic, the derivative is equal to zero. The actual value of the adhesion coefficient can be replaced by an actual value of the adhesion force in (3.44). Therefore, it is difficult to get the derivative according to (3.44) equal to zero [22]

Equation (3.44) can be simplified and rewritten as follows:

$$\frac{\mathrm{d}\mu}{\mathrm{d}t} \cdot \frac{\mathrm{d}t}{\mathrm{d}v_s} \approx \frac{\mathrm{d}\mu}{\mathrm{d}t} \tag{3.45}$$

The simplification can be done because the slip velocity has a small value and the slip velocity change during acceleration is also small. The (3.45) removes a problem with the train velocity, which is difficult to determine when all wheels are driven because the measured wheel velocity is higher than the train velocity about the slip velocity. The second problem is with division by zero that can occur when the slip velocity has a constant value.

The slip controllers based on the adhesion-slip characteristic slope determination based on disturbance observers, described in chapter 2.2.4.1, have a known weaknesses. The main weakness is the possible fail when the static adhesion-slip characteristic has a plateau instead of the peak [81]. The second problem is with the actual adhesion-slip characteristic changes. The

slip controllers work as expected if the slip controller is tested on a mathematical model with a static adhesion-slip characteristic that is depicted, e.g. in Figure 2.2. When a measured velocity is used as the slip controller input, the slip controller can fail due to the actual adhesion-slip characteristic shape. The adhesion-slip characteristic shape changes during the train runs, e.g. due to the train speed and wheel surface contamination. Measured adhesion-slip characteristics are published, e.g. in [40] and [125], and an example of measured data from [40] are shown in Figure 3.5. The operating point oscillates around its stable position due to the characteristic changes. Therefore, the slope of the adhesion-slip characteristic changes too. In this case, the derivative can be positive, negative or zero, although the position is set to the stable area during the train run.

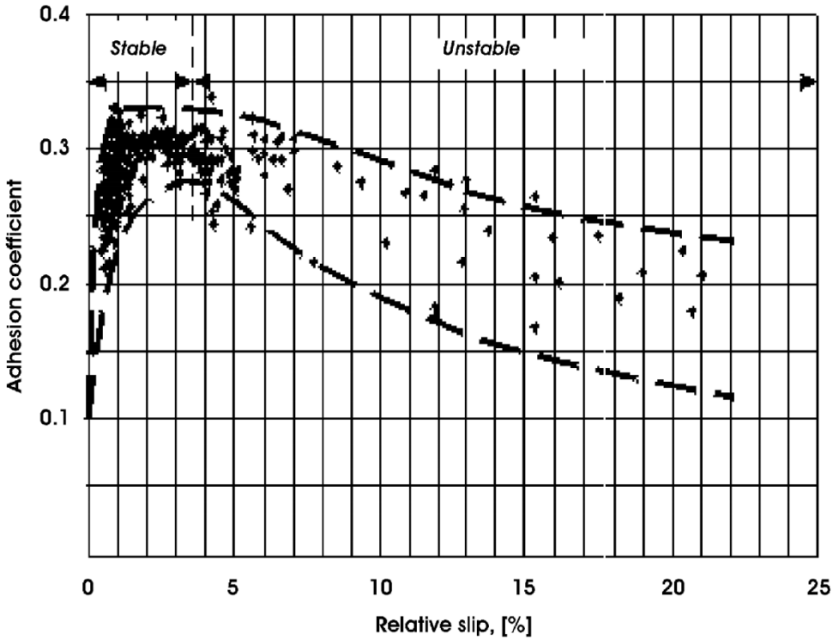

Figure 3.5 Example of measured adhesion-slip characteristic [40]

The slip controller function according to (3.44) and (3.45) is demonstrated in Figure 3.6. The slip controller input data are measured data that were measured on a locomotive that hauls a freight train. A measured wheel velocity, train velocity, one wheelset force and calculated adhesion force, and derivatives of the estimated force according to (3.44) and (3.45) are shown in Figure 3.6. The adhesion force was calculated by a first order disturbance observer according to [22]. The input data are for the case when the train accelerates, and slippage occurs at the end of the record. The applied tractive force has a constant value. The calculated derivative according to (3.44) is mainly positive in the part where the slippage does not occur of the record, but the calculated derivative oscillates around zero. The adhesion force derivative according to (3.45) is smoother, but it also oscillates around zero. The oscillations are caused by the adhesion-slip characteristic changes and wheel velocity measurement noise. The noise of the wheel velocity signal can be eliminated by a filter that causes an additional time delayed and a slip controller delay response.

Based on the previous conclusions a slip controller based on a UKF was designed. The proposed slip controller eliminates the described weakness of the classical slip controllers. The proposed slip controller does not directly estimate the actual value of the adhesion coefficient or the adhesion force. The slip controller estimates a relative adhesion force. The estimated relative adhesion force corresponds to the adhesion force in the time course, but not in absolute value.

The estimated relative adhesion force is shifted to zero in normal conditions, and become negative when the adhesion force starts decreasing. Therefore, the estimated force can be used directly to the control part of the slip controller.

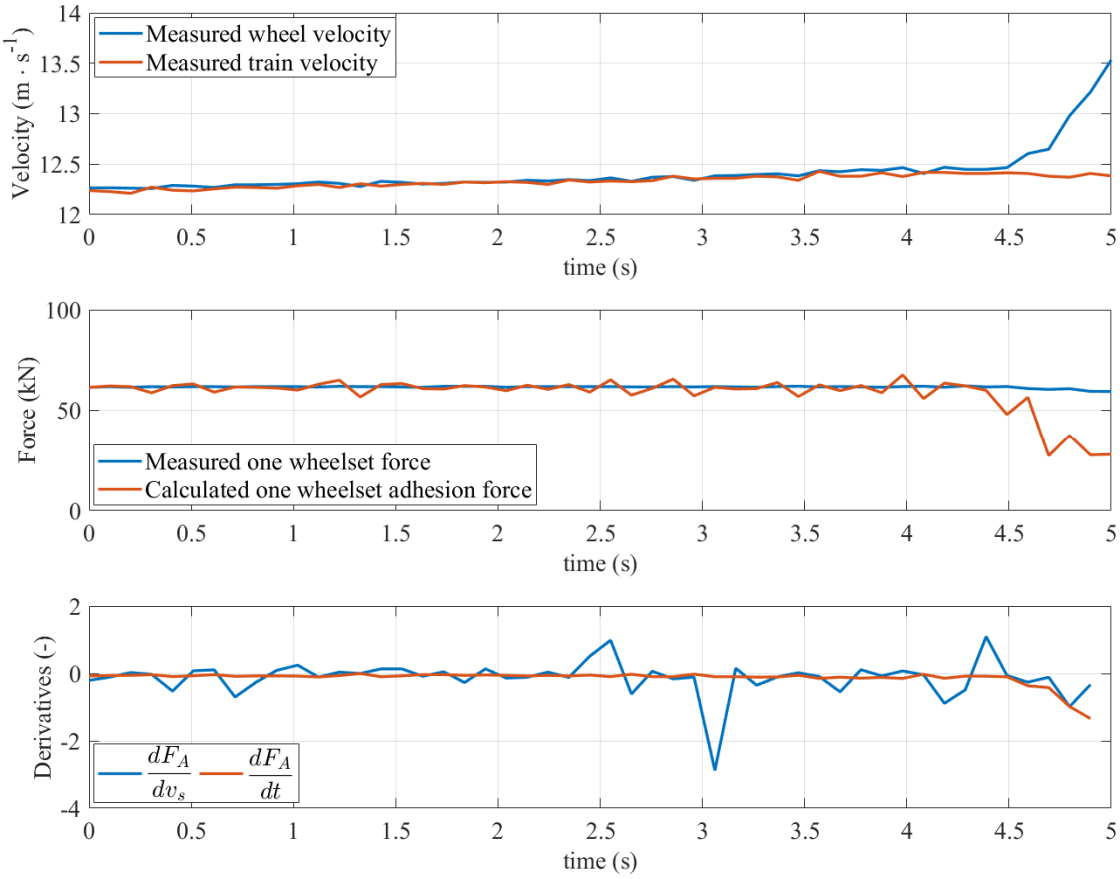

Figure 3.6 Demonstration of the work of the classical slip controller

3.2.2 Proposed Slip Controller Principle

The slip controller block diagram for one wheelset is shown in Figure 3.7. The block diagram contains a *Wheelset mechanical and electrical system* block and a *Locomotive computer* block. The *Wheelset mechanical and electricals system* block contains a *Converter*, *Motor*, *Gearbox and wheelset* and *Speed measurements* blocks. These blocks depend on locomotive configurations. The configuration depicted in the figure measures wheelset velocity, but the configuration that measures motor velocity is also possible. The measurement measures pulses from an incremental encoder and the wheelset velocity are calculated in the locomotive computer and then the signal is used by slip controller and electric drive controller. However, for greater clarity, the signal is marked as measured velocity. The locomotive computer block contains the *Electric drive controller* and *Slip controller* blocks. The slip controller is created by the *UKF algorithm with nonlinear function* and *Controller part of the slip controller* blocks. The *UKF algorithm with nonlinear function* block creates the slope detection part of the slip controller. The block diagram input is a required tractive force F_{T}^{*}. The required tractive force is multiplied by the slip controller output, and calculated tractive force F_{T} is led to the *Electric drive controller block*. The block generates control signals for the *Wheelset mechanical and electrical system* block. The output of the *Wheelset mechanical and electrical system* block is a wheel velocity v_{C}. The wheel velocity is led to a *UKF algorithm with nonlinear function* block. The *UKF* block output is an estimated relative adhesion force $i_{\mathrm{FAdhesion}}$ that is compared

with required relative adhesion force $i^*_{\mathrm{FAdhesion}}$. The calculated error e is led to a controller that limits required tractive force.

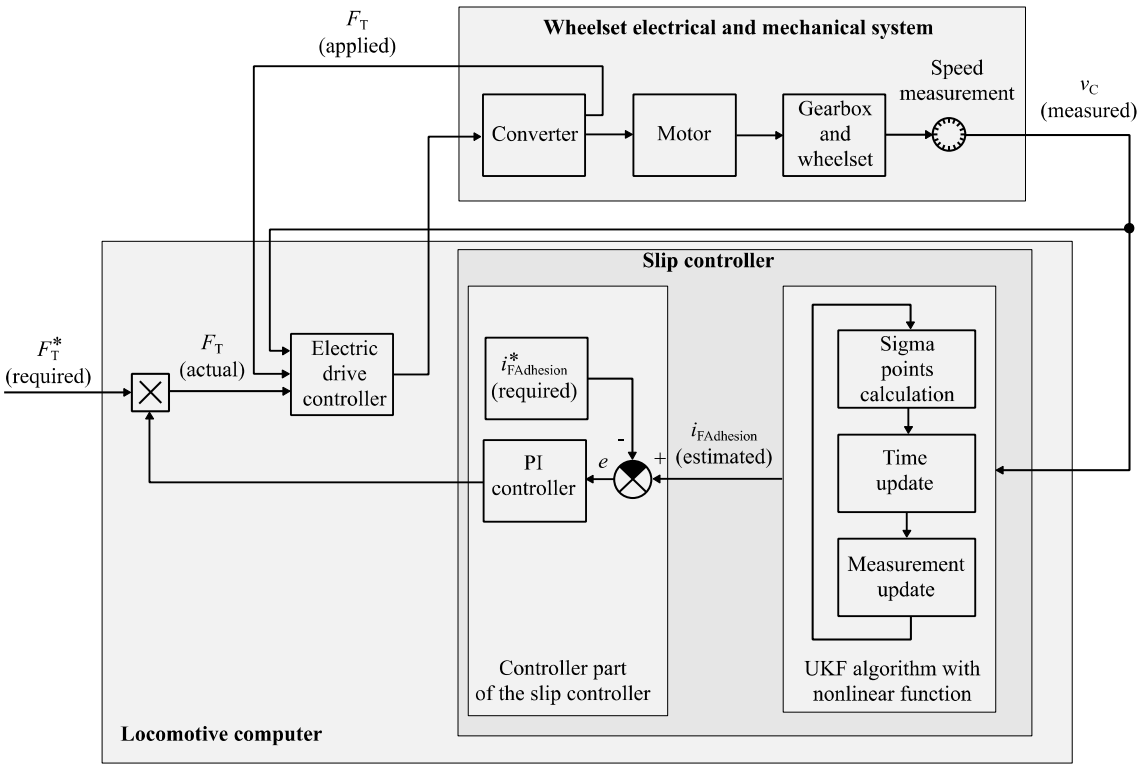

Figure 3.7 Proposed slip controller block diagram and its relation to the other locomotive components

The block *Wheelset mechanical and electrical system* represents one wheelset mechanical parts and a wheelset electric drive. This block is not part of the slip controller. Figure 3.7 depicts all blocks to explain the slip controller position against the electric and mechanical parts.

The block *Electric drive controller* control the block *Wheelset mechanical and electrical system* and the block are located in the *Locomotive computer* block.

The block *UKF algorithm with nonlinear function* contains the UKF, which algorithm is described in chapter 3.1.1 in detail. The UKF needs a nonlinearity description. The nonlinearity is based on an idealised adhesion-slip characteristic description. The nonlinearity is described below in detail.

The *Controller part of the slip controller* block can be, basically, any controller type and it is the second part of the *Slip controller block*. The controller output is limited from 0 to 1. Therefore, the controller can only decrease the required tractive force. In the results, it is the slip controller functionality demonstrated by using a PI controller.

3.2.2.1 Output of the Slip Controller Detection Part

The UKF output is not an estimation of an adhesion coefficient or an adhesion force as it is common in classical slip controllers. The output is an estimation of a relative adhesion force. As was stated above, the relative adhesion force has the same time course as the actual adhesion force, but the value is different. The relative adhesion force is shifted to zero when the operating point is in the stable area of an adhesion-slip characteristic. The tractive force is considered as

noise from the point of view of the estimation of the states. Therefore, when the operating point is in the stable area of the adhesion-slip characteristic, the relative adhesion force has zero value, and when the operating point is in the unstable area the value is negative. When an operating point is at the maximum point of the adhesion-slip characteristic the relative adhesion force has a small negative value.

The relative adhesion force waveform is shown in Figure 3.8. There are shown a wheel velocity, train velocity, relative adhesion force and required relative adhesion force in the figure. When the operating point is in the stable area of the adhesion-slip characteristic, the relative adhesion force has zero value. The value is noisy because the wheel velocity is noisy too. The noise can be reduced by the UKF settings, but the higher filtration level causes the UKF output delay against its input. The relative adhesion force value starts to decrease when a slip velocity starts to increase with a time delay. A controller can start acting when the relative adhesion force gets below a required relative adhesion force.

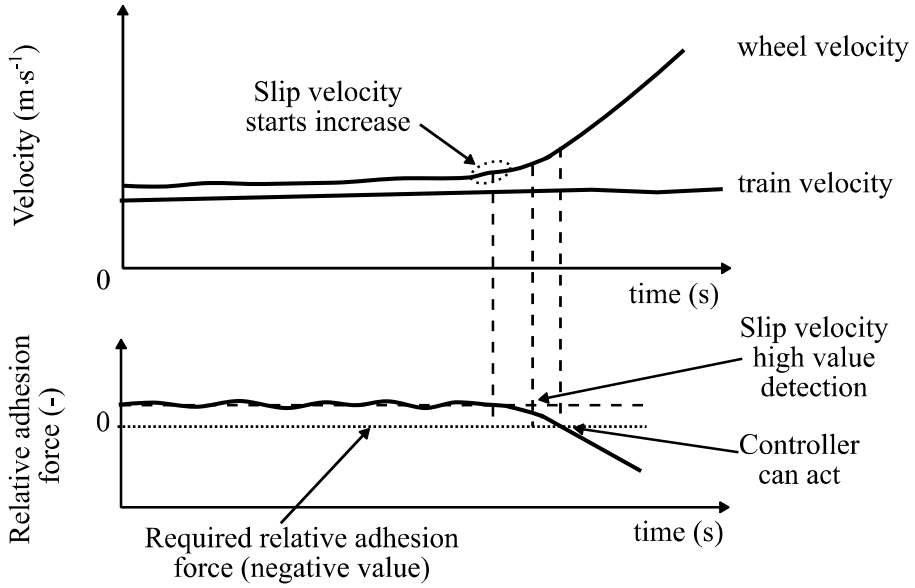

Figure 3.8 The proposed slip control slip controller detection part output

The comparison of the proposed slip control method output with the methods that calculate derivative of the estimated adhesion coefficient is depicted in Figure 3.9. The calculated derivatives are the same as depicted in Figure 3.6, and the settings are also the same. The value of the relative adhesion force is almost zero in contrast to the derivatives. Therefore, the relative adhesion force is again depicted below the derivatives. The estimated relative adhesion force is less noisy, and according to the value, the increasing slip velocity can be detected.

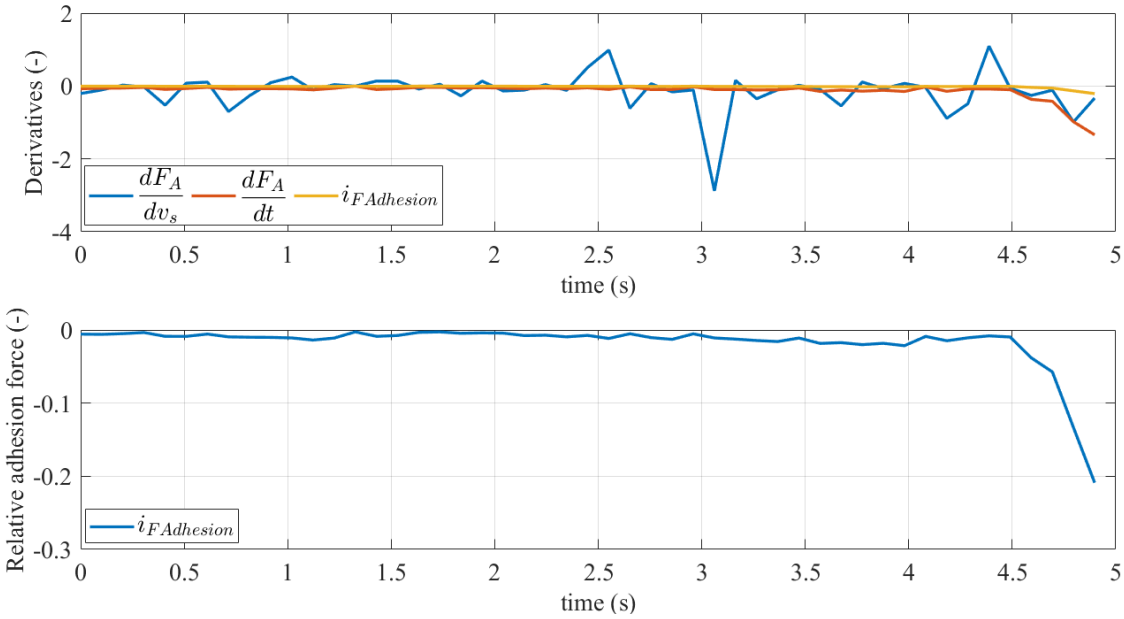

Figure 3.9 Comparison of the proposed slip controller output with classical methods

3.2.2.2 Description of the Nonlinear Adhesion Function

The UKF needs a nonlinearity description for the proper work. The nonlinearity is caused by the adhesion-slip characteristic in this case. When the adhesion-slip characteristic has to be described by equations, the description is complicated due to the characteristic changes. The adhesion-slip characteristic is described in chapter 2.1, and the modelling of the adhesion-slip characteristic is described the chapter 2.1.5 in detail. Measurement results from other authors and models are also described in the chapter. Different models use different approaches to describe an adhesion-slip characteristic. Generally, the adhesion-slip characteristic consists of a stable area, maximum peak and unstable area. Using complex description is not required because the actual characteristic shape is not known. Therefore, a model that describes this type of nonlinearity is required only for the UKF proper calculation. Therefore, the nonlinear function is derived from (2.12). The equation transformation from the adhesion coefficient to the relative adhesion force was made to ensure correct calculation. The nonlinear function estimates the maximum value of the current value of the relative adhesion force that represents the maximum point on the current adhesion-slip characteristic:

$$i_{\mathrm{FAdheisonMAX}} = \pm K_{\mathrm{S}} \cdot \sqrt{\frac{i_{\mathrm{FAdhesion}}}{v_{\mathrm{SEst}} \cdot (2 \cdot K_{\mathrm{S}} - i_{\mathrm{FAdhesion}} \cdot v_{\mathrm{SEst}})}} \tag{3.46}$$

The positive value is valid in traction and negative in a brake. The equation (3.46) needs K_s, $i_{\mathrm{FAdhesion}}$ and v_{SEst} values for its solution. The K_s is a pre-set known constant value. The value of the actual relative adhesion force $i_{\mathrm{FAdhesion}}$ is estimated by the UKF. The v_{SEst} value can be estimated by the UKF or calculated in a different way. The calculation by the UKF requires extending the system matrix and needs more computing power to calculate the UKF. The system matrix extension is described in chapter 2.3. The slip velocity can be calculated from the wheel velocity as it is used in classical slip controllers. Another possible way is to calculate the slip velocity according to the estimated adhesion. The calculation is used in the slip controller and described next in chapter 3.2.2.3 in detail.

To enable calculation of (3.46) the denominator cannot be zero and the expression under the root has to be positive. The variables $i_{\mathrm{FAdhesion}}$ and v_{SEst} are positive and greater than zero in the traction mode. The v_{SEst} can be zero during coasting, but the slip controller has no meaning in this regime. Therefore, the expression in the bracket has to be nonzero and positive. Conditions to get a valid solution of the fraction:

$$K_S \neq \frac{i_{\mathrm{FAdhesion}} \cdot v_{\mathrm{SEst}}}{2} \tag{3.47}$$

Conditions to get the real solution for traction:

$$K_S > \frac{i_{\mathrm{FAdhesion}} \cdot v_{\mathrm{SEst}}}{2} \tag{3.48}$$

The value of the K_s variable should not be greater than 1, and its value should be constant. Equations (3.47) and (3.48) should be valid in a normal operation when the operating point is in the stable area or near the maximum value in the unstable. If the (3.48) is not met, the result of (3.46) is a complex number and the method calculation fails. The (3.48) is met for the normal operating range in the stable area and the unstable area near the maximum point of the adhesion-slip characteristic. When the slippage is very high, the right-side of (3.48) can be greater than the left side. However, this situation is not acceptable and (3.46) can be limited to fit (3.48).

3.2.2.3 Slip Velocity Estimation

Equation (3.46) requires the slip velocity value to its proper work. The actual train velocity can be calculated by the estimator according to the principle described in chapter 2.3. The method is described in [86] for the UKF and in [92] and [91] for the EKF and KF cases. However, the method increases the computational complexity of the estimator. The second way is to use an extra method that estimates the slip velocity independently on the estimator. A method for train velocity estimation based on the fuzzy logic [90] can be used for the slip control purpose. However, the slip velocity can be estimated more straightforwardly if an assumption of the noise signal is taken into account because the UKF can cope with the noise signal. If the tractive effort is considered as noise, the actual slip velocity can also be considered as a highly noisy. Therefore, the actual slip velocity value is not required. The slip velocity time course nevertheless has to be preserved. The velocity can be calculated by the estimator on a similar principle as (2.11). The tractive effort can be used, but integration is required as an additional operation. However, the state vector of the mathematical model, described by equation (4.11) in the next chapter, contains a difference of angles on the different shaft ends $\Delta\varphi$. This difference corresponds to the torque. The difference is part of the state vector, and it is integrated by the estimator principle. The proposed slip velocity estimation method is a by-product of the nonlinear function calculation in the estimator. Therefore, the slip controller requires minimal additional computation power. The estimated relative adhesion force becomes more independent on the measured value by using the described principle, but the principle and reaction are still correct.

3.2.2.4 Control Part of the Slip Controller

The system is nonlinear, but the output of the estimator is linear. Therefore, a linear controller can be used. The proposed slip controller uses a PI controller. However, the controller can be substituted by any controller type. The PI controller algorithm is described in [126]. The described algorithm form can be directly implemented into a microcontroller:

$$e = i_{\mathrm{FAdhesion}} - i^{*}_{\mathrm{FAdhesion}} \tag{3.49}$$

$$out_{\mathrm{T}} = sum + e \cdot K_{\mathrm{p}} \tag{3.50}$$

$$out = \begin{cases} out_{\max} & \text{if } out_{\mathrm{T}} > out_{\max} \\ out_{\min} & \text{if } out_{\mathrm{T}} < out_{\min} \\ out_{\mathrm{T}} & \text{otherwise} \end{cases} \tag{3.51}$$

$$ex = out_{\mathrm{T}} - out \tag{3.52}$$

$$sum = sum + e \cdot K_{\mathrm{i}} - ex \cdot K_{\mathrm{c}} \tag{3.53}$$

Where e is an error, out_{T} is a temporary output value, $out_{\max}$ and $out_{\min}$ are the output limits, out is the PI controller output value, ex is excess, sum is a sum of previous values, K_{p}, K_{i} and K_{c} are the PI controller coefficients.

The theoretical slip controller function with a controller is demonstrated in Figure 3.10. The two top time courses are similar to the time course depicted in Figure 3.8. The difference is in the controller reaction that limits the tractive force and suppresses the slippage. The controller does not react immediately when the slip velocity starts to increase. The reaction is delayed about time that the UKF out value steps below the required value. The force and velocity time courses depend on the PI controller settings. If a different controller type is used, the difference occurs only in the part when the estimated relative adhesion force decreases below the required value of the relative adhesion force. Therefore, the controller influence to the slip controller performance is limited, and the PI controller can provide effective control.

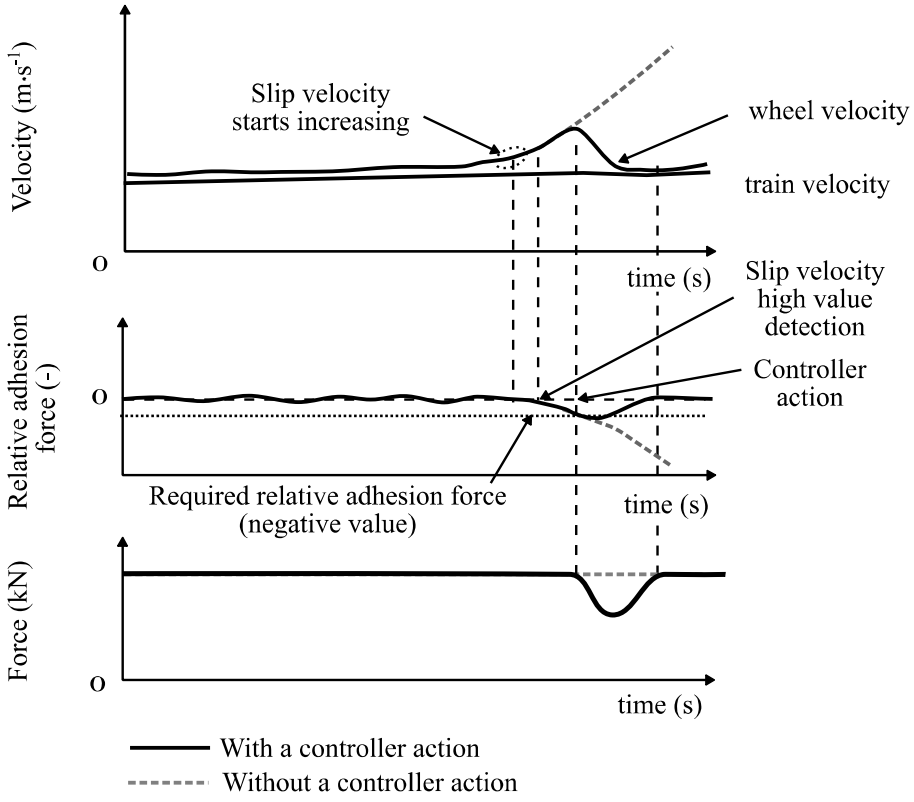

Figure 3.10 Controller action

3.2.2.5 Relation between the Nonlinear Function and the Adhesion Slip Characteristic

The slip controller is based on the UKF with nonlinear function. However, the original slip controller works with the KF is without the linearized function. If the UKF has no nonlinear function, the slip controller behaves as the slip controller with the KF. The nonlinear function improves the slip controller function and stability. The used nonlinear function is based on the approximation of the adhesion-slip characteristic. The principal assumption is that the approximation is correct for the most of cases that can occur during the train run. The difference between the proposed nonlinear function and the actual adhesion-slip characteristic can occur. The first difference type is based on the different parameters than proposed. This situation is, e.g. depicted in Figure 2.4 for a wet sand case. The second type of the difference of the adhesion-slip characteristic is based on the assumption that the characteristic is entirely different. However, this case contradicts with the measurement presented in papers and described in chapter 2.1, and the case is unlikely.

If the adhesion-slip characteristic has different parameters than it is assumed, the slip controller still works as it is proposed. The possible situation is depicted in Figure 3.11, Figure 3.12 and Figure 3.13.

The first case describes the situation when the maximum point of the actual adhesion-slip characteristic is shifted to the higher slip velocity that it is assumed according to the nonlinear function. The situation is depicted in Figure 3.11. The controller increases the tractive force until the required slope is not achieved. The slopes are the same, and the correct operating point is set to the actual optimal position on the actual adhesion-slip characteristic, and tractive force is F_T. The same result is valid for the case when the maximum point is shifted to the lower slip velocity.

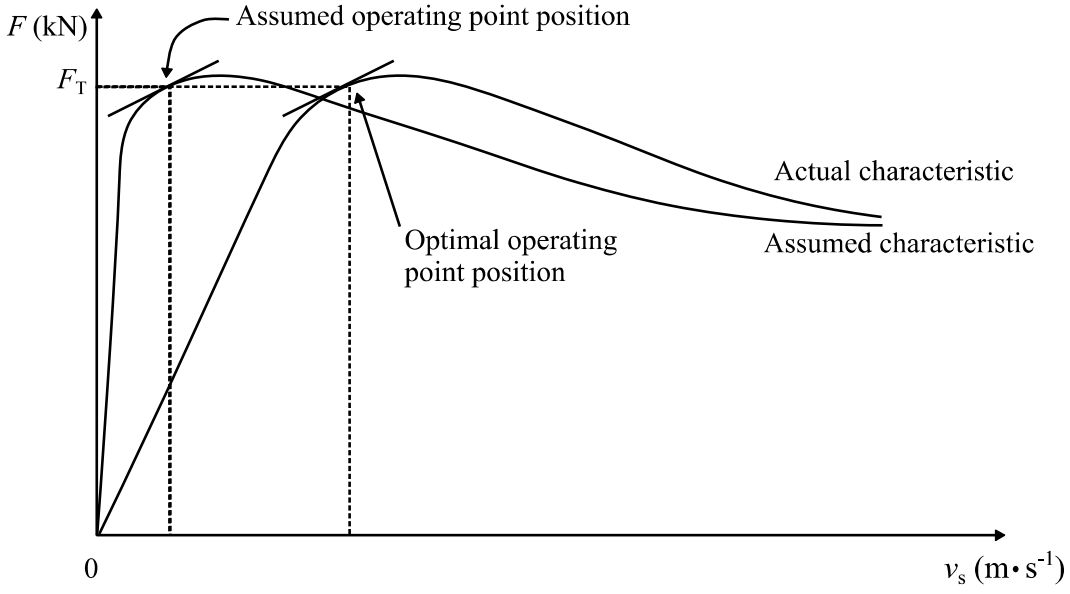

Figure 3.11 Characteristics mismatch for case when the maximum point is shifted to a higher slip velocity

The situation when the operating point is shifted to the higher slip velocity and lower adhesion as is depicted in Figure 3.12. In the case, the controller increases the required tractive force until the required slope is achieved. The corresponding tractive force is F_{T1}. The controller will not

increase the tractive force because the required slope is achieved, and the operating point is set to the optimal position. The maximum point is shifted to the lower slip velocity and higher adhesion in the last case.

The situation is depicted in Figure 3.13. The required slope should be achieved at applied tractive force F_{T1}. However, the detected slope is different, and the tractive force is increased until the required slope is not achieved. The operating point is set up to the correct position with the tractive force F_{T2}. The slip controller works if the characteristic has the assumed shape regardless the characteristic parameters.

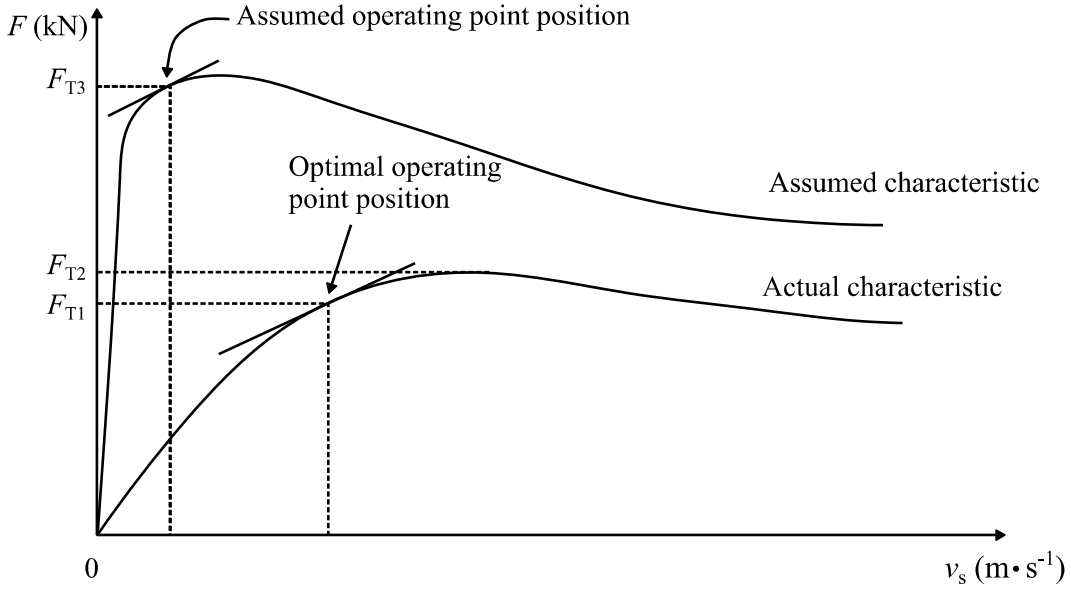

Figure 3.12 Characteristics mismatch for case when the maximum point is shifted to a higher slip velocity and lower force value

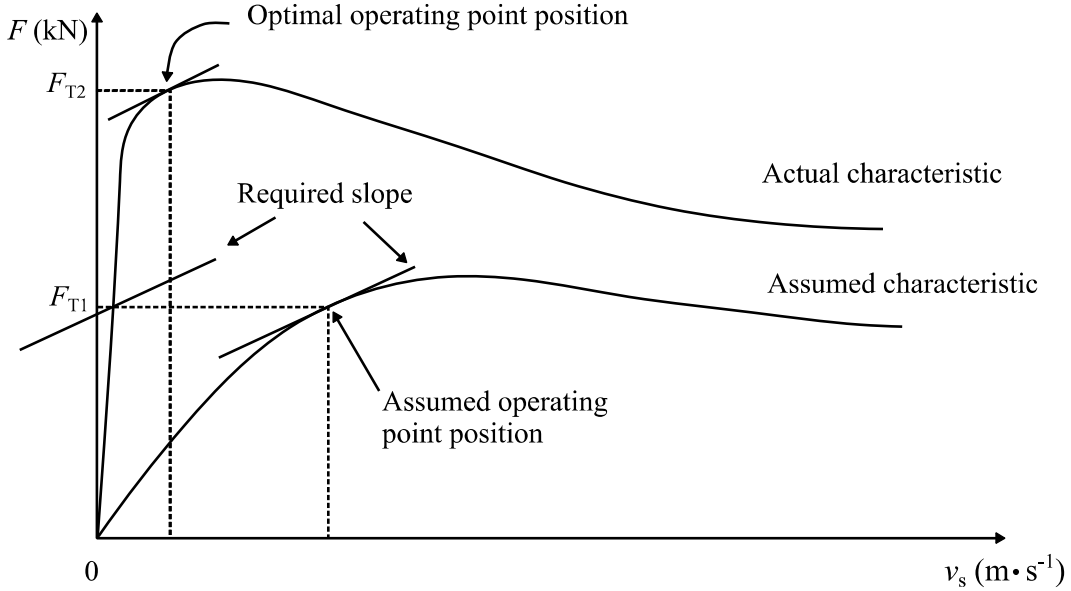

Figure 3.13 Characteristics mismatch for case when the maximum point is shifted to a lower slip velocity and higher force value

3.2.2.6 Gradual Slip Velocity Increase

The gradual slip velocity increase can occur when the adhesion conditions become gradually worse or when the train accelerates. Some existing slip controllers can cope with a gradual slip velocity increase. However, many slip controllers can fail when the slip velocity increased gradually. This failure can occur when the characteristic has a plateau instead of a peak. An example of the characteristic is shown in Figure 2.9 for a wet (dew) case. If the slip controller cannot cope with the problem, the slip velocity can increase to very high value. Therefore, the slip controller weakness has to be taken into account during the slip controller implementation and an additional slip controller or protection has to be added to the slip controller to avoid these cases.

The proposed slip controller is resistant to the gradual slip velocity increasing. The slip controller endurance is demonstrated in Figure 3.14. Adhesion-slip characteristics, two sets of tangents that represent the required characteristic slope, and positions of the maximum point on the characteristics are depicted in the figure. The operating point moves to the highest slip velocities when the adhesion-slip characteristic becomes worse. The operating point position moves to an exponential function that is different from functions on which moves the maximum point. Therefore, the slip velocity is lower than the slip velocity at the maximum point. The tangent sets represent two different controller limit settings. Both settings utilise the adhesion similarly when the adhesion is good. The second limit eliminates the high slip velocity in bad adhesion conditions. The high slip velocity that occurs at the worst case in Figure 3.14 is approximately 3 km·h^{-1} in one case and 2 km·h^{-1} in the second one. The slip velocity around 2 km·h^{-1} is considered as the acceptable value. Therefore, it is better to use stepper slope than try to achieve the adhesion-slip characteristic maximum value.

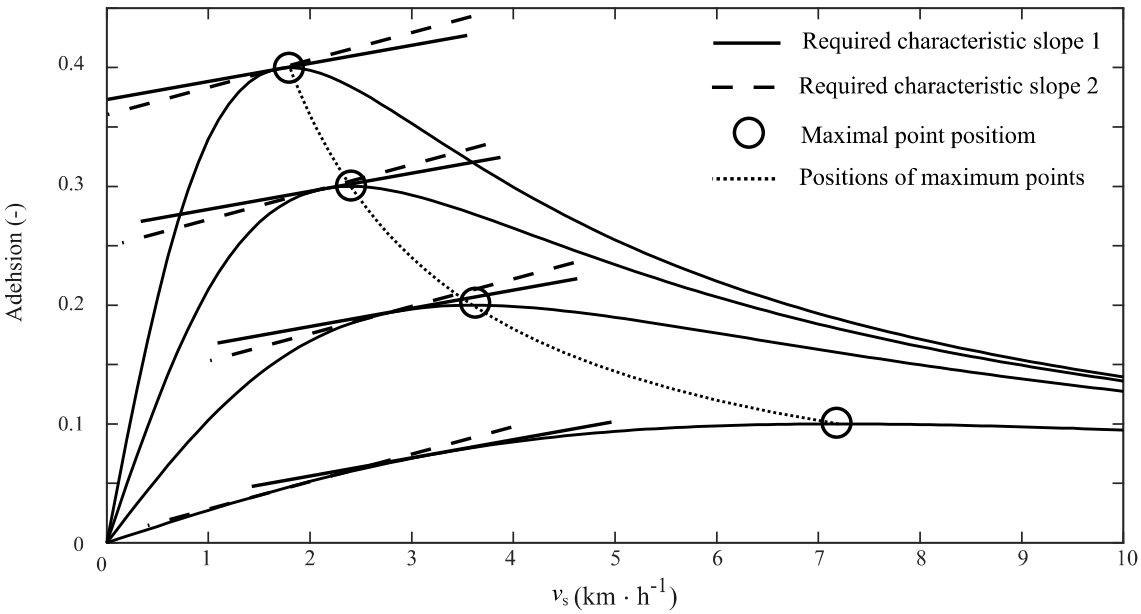

Figure 3.14 Proposed slip controller performance

3.3 Proposed Slip Controller Overview

The proposed slip controller is based on the adhesion-slip characteristic slope. The disadvantage of the classical slip controllers, which are based on the same principle, is described in the chapter. The classical methods require a high filtration level of input signal to eliminate the actual adhesion-slip characteristic changes. The proposed slip controller can cope with the

problem because the slip controller does not calculate a derivative from the estimated adhesion coefficient. The slip controller calculates the relative adhesion force that can be used for an error value calculation that is used as a filter input. The proposed slip controller requires a nonlinear function calculation. The function requires the actual slip velocity. The slip velocity is calculated from the estimated angles difference by the proposed nonlinear function. This solution eliminates the problem with the slip velocity calculation from the wheels velocity or calculation by an estimator. The slip controller uses the nonlinear function that describes an adhesion-slip characteristic. The nonlinear function is essential for the slip controller operation. The nonlinear function improves the estimator performance and stability. Therefore, the disagreement between the adhesion-slip characteristic described by the nonlinear function and the actual adhesion-slip characteristic is also discussed. The slip controller output has to be connected to a controller. The theoretical function of the controller is also presented in the chapter.

The proposed slip controller is based on the UKF that enables to estimate states of nonlinear systems. The UKF algorithm is described in chapter 3.1.1 in detail. The used model is a two-mass model that is further described in chapter 4.1.2.2 in detail. The UKF output is an estimation of the relative adhesion force. The relative adhesion force corresponds to an actual adhesion force or an adhesion coefficient in the time course, but not in absolute value. The relative adhesion force can be directly used as a controller input without any additional calculation. The slip controller is designed to use the measured wheel velocity. The slip controller is designed to control one wheelset. Therefore, every wheelset has to have its controller. If more than one electric drives are powered by one converter or inverter, the slip controller limits tractive force for all powered electric drive. The slip controller can be implemented for an electric locomotive. The UKF can be replaced by the EKF. However, the correct function in all possible cases is not guaranteed due to the EKF possible divergence, but if preventive measures are made, the EKF can be used. The UKF can also be replaced by the KF. However, the advantage of the nonlinear function is unused it the case.

4 DESIGN OF THE PROPOSED SLIP CONTROLLER

The chapter describes a model design of the proposed slip controller. The development requires mathematical models of locomotive mechanical parts. The mathematical models are used for two different purposes during the design. The first model type is used for the system modelling in Matlab software as a substitution of a real system for the slip controller design. The second model type is used by the estimator. The block diagram of the design process is depicted in Figure 4.1. The design process requires the locomotive model and the designed slip controller model. The model for the estimator is included in the model of the slip controller. A model of adhesion, normal force and a train mass has to be also modelled. However, these models are not part of the locomotive model.

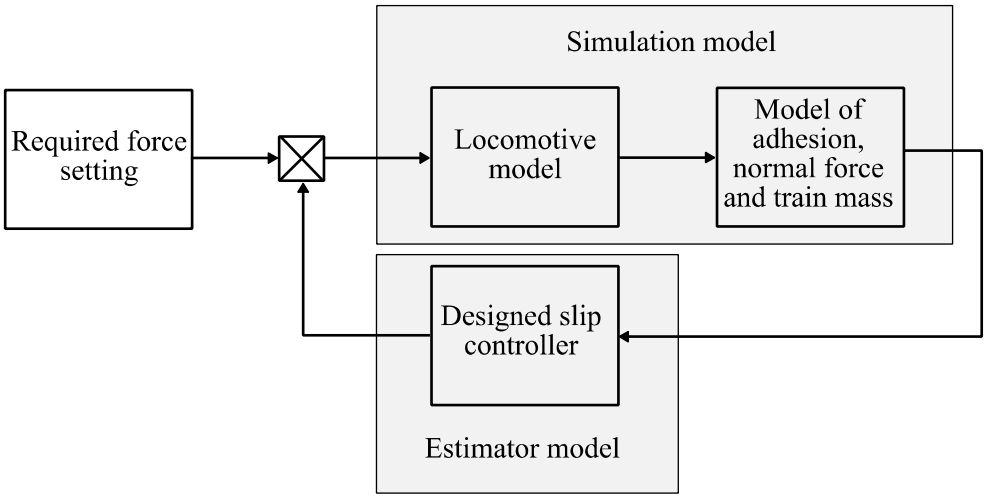

Figure 4.1 Block diagram of the design of the proposed slip controller

The chapter briefly describes requirements of the mathematical model and a general structure of the whole model design. Then, the mathematical model of locomotive parts used in simulations in Matlab software and for an estimator is described. The model for simulation is a five-mass model, and developed models for estimator are a tree-mass model and two-mass one. All models are discussed, and their features are compared among themselves. Moreover, the features of the models are compared with measurement. Finally, the model simulation process is described because a continuous-time model and a discrete-time model have to be running simultaneously. The model used for the system modelling in Matlab software is called as a simulation model, and model for an estimator is called as an estimator model in the chapter for greater clarity.

4.1 Mathematical Model

Mathematical models of locomotive mechanical parts for the modelling in Matlab software are more complex than the model for an estimator. The results of the model design depend on the model parameters. Therefore, the model has to capture the most significant processes that occur in the real system. Different model types with different complexity are described in the literature. The model can describe whole train or locomotive. Simpler models describe some locomotive parts that are the most important for the simulation, e.g. bogie or wheelset with an electric drive. Model for estimators should be more straightforward than the simulation model because of a request for the model observability and real-time calculation. When the model contains unobservable parts, the parts are unnecessary for the estimator purpose. The

requirement of observability is no need for models for the system modelling. The second reason for the model simplicity is the model implementation into a DSP and its real-time calculation. In this case, more straightforward model as possible is preferred. The model complexity depends on the used estimator computational complexity. For example, the KF can use more complicated model than the UKF at the same time requirements.

Description of complete train or locomotive is a difficult task because many dynamic motions which occur during the train moving. Simplified forces and movement around axes applied to a moving vehicle are shown in Figure 4.2. The main forces are a tractive force and a tractive resistance. These forces are directly connected with the vehicle movement. Side forces and forces caused the locomotive moving around axes are other types of forces applied to the locomotive. Movements around the axes are called as yaw, roll and pitch. These movements cause locomotive deviations from its ideal straight movement. Yaw causes well-known hunting oscillations. Simulation of all forces and movements is difficult and time-consuming. For example, the model described in [66] has 21 degrees of freedom and model described in [127] has 266 degrees of freedom. Therefore, forces and movements that are important for the simulation purpose could be only taken into account to get more straightforward and accurate model. Examples of components arrangement that can be used for a locomotive modelling are depicted in Figure 4.3. The model can be created from wheelset models, gearboxes and electric drives that create a bogie. Bogies are connected to a locomotive frame. Every bogie and wheelset is loaded by different forces that are caused by movement around axes and interaction with a locomotive load. Moreover, wheel-rail interactions have to be taken into account as well.

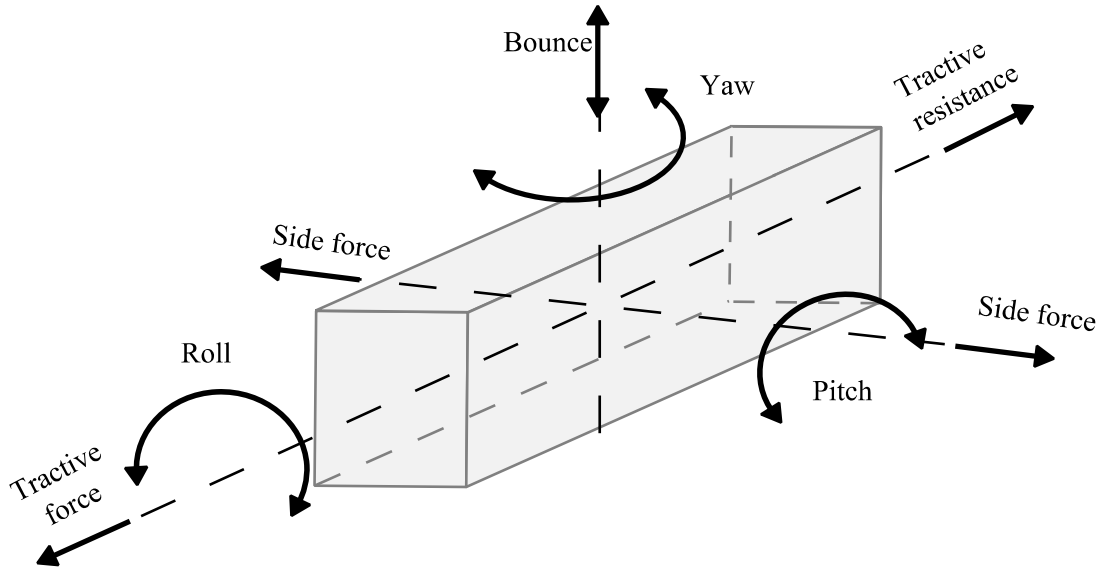

Figure 4.2 Simplified forces and movement around axes during vehicle motions

The goal of resulting model is the simple estimator model and the simulation one that is intended for estimator verification and the whole slip controller verification. The structure of the simulation model depends on the locomotive structural arrangement. The torque transfers from a motor to a wheel can be various. For example, the torque can be transferred by a shaft or by a hollow shaft. These two constructions have to be described by two different models. Therefore, the complex model which describes the real locomotive is a single purpose model. A detailed description of all possible locomotive configurations and their models is not the target of this chapter. The estimator models typically describe the main features of the real

vehicle for its higher versatility of the estimator model. The estimator models describe a torque transfer from a motor to wheel [23] and [128]. The model is sometimes simplified to an equation of motion [29] and [52]. The simulation model used for a slip control or load torque estimation or control contains one wheelset model with a gearbox and electric drive [128], [129] and [130]. For slip controller verification, the simulation model has to be complemented by an adhesion model.

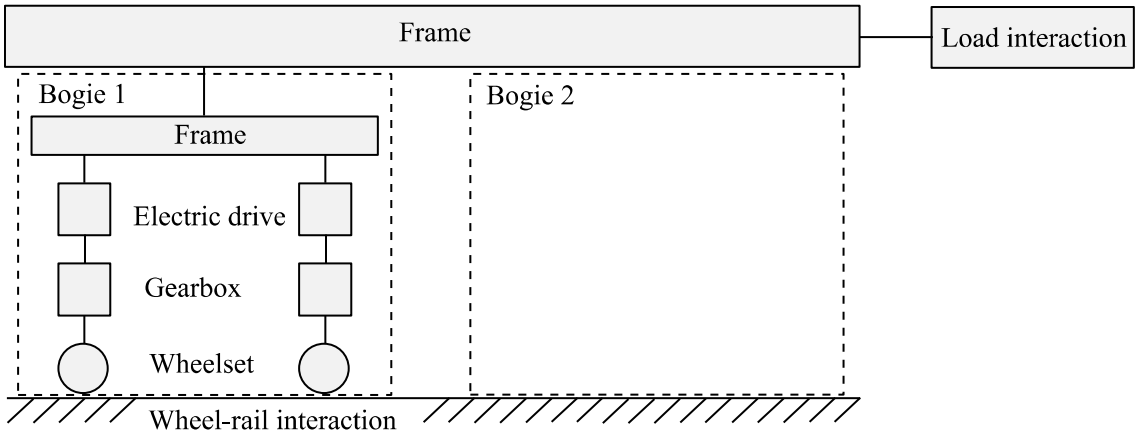

Figure 4.3 Simplified locomotive model arrangement

The proposed simulation model is used as a base for the estimator model derivation. The simulation model is based on the wheelset model. The individual components of the wheelset are:

1. Electric drive, which can be simulated as a complete model of motor and inverter with the motor control or directly as the electric drive transfer function and its time delay. Induction motors are typically used in the locomotives nowadays. However, DC motors were used typically in older still operated locomotives. The complete model of electric drive is created from the motor, inverter and its control. The model is complicated, but it is used [129]. More appropriate model of electric drive is a transfer function and time delay or the electric drive can be replaced by the torque or force [128]. This reduced model is more appropriate than the complete model because the electric drive response is needed for the slip control, and processes in the motor and inverter are not necessary to know.
2. Gearbox, which is created by gear wheels that can have different teeth types. The wheel types, which are typically used are a spur, helical or double helical. The wheel type influences the gearbox properties, e.g. the spur wheels change stiffness between wheels during the rotation of the wheels. Modelling of these behaviours increases computation time. Therefore, the gearbox is typically represented by its gear ratio and its masses.
3. Locomotive wheelset, which is created by two wheels connected by a shaft in a simple construction case. The gear wheel is mounted on the shaft. The wheels have a different diameter, load and adhesion conditions. Therefore, every wheel can transfer different force to rails. When the slippage occurs, one wheel velocity starts increasing first, and whole bogie rotation is a result. This behaviour is used by some slip controllers for slippage detection. For most of the slip controllers, this behaviour is not needed. However, between the wheels, torsional vibrations occur. These vibrations are caused by a non-rigid shaft. The vibrations can be measured by a speed sensor. The same vibrations occur between the gearbox and motor. The torsional vibrations are also used by some slip controllers.

However, the torsional vibrations modelling are not needed for the most of the slip controllers. Therefore, the wheelset is sometimes replaced by one wheel.

The components mentioned above are represented by its masses. The masses are connected by shafts that are not rigid. Therefore, the shafts are represented by is stiffness and elasticity.

4.1.1 Proposed Simulation Model

The author has available data measured on a Skoda 93E electric locomotive. The locomotive is intended for a freight train hauling. The model possible using for different locomotives is discussed after the model developing at the end of the chapter. The Skoda 93E locomotive has three bogies and six wheelsets. The locomotive parameters are given in Table 4.1. The locomotive has the maximum tractive force 575 kN that cannot be reached by the locomotive because the maximum adhesion force for the locomotive is 360 kN when the adhesion coefficient value is 0.3. The high possible tractive force occurs due to the locomotive rebuild. The locomotive photo is depicted in Figure 4.4.

Table 4.1 Parameters of Skoda 93E locomotive

Parameter	value
Nominal voltage	3.0 kV
Weight	123 tonnes
Maximum speed	95 km·h^{-1}
Nominal speed	51 km·h^{-1}
Maximum power	5220 kW
Maximum tractive effort	575 kN
Tractive effort at 50 km·h^{-1}	355 kN
Number of wheelsets / bogies	6 / 3
Gear ratio	81:18

Figure 4.4 Photo of Skoda 93E locomotive

The locomotive wheelsets are driven by DC motors. One DC motor drives one wheelset. Two DC motors are connected to one converter in series. An incremental encoder is mounted on every wheelset. The encoders are mounted on one locomotive side, but due to the wheelset configurations, one encoder measures velocity on the directly driven side and the second in the indirectly driven side as it is shown in Figure 4.5.

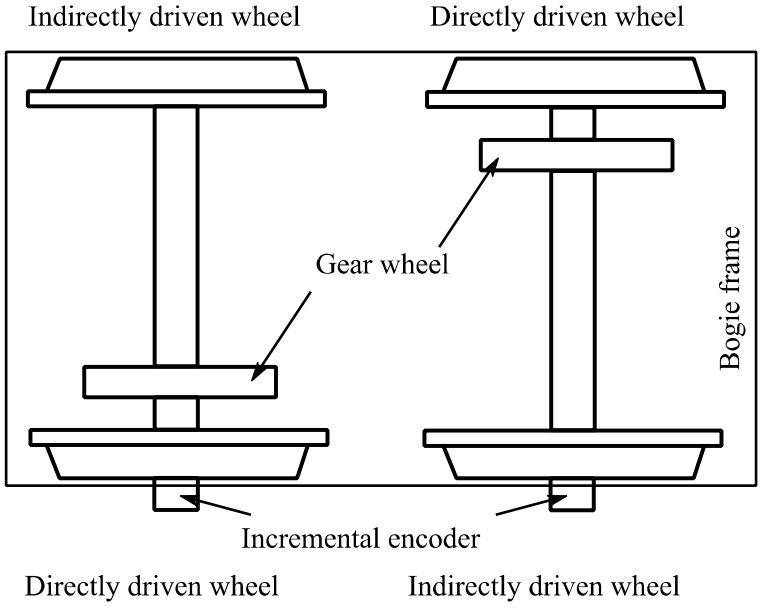

Figure 4.5 Skoda 93E bogie schema [30]

The proposed simulation model describes one wheelset with gearbox and motor. The simulation model is a five-mass model. The masses of the model are a motor rotor, pinion, gear wheel, directly driven wheel and indirectly drive wheel. The model is based on equations presented in [131]. The model is intended for simulations of a locomotive behaviour in Matlab software. The model is intended for a slip controller performance evaluation when the slip controller is supplemented by a controller. Therefore, the model can be more complex than an estimator model. The model contains some components that are not needed for an estimator. However, these components made the model more precise and close to the measured data. The simulation model preserves eigenfrequencies that were identified on the locomotive during measurement. The simulation model describes the torque transfer from the motor through the gearbox to the directly driven wheel and indirectly wheel. The directly driven wheel and indirectly driven wheel are placed on the wheelset. The wheel, which is nearer to gear wheel, is the directly driven wheel. The wheelset configuration that is used for the wheelset simulation model is shown in Figure 4.6. Every mass is represented by its moment of inertia J. The torque is transferred through shafts that are elastic elements. The shafts are represented by a damping d and stiffness c. Three shafts are shown in Figure 4.6. Every shaft has a different value of the damping and stiffness. The first shaft connects a motor to a gearbox. The second and third shaft connects the gear wheel with wheels. The main difference between directly driven wheel and indirectly driven one leads in the shafts parameters. The shorter one has higher stiffness. Phenomena that occur in the gearbox are neglected, and the gearbox is represented by its moment of inertia and by its gear ratio. The shafts are not rigid. Therefore, elements, which are connected by a shaft, can have different actual angular velocities.

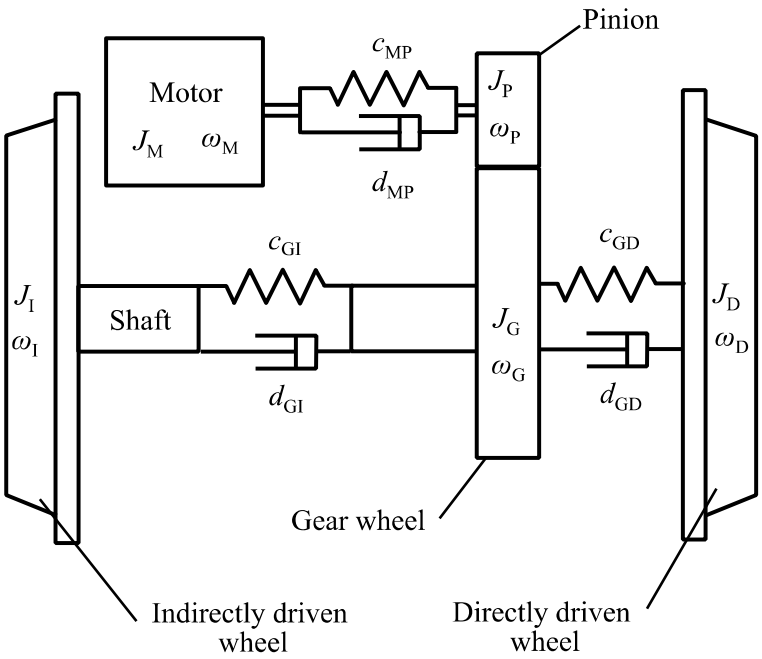

Figure 4.6 Wheelset simplified configuration for the five-mass model

The general equation that describes the wheelset is:

$$T = \mathbf{J}_m \cdot \epsilon + \mathbf{D}_m \cdot \omega + \mathbf{C}_m \cdot \varphi \tag{4.1}$$

Where $\mathbf{J}_m$, $\mathbf{D}_m$ and $\mathbf{C}_m$ are matrices of moments of inertia, damming and stiffness respectively, ω is angular velocity, ϵ is an angular acceleration and φ is an angle.

For simulation purpose is more appropriate a state-space representation:

$$\frac{\mathrm{d}\mathbf{x}}{\mathrm{d}t} = \mathbf{A} \cdot \mathbf{x} + \mathbf{B} \cdot \mathbf{u} \tag{4.2}$$

The state vector is defined as:

$$\mathbf{x} = \begin{bmatrix} \varphi_M \\ \varphi_P \\ \varphi_G \\ \varphi_D \\ \varphi_I \\ \omega_M \\ \omega_P \\ \omega_G \\ \omega_D \\ \omega_I \end{bmatrix} \tag{4.3}$$

Where the subscript M means motor, P pinion, G gear wheel, I indirectly driven wheel and D directly driven wheel.

The system matrix **A** structure is defined as:

$$\mathbf{A} = \begin{bmatrix} 0 & I \\ -\dfrac{\mathbf{C}_\mathrm{m}}{\mathbf{J}_\mathrm{m}} & -\dfrac{\mathbf{D}_\mathrm{m}}{\mathbf{J}_\mathrm{m}} \end{bmatrix} \tag{4.4}$$

The matrixes $\mathbf{J}_\mathrm{m}$, $\mathbf{C}_\mathrm{m}$ and $\mathbf{D}_\mathrm{m}$ are defined as:

$$\mathbf{J}_\mathrm{m} = \begin{bmatrix} J_\mathrm{M} & 0 & 0 & 0 & 0 \\ 0 & J_\mathrm{P} & 0 & 0 & 0 \\ 0 & 0 & J_\mathrm{G} & 0 & 0 \\ 0 & 0 & 0 & J_\mathrm{I} & 0 \\ 0 & 0 & 0 & 0 & J_\mathrm{D} \end{bmatrix} \tag{4.5}$$

$$\mathbf{C}_\mathrm{m} = \begin{bmatrix} c_\mathrm{MP} & -c_\mathrm{MP} & 0 & 0 & 0 \\ -c_\mathrm{MP} & c_\mathrm{MP} + c_\mathrm{PG} & -c_\mathrm{PG} & 0 & 0 \\ 0 & -c_\mathrm{PG} & c_\mathrm{PG} + c_\mathrm{GD} + c_\mathrm{GI} & -c_\mathrm{GD} & -c_\mathrm{GI} \\ 0 & 0 & -c_\mathrm{GD} & c_\mathrm{GD} & 0 \\ 0 & 0 & -c_\mathrm{GI} & 0 & c_\mathrm{GI} \end{bmatrix} \tag{4.6}$$

$$\mathbf{D}_\mathrm{m} = \begin{bmatrix} d_\mathrm{MP} & -d_\mathrm{MP} & 0 & 0 & 0 \\ -d_\mathrm{MP} & d_\mathrm{MP} + d_\mathrm{PG} & -d_\mathrm{PG} & 0 & 0 \\ 0 & -d_\mathrm{PG} & d_\mathrm{PG} + d_\mathrm{GD} + d_\mathrm{GI} & -d_\mathrm{GD} & -d_\mathrm{GI} \\ 0 & 0 & -d_\mathrm{GD} & d_\mathrm{GD} & 0 \\ 0 & 0 & -d_\mathrm{GI} & 0 & d_\mathrm{GI} \end{bmatrix} \tag{4.7}$$

The equations above describe the wheelset mechanical model without the adhesion influence, resistance forces, normal force and train mass. These parameters are described separately. The system contains 9 unobservable states.

The five-mass model parameters are described in Table 4.2. The verification of the parameters is difficult because the parameters for locomotive Skoda 93E are not presented. However, the parameters for a locomotive BR120 are presented in [132]. The locomotive BR120 has a different wheelset configuration because it has hollow shafts and induction motors. However, the parameters of the locomotive BR120 can be used for checking if the parameters of Skoda 93E are at least approximately similar and the parameters are also summarized in Table 4.2. The parameters are approximately the same except stiffness c_MP and c_GI. However, the values of the stiffness are interchanged. This is caused by the different configuration. Values in Table 4.2 are recalculated to wheels.

Table 4.2 Five-mass model parameters and its comparison with another locomotive

Variable	Skoda 93E	BR120
c_MP (kNm)	9720	150000
c_GI (kNm)	137000	10097.7
c_GD (kNm)	10956	7057
d_MP (Nms)	1215	920
d_GI (Nms)	111	105
d_GD (Nms)	29.6	53.6
J_M (kgm^2)	810	466.6
J_P (kgm^2)	4.3	55
J_G (kgm^2)	57.7	
J_I (kgm^2)	130	163
J_D (kgm^2)	130	157.4

4.1.2 Proposed Estimator Models

Two models for observes were gradually developed. The first model is a three-mass model and the second model is a two-mass model. Both models are based on the five-mass simulation model. The five-mass model has two inappropriate properties. The first property is the model complexity and related computational complexity. The computation complexity can be demonstrated on a simple example. The system matrix size of a five-mass model is 10×10 and for a two-mass model is the system matrix size 4×4. If the system matrix has to be multiplied with another matrix of the same size, 1000 multiplications and additions have to be done in the five-mass model. On the other hand, 64 multiplications and additions have to be done in the two-mass model case. Therefore, the simulation model can be used in Matlab software, but the model is inappropriate for the real-time calculation. The second negative property is related to the system observability. The five-mass model is unobservable. Therefore, some parts of the model have to be reduced.

4.1.2.1 Three-Mass Model

The three-mass model was presented in [30], [32] and [122]. The five-mass model contains a motor, pinion, gear wheel and two wheels. There are two significant eigenfrequencies between the motor and wheelset, and between the wheels in the model. The motor has to be preserved in the model to preserve eigenfrequency between motor and wheelset. The pinion and gear wheel can be connected to one mass. When one wheel is connected to the gear, the eigenfrequency between wheels can slightly change. However, the eigenfrequency will more or less remain. The possible configuration is depicted in Figure 4.7.

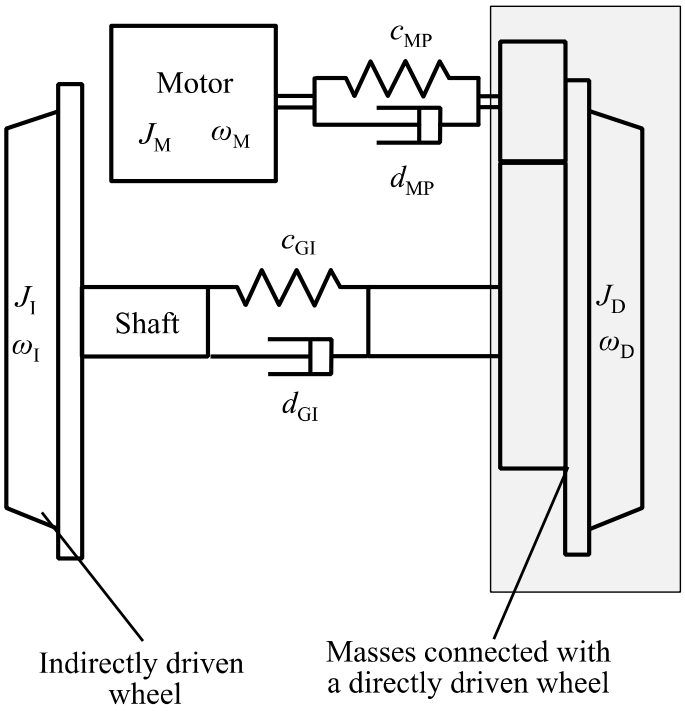

Figure 4.7 Reduction of the five-mass model to the three-mass model

The reduced three-mass model contains three masses. The motor creates one mass. The pinion with a gear wheel and directly driven wheel creates the second mass. The third mass creates indirectly driven wheel. Between masses are elastic elements with stiffness c and damping d. The system vector has a different structure than the system vector of the five-mass model described by (4.3). The difference is due to the estimator structure and the relative adhesion

force implementation into the model. The state vector for the two-mass model is defined as follows:

$$\mathbf{x} = \begin{bmatrix} \omega_{\mathrm{M}} \\ \omega_{\mathrm{D}} \\ \omega_{\mathrm{I}} \\ T_{\mathrm{MD}} \\ T_{\mathrm{MI}} \\ i_{\mathrm{FAdhesion}} \end{bmatrix} \tag{4.8}$$

T_{MD} and T_{MI} are torques between the motor and the directly driven wheel and the indirectly driven one respectively, $i_{\mathrm{FAdhesion}}$ is the relative adhesion force.

The Matrix **A** is based on matrix presented in [30] and the matrix is defined as follows:

$$\mathbf{A} = \begin{bmatrix} 0 & 0 & 0 & \frac{1}{J_{\mathrm{M}}} & \frac{1}{J_{\mathrm{M}}} & 0 \\ 0 & 0 & 0 & \frac{1}{J_{\mathrm{D}}} & 0 & -\frac{1}{J_{\mathrm{D}}} \\ 0 & 0 & 0 & 0 & \frac{1}{J_{\mathrm{I}}} & -\frac{1}{J_{\mathrm{I}}} \\ c_{\mathrm{MD}} & -c_{\mathrm{MD}} & 0 & -\frac{d_{\mathrm{MDI}}}{J_{\mathrm{D}}} & \frac{d_{\mathrm{MD}}}{J_{\mathrm{D}}} & -\frac{d_{\mathrm{MD}}}{J_{\mathrm{D}}} \\ c_{\mathrm{DI}} & 0 & -c_{\mathrm{DI}} & \frac{d_{\mathrm{DI}}}{J_{\mathrm{I}}} & -\frac{d_{\mathrm{MDI}}}{J_{\mathrm{I}}} & -\frac{d_{\mathrm{DI}}}{J_{\mathrm{I}}} \\ 0 & 0 & 0 & 0 & 0 & 0 \end{bmatrix} \tag{4.9}$$

The system output matrix is:

$$\mathbf{y} = [0 \quad 1 \quad 0 \quad 0 \quad 0 \quad 0] \tag{4.10}$$

The state vector (4.8) can contain angular velocities ω and swivelling angles φ. In the case, the structure will be the same as for the five-mass model. If swivelling angles are replaced by its difference φ_{M}-φ_{D} and φ_{M}-φ_{I}, the torques T_{MD} and T_{MI} can be used [132]. The torques are used because the model with the state vector that contains swivelling angles is unobservable. The reduced model is fully observable now. The relative adhesion force $i_{\mathrm{FAdhesion}}$ is added to the model to make the calculation of the relative adhesion force possible. The relative adhesion force is not a part of the locomotive mechanical model. The three-mass model disadvantage is its higher complexity than the two-mass model, and some parts can be considered as redundant although the whole system matrix is observable.

4.1.2.2 Two-Mass Model

The two-mass model was presented in [120]. The two-mass model was designed to preserve eigenfrequency between the motor and the wheel from the five-mass model. Other eigenfrequencies cannot be preserved due to the model character. The reduced model is depicted in Figure 4.8. The motor forms one mass and the second mass is created by a pinion, gear wheel and a directly driven wheel. The masses are connected by a shaft that represents an elastic element.

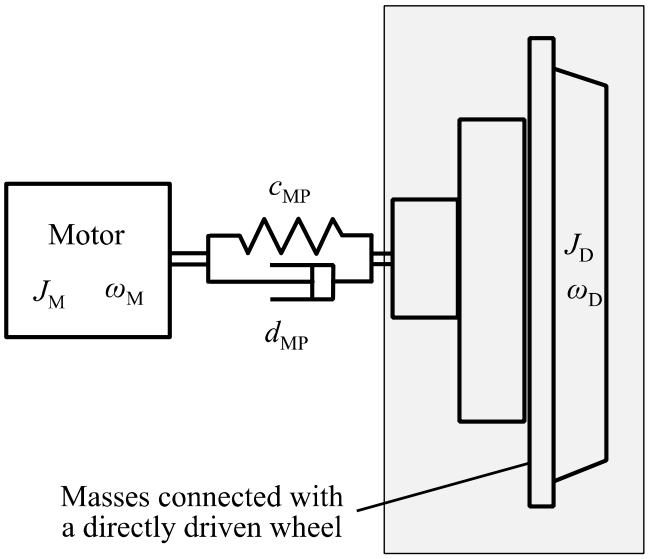

Figure 4.8 Reduction of the five-mass model to the two-mass model

The two-mass model state vector is defined as:

$$\mathbf{x} = \begin{bmatrix} \Delta\varphi \\ \omega_M \\ \omega_D \\ i_{FAdhesion} \end{bmatrix} \tag{4.11}$$

Where $\Delta\varphi$ is shaft torsion between motor and pinion, ω_M is a motor angular velocity, ω_D is a directly driven wheel angular velocity, and $i_{FAdhesion}$ is an estimated relative adhesion force.

A Matrix **A** is defined as follows:

$$\mathbf{A} = \begin{bmatrix} 0 & 1 & -1 & 0 \\ -c_{MD} & -d_{MD} & d_{MD} & 0 \\ c_{MD} \cdot r_J & d_{MD} \cdot r_J & -d_{MD} \cdot r_J & -\frac{1}{J_D} \cdot R_g \\ 0 & 0 & 0 & 0 \end{bmatrix} \tag{4.12}$$

Where r_J is a ratio of moments of inertia J_M and J_D.

Table 4.3 Two-mass model parameters

Variable	Value
c_{MD} (kNm)	4.52
d_{MD} (Nms)	0.55
r_J (-)	2.12
J_D (kgm^2)	174.93
R_g (-)	4.5

4.1.3 Models Comparison

The five-mass model, three-mass model and two-mass models are compared between themselves in the subchapter. Bode plot and system poles are used for the comparison. The five-mass model performance comparison with measurements is discussed in chapter 5 in detail.

The five-mass and three-mass models can be applied to different locomotives that have the same configuration of the wheelset and electric drives. The two-mass model is universal and can be applied to different types of locomotives with a different configuration. The change of the parameters is only required. Two eigenfrequencies of 18 Hz and 61 Hz were detected from measured data in Skoda 93E locomotive [134]. The 18 Hz was determined as a frequency between the motor and the wheel, and 61 Hz is the frequency between the directly driven wheel and the indirectly drive wheel. If the models are tuned correctly and describe the mechanical system correctly, the eigenfrequencies should be in the comparison. The five-mass model and three-mass model contain both frequencies, and the two-mass model only contains 18 Hz. The difference between the models is shown in Figure 4.9. The comparison is made with their poles.

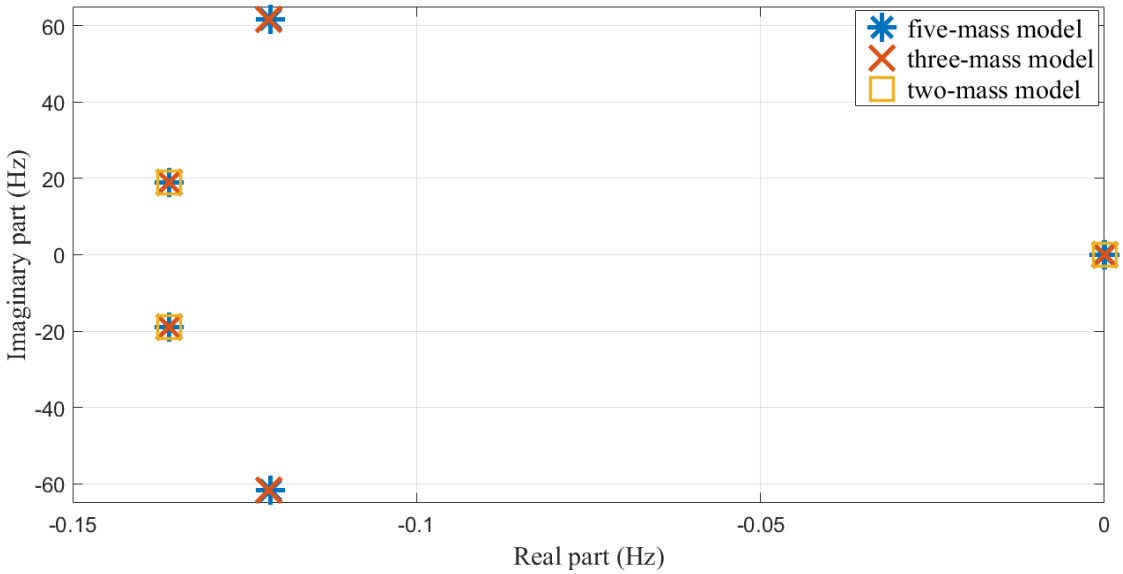

Figure 4.9 Comparison of the Models poles position

Bode plot is shown in Figure 4.10. The plots for the five-mass model and the three-mass model are almost identical. The plot of the two-mass model is different in a higher frequency that is not preserved in the model.

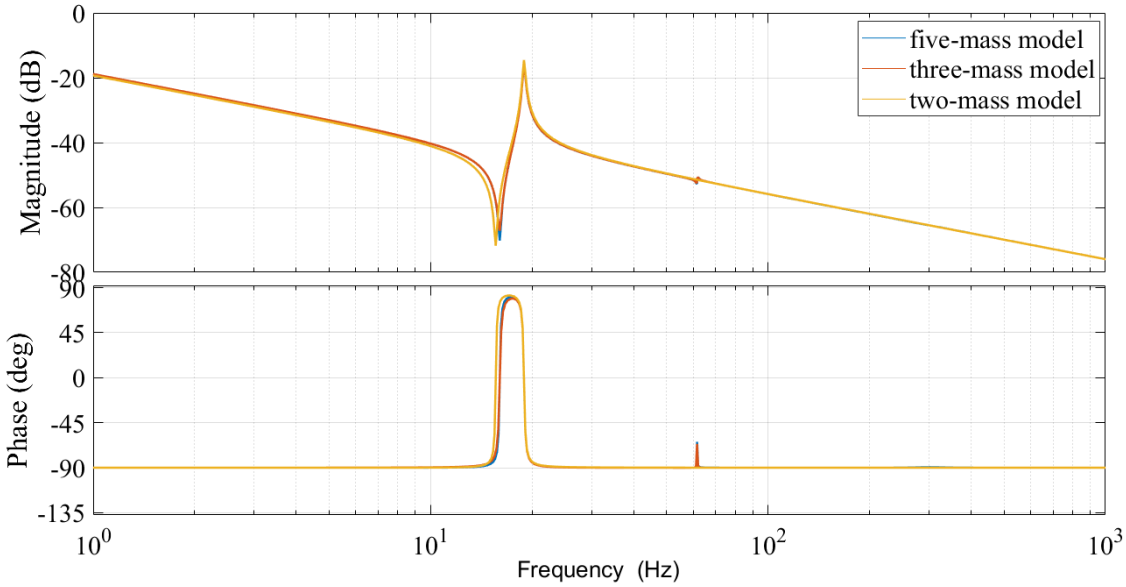

Figure 4.10 Bode plots of the five-mass model, three-mass model and two-mass model

4.2 Principle of the Slip Controller Simulation

The developed simulation model and the proposed slip controller have to be implemented into one simulation model during the model design of the slip controller. The block diagram of the simulation is depicted in Figure 4.11.

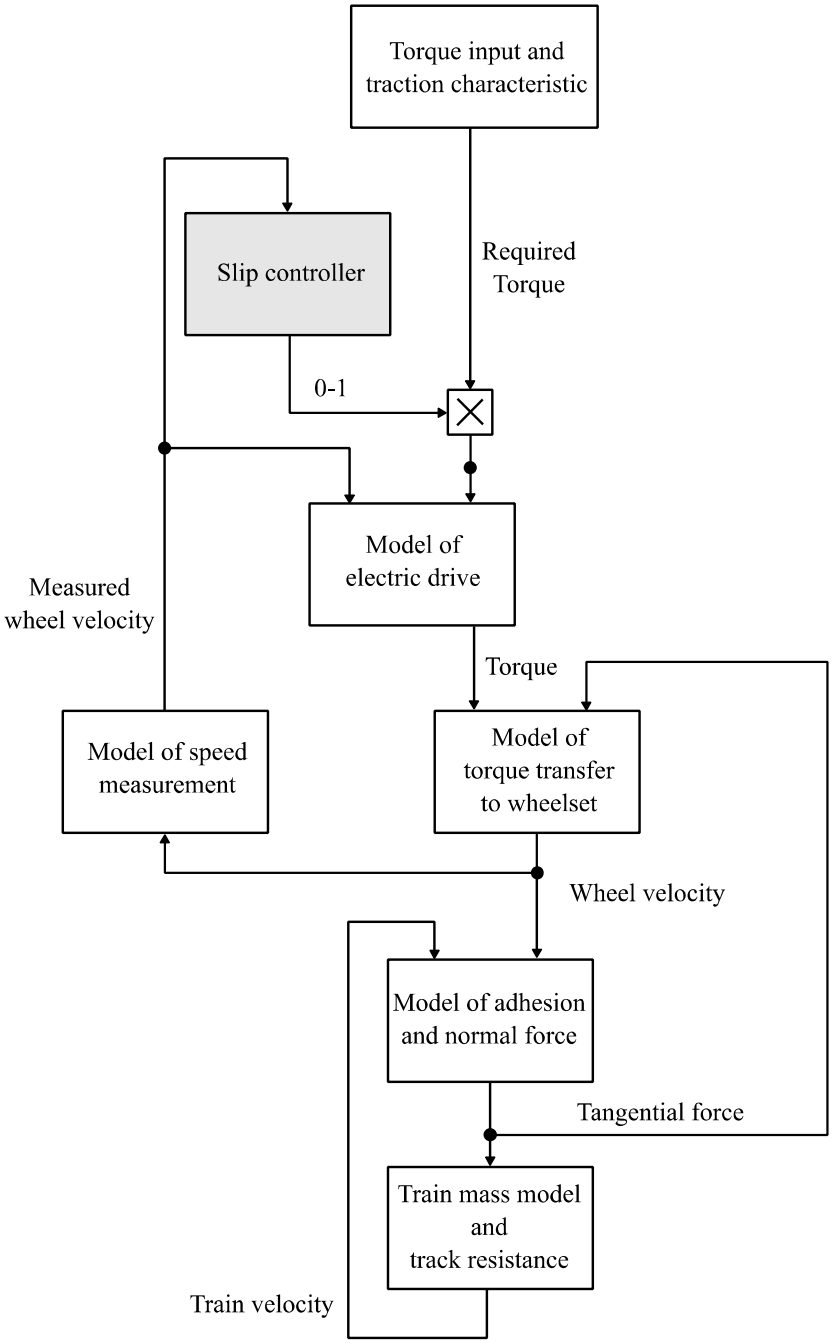

Figure 4.11 Simulation block diagram of one wheelset

The model input is the required torque value that is limited by a traction characteristic. The traction characteristic limits the required force according to train velocity due to the adhesion force dependence on the train velocity. The train velocity is calculated from the wheel velocity as it is calculated in a locomotive. The force is multiplied by the slip controller output that is limited to a value from 0 to 1. The limited force is led to the model of electric drive. The slip controller input is a measured wheel velocity. Model of electric drive generates a motor torque.

The motor torque is led to the model of a torque transfer to wheelset block. The block output is a wheelset velocity. The wheelset velocity is led to the model of adhesion and normal force and the velocity measurement. The model of adhesion and normal force generates an adhesion force that is led back to the model of torque transfer to wheelset and the block train mass and track resistance. The last block generates train velocity.

The block *Torque input and traction characteristic* is represented by a required tractive effort value that is present at the simulations begging. The required force is limited by the traction characteristic according to the train velocity. The train velocity generated by the train mass model and track resistance is not available in the real locomotive, and the train velocity is calculated from all wheelset velocity. However, the model simulates only one wheelset, and other wheelsets velocities are not available. Therefore, the train velocity for the block purpose is the wheelset velocity without slippage.

The block *Slip controller* is represented by a proposed slip controller, or it can be another slip controller if it is desired. The block contains an estimator model.

The block *Model of electric drive* is represented by a transfer function and time delay of the electric drive.

The block *Model of torque transfer to wheelset* contains the five-mass simulation model that is described in subchapter 4.1.1 in detail.

The block *Model of adhesion and normal force* is represented by equation (2.12) with a random disturbance of the normal force.

The block *Train mass model and track resistance* are represented by a train mass and the train resistance force F_R is calculated according to Davis formula in a form [82]:

$$F_R = k_0 + k_1 \cdot v_T + k_2 \cdot v_L^2 \tag{4.13}$$

Where k_0, k_1 and k_2 are coefficients.

The formula gains importance at high velocities. The coefficient k_0 can be associated with rolling resistance, k_1 with other mechanical resistance, and k_2 with the aerodynamic resistance [133].

The slip controller with the simulation model has to run simultaneously for simulation purpose. The problem of this simulation is that the simulation model has to be simulated in continues time, and the slip controller has to run in discrete time. The simulation model has to run in continues time to provide similar results as a measurement on the real locomotive. The slip controller has to run in discrete time to provide the almost identical results as an estimator implemented in a DSP. Moreover, the simulation model simulates a locomotive mechanical part, but a control part and measurement part have to run in the continuous model too. Therefore, the simulation model has to run in continuous time solver, and the estimator and the controller have to run in discrete time model. Models cooperation is depicted in Figure 4.12.

The whole model consists of a discrete time model, which is solved by a discrete time solver and a continuous time model solved by a continuous time solver. The superior solver is the discrete time solver, and its every step represents one locomotive control system period, e.g.

400 μs or 1 ms. The continuous solver runs once in one discrete time solver step. The simulation runs in a loop. A required torque is set up firstly. The continuous solver runs for one locomotive control system period, next. After that, the continuous time solver is stopped and is results are transferred to a discrete time solver. The discrete time solver processes the results in a *Measurement* block, *Estimator* block and *Controller* block. The required torque is adjusted by a controller output, and the one loop run is finished. The actual adhesion is modelled in the continues-time model according to actual velocity and pre-set adhesion coefficient that is set up in the discrete-time model. The blocks are simplified, and all signals and auxiliary blocks are not depicted in Figure 4.12.

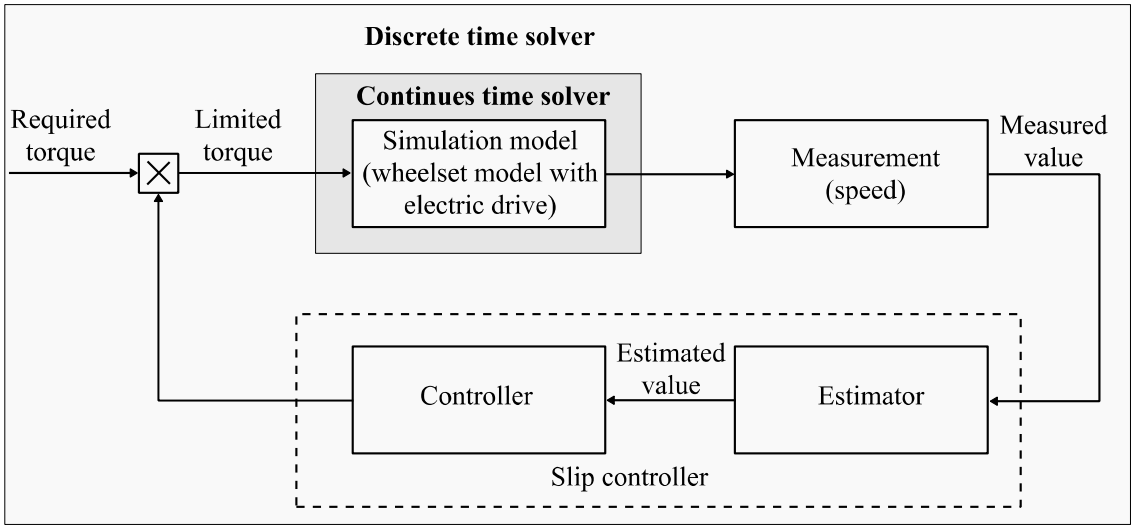

Figure 4.12 Simulation model and the slip controller implementation

4.3 Design Summary

The chapter describes the development tool for proposed slip controller development. The main part of the chapter describes mathematical models. The presented models describe one wheelset with an electric drive of the Skoda 93E locomotive. The five-mass model and three-mass models maintain the locomotive structure. The electric drive is replaced by the transfer function and time delay. Therefore, the type of used motor, inverter and control strategy can be simply changed by the electric drive model parameters. Therefore, the models can model a different locomotive with the same structural arrangement. The two-mass model does not maintain the locomotive structure, and after careful consideration, the model can be used for a different locomotive with a different structure. When any of the models are used for a different locomotive type the masses, damping and stiffness have to be replaced by proper values. The simulation model has to describe the real system with appropriate accuracy. The five-mass model is described as the simulation model in the chapter. The model eigenfrequencies correspond to eigenfrequencies identified on a locomotive. On the other hand, the estimator model has to be as simple as possible. The three-mass models and two-mass model are described in the chapter. The tree-mass model preserves the two most significant eigenfrequencies from the five-mass model. The two-mass model preserves only one eigenfrequency. The two-mass model is the most straightforward model from the described models. The models are compared between themselves in the chapter. The comparison is based on the system poles and Bode plot. Finally, the simulation implementation is described in the chapter.

5 SIMULATION RESULTS

The chapter describes the simulation results of the proposed slip controller. The simulations are mainly focused on the proposed slip controller with the UKF. However, the KF and EKF are also simulated to get a comparison between the slip controller performances with different estimators. The simulations are verified by measured data. The measurement and measured data are described first in the chapter. Then, simulations that verify the five-mass simulation model according to the measured data are presented. Next, the proposed slip controller verification is made in the simulation model and comparison with the slip controller with the KF and EKF and with conventional methods based on LO and DO are presented. Finally, the possibility of the slip controller implementation into a DSP is described.

5.1 Measured Data

The measured data were measured on a train with the electric locomotive Skoda 93E during the train operation. During measurement were recorded data that were measured by locomotive computer and data that were measured by additional sensors. The locomotive computer measured wheelsets velocity and tractive force. These data were available for the locomotive control. Position and velocity by GPS and acceleration measured by accelerometers were measured additionally. During one measurement were recorded pulses from incremental encoders to get non-filtered information about wheels velocity. This measurement was made because the locomotive computer provides filtered wheel velocity and many phenomena are hidden due to the filtration. This measurement enables to record torsion vibrations that occur during the slippage. Measurements of torsional vibrations between wheels were also made. The measurement was made by using barcodes that were glued on wheels and measured by the laser sensor.

5.1.1 Measurement Arrangement

The measurement configuration is shown in Figure 5.1. The block diagram describes one boogie, and the block consists of a DC/DC converter, two motors, gearboxes and incremental encoders. Every motor drives one wheelset. For simplicity, other parts are not depicted in Figure 5.1. Two types of signals led from the block. From the first signal is calculated entire wheelset torque. The second signal type is a quadrature signal from encoders. From the signals are calculated wheelset velocities in the locomotive computer. The data from the locomotive computer are sent through an RS-232. The laptop is connected to USB to the RS-232 converter. Data from accelerometers and GPS are sent to the laptop through USB. The accelerometers were mounted on the wheelsets during one measurement and in the locomotive cab during another measurement. During one measurement was measured a signal from an incremental encoder that was measured and recorded by a logic analyser. Therefore, the signals had to be offline synchronised.

5.1.2 Example of Measured Data

The locomotive is equipped with a re-adhesion controller. The re-adhesion controller switching off was not possible during measurements. Therefore, the measured data are affected by the re-adhesion controller reactions when slippages occur. The recorded tractive forces, wheels velocity, GPS velocity and altitude are shown in Figure 5.2. There are only shown velocities of the first and second wheelset from the first bogie, and the first wheelsets from the second bogie, signed as the third wheelset in Figure 5.2. There are shown slippages and reaction of

implemented re-adhesion controller in the figure. The second bogie was switched off. Recorded traction, brake and coasting modes are depicted in the figure.

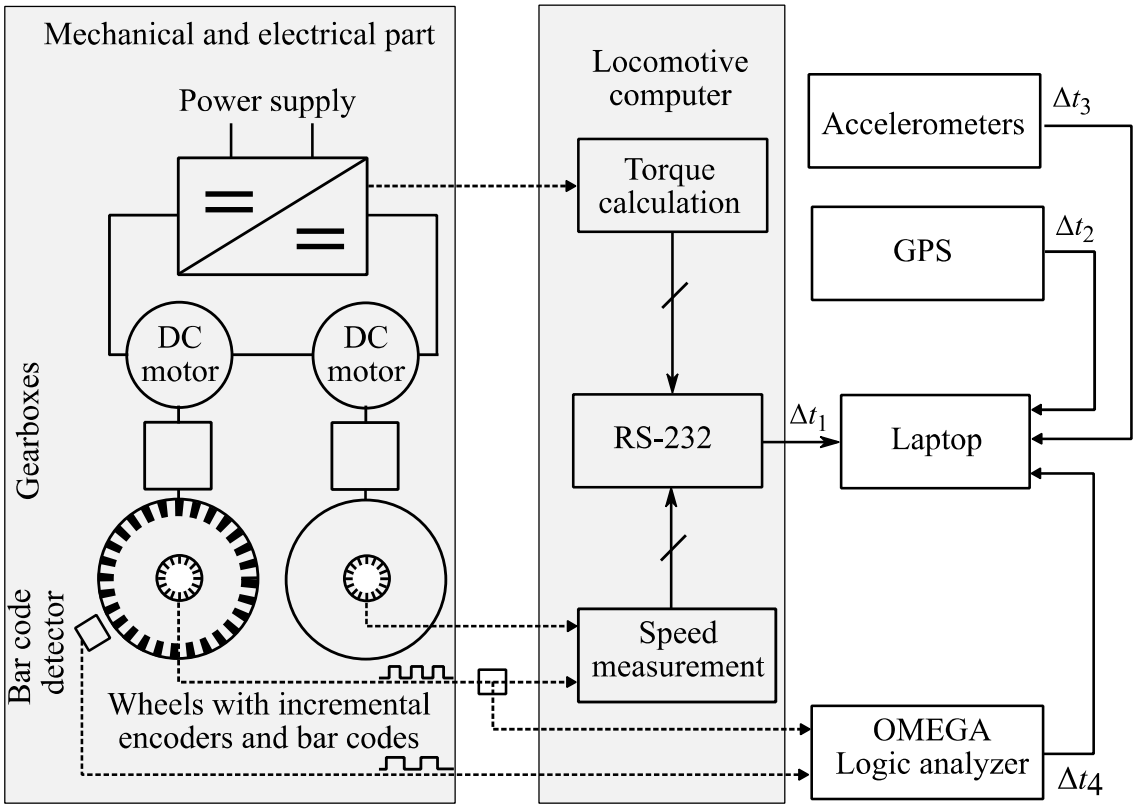

Figure 5.1 Measurement configuration

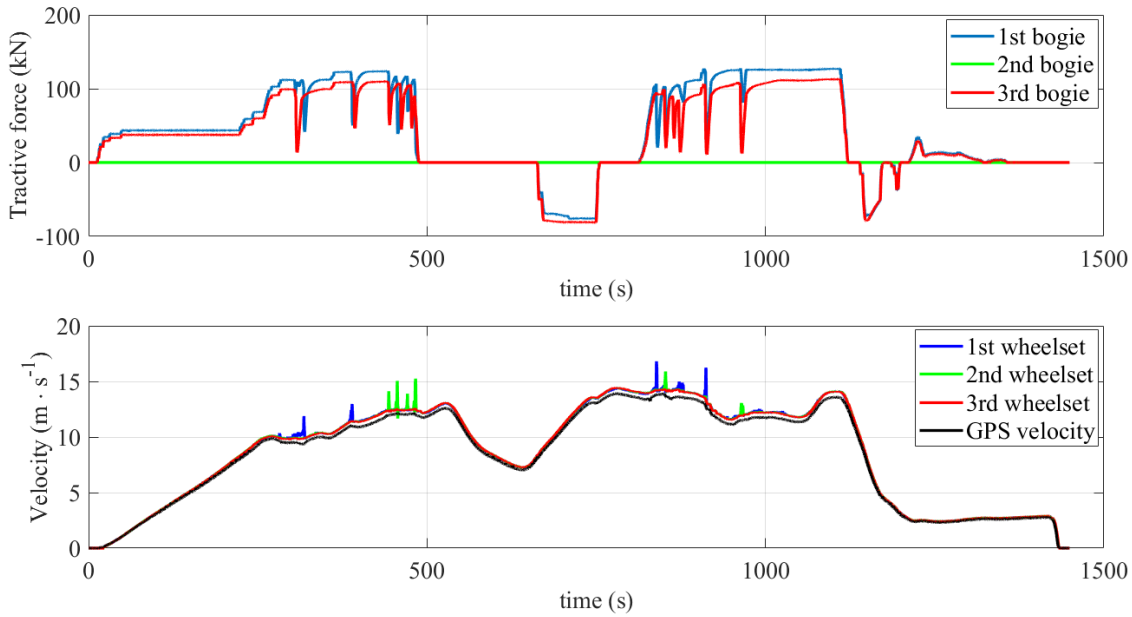

Figure 5.2 Example of measured data

Detail of measured data is shown in Figure 5.3. The detail shows the tractive force, first and second wheelsets velocity and a train velocity measured by GPS. Three slippages are shown in the figure. The slippages are suppressed by a re-adhesion controller that decreases a bogie tractive force by more than 80 % in the worst case. Every decrease of the tractive force lasts

several seconds. The re-adhesion controller decreases the tractive force to suppers the slippage at the beginning, and after that starts to increase the tractive force to the initial value. The applied tractive force is near the maximum transferable force. Therefore, when the force begins to approach to the initial force value, the new slippage occurs again. The re-adhesion controller cannot prevent the new slip generation.

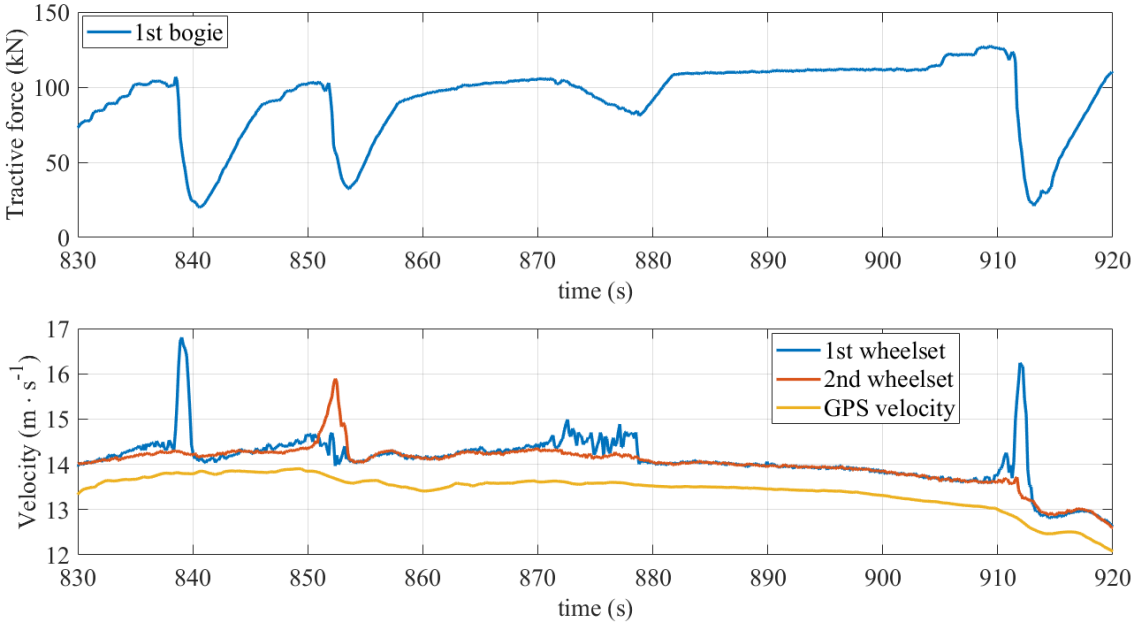

Figure 5.3 Detail of measured data

5.2 Comparison of the Simulation Model Output with the Measured Data

The subchapter aim is to demonstrate that the simulation model can produce similar results as measurement and thus can be simulation used as a locomotive model. The first slippage from Figure 5.3 shows Figure 5.4 in detail. The theoretical maximum adhesion force is also depicted in Figure 5.4. The adhesion force is calculated from the velocity measured by the GPS according to the Curtius and Kniffler formula. Therefore, the adhesion force does not decrease during the slippage even if it is evident that the adhesion force has decreased and also because that the actual adhesion force is not known. The depicted tractive force is recalculated from the bogie force to one wheelset force. The tractive force is near the maximum value of the adhesion force, and any decrease can cause the slippage. The tractive force decreases about 80 %, and the slip velocity is lower after slippage suppression than at the slippage beginning. The adhesion probably increased to the original adhesion-slip characteristic after the slippage suppression because if the adhesion-slip characteristic remains to the new adhesion-slip characteristic, the slip velocity should be higher due to the maximum point new position. This situation is possible because the slippage increasing part takes approximately 1 second and decreasing part also takes 1 second, and the train approximately moves about 24 metres that are enough to the adhesion condition of the track take change.

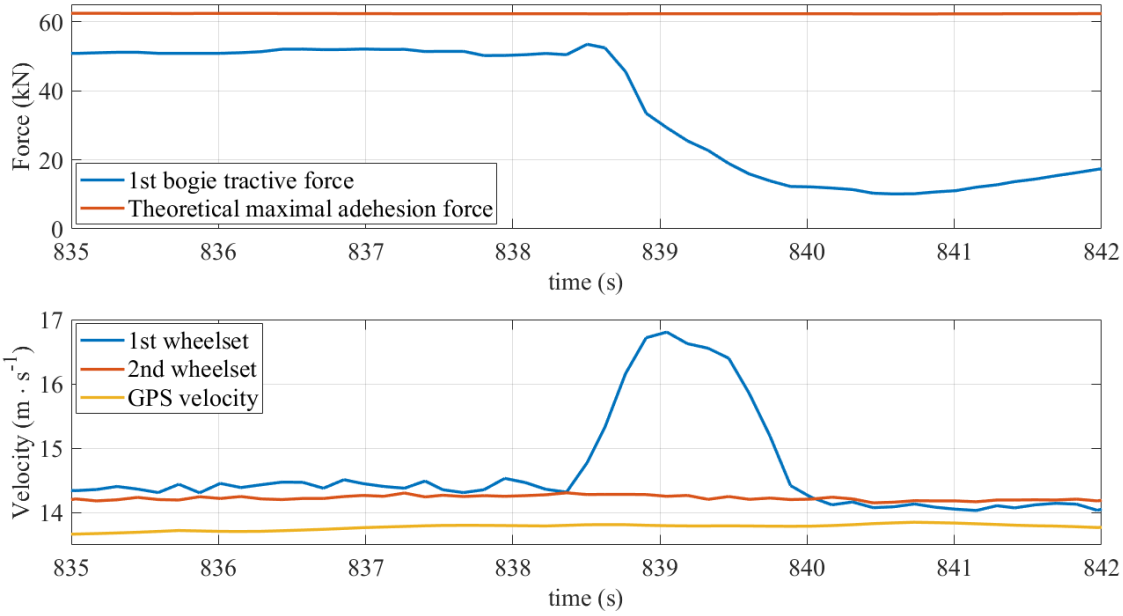

Figure 5.4 Detail of measured data with one slippage

The re-adhesion controller simulations of the designed five-mass simulation model are shown in Figure 5.5. The simulation is made to get the adhesion-slip characteristic parameters for the proposed slip controller and compare the model performance with the measured data. The wheel velocity contains random noise. The time course is similar to the measured data. The simulation results enable to calculate the adhesion. The adhesion force on real measurement is unknown. Therefore, the adhesion force in simulation results is only probable adhesion force. The adhesion coefficient starts to decrease at time 2.9 seconds with slope 125% per second for 0.5 second interval. The slip velocity starts to increase when the adhesion force decreases below the tractive force at time 3.1 seconds. The tractive force is decreased to reduce the slip velocity, and the tractive force decrease has to be high to reduce the slippage. The operating point trajectory derived from the adhesion-slip characteristic and the operating point trajectory derived from the tractive force is depicted in Figure 5.6. The operating point trajectory is calculated from internal adhesion coefficient, and it depicts the actual trajectory. The arrows show the direction of the operating point movement. The operating point trajectory that is calculated from the applied force is more extensive than the operating point trajectory calculated from the adhesion. The trajectories should be close to getting better performance. The static adhesion-slip characteristics are depicted in Figure 5.7. The original characteristic is marked as characteristic 1, and the characteristic during slippage is marked as a characteristic 2. The comparison between the measured data with simulation results is summarized in Table 5.1.

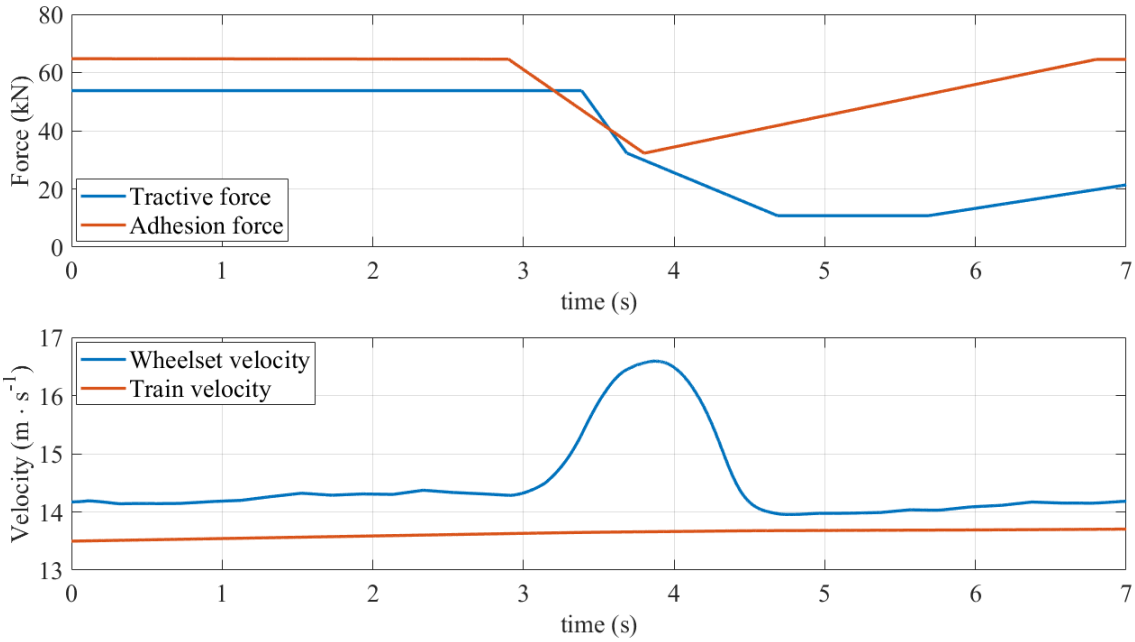

Figure 5.5 Simulation results for the re-adhesion controller

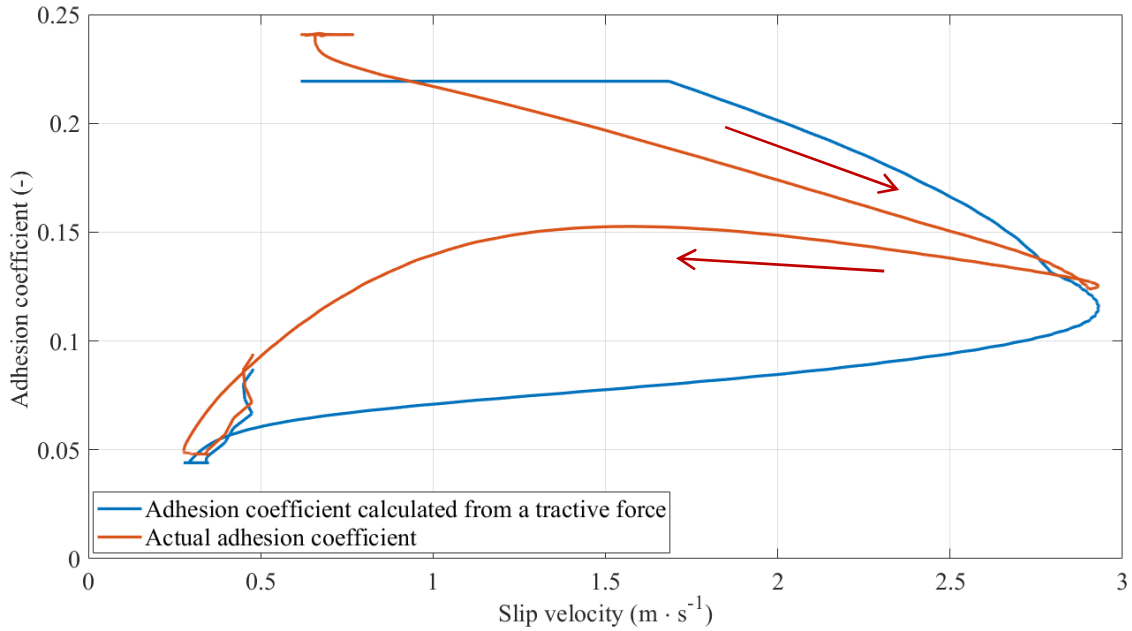

Figure 5.6 Operating point trajectory during simulation of the re-adhesion controller

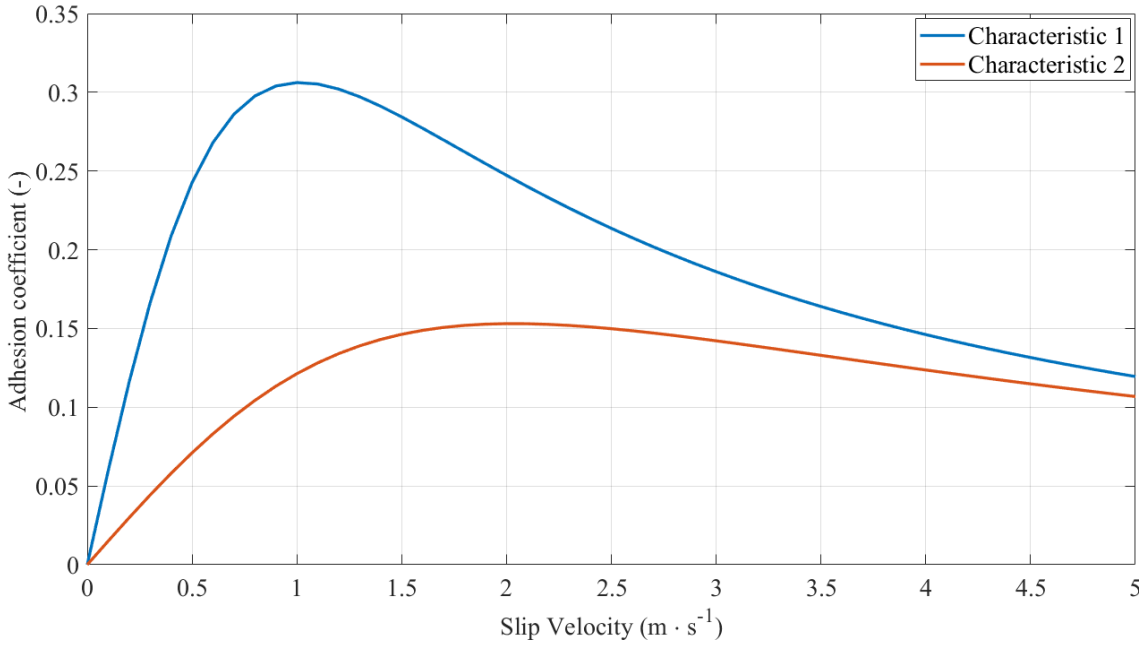

Figure 5.7 Static adhesion-slip characteristic used during simulation

Table 5.1 Model and measurement comparison

	Measurement	Simulation
Slippage duration (s)	1.65	1.7
Maximum slip velocity (m·s^{-1})	3.0	2.9
Maximum force decreasing (kN)	42.3	43.0

5.3 Proposed Slip Controller Performance

The proposed slip controller is based on the UKF. Therefore, the main simulations are made with the slip controller with the UKF. The proposed slip controller with the UKF is compared with the slip controller that is based on the KF and EKF. The comparison is made according to evaluation criteria, which are mentioned below. The criteria are divided into two groups. The first group of criteria evaluates the estimator performance without the slip controller control part, and the second group of criteria evaluates the slip controller. The first group of the criteria can be used for simulations and the measured data. The second group can be applied only to simulations.

The first group defines the estimator performance. All criteria are depicted in Figure 5.8. In this group is evaluated these criteria:

- The primary criterion is a detection time delay of an estimator output $t_{\mathrm{iOutDelay}}$. The time delay defines how fast the estimator enables to detect the beginning of the high slip velocity rising. The time delay is defined as a time between the slip velocity steps over a slip velocity threshold value v_{ST} to the estimator output decrease below defined required relative adhesion force. The velocity threshold is a velocity that traces a wheel velocity value, and its value is over velocity noise peaks. When the velocity exceeds the threshold value, the slippage occurs. The parameter is important because on it the controller settings depend.
- The second criterion is a required relative adhesion force value $i^{*}_{FAdhesion}$. The value is defined by the amplitude of an estimator output noise. The noise is transferred from the estimator input to its output. The input noise is caused by the measured velocity. The

criterion closely relates to the first criterion. The value is two times greater than maximum noise peaks detected in the part where no slippage occurs.

The second group of criteria evaluates the overall slip controller performance, i.e. the estimator with a controller. All criteria are depicted in Figure 5.9. In this group are evaluated these criteria:

- The train velocity v_L at the end of slippage is one of the most important parameters. The train velocity is measured one second after the slip velocity decreases below the slip velocity threshold. One second delay was chosen because there can be some transient oscillations when slippage is suppressed due to, e.g. a controller action.
- The slip velocity peak value v_{SPeak}. The value describes the maximum value of the slip velocity that reaches during a controller action when the slippage occurs. The value is measured against the slip velocity threshold v_{ST}.
- The time duration of the slippage t_s. The time is measured from the slippage start to its suppression. The time is measured from the time when the wheel velocity exceeds the velocity threshold v_{TS} to the time when the wheel velocity decreases below the threshold.
- Force drop F_{SDrop} is the maximum force drop due to a controller action.
- Power loss is a power P_{SLoss} that is converted to heat in a wheel-rail contact. The maximum power loss is calculated during the slippage. This parameter is connected to mechanical wear of wheels and rails.
- Impulse I_S during the slippage. This parameter better describes the tractive force decreasing than tractive force drop because the parameter takes into account the tractive force time course.

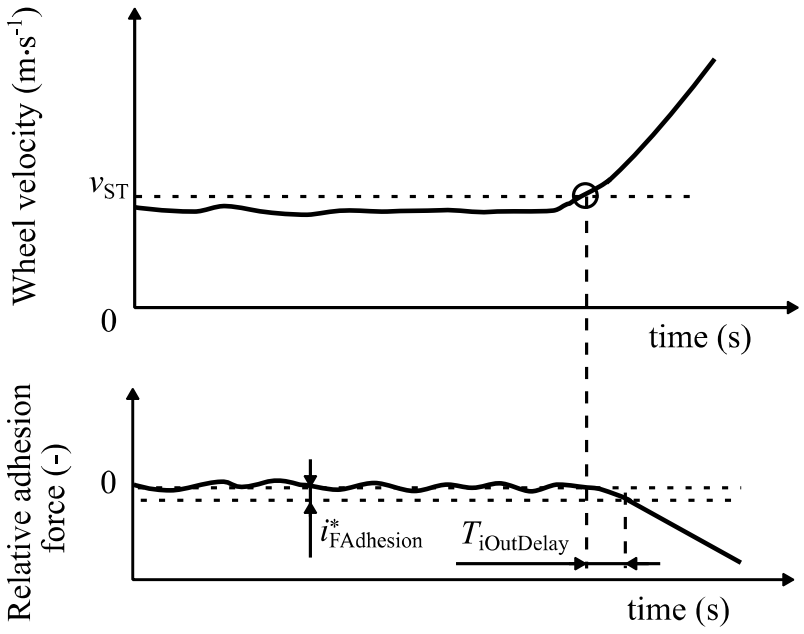

Figure 5.8 Estimator evaluation criteria definition

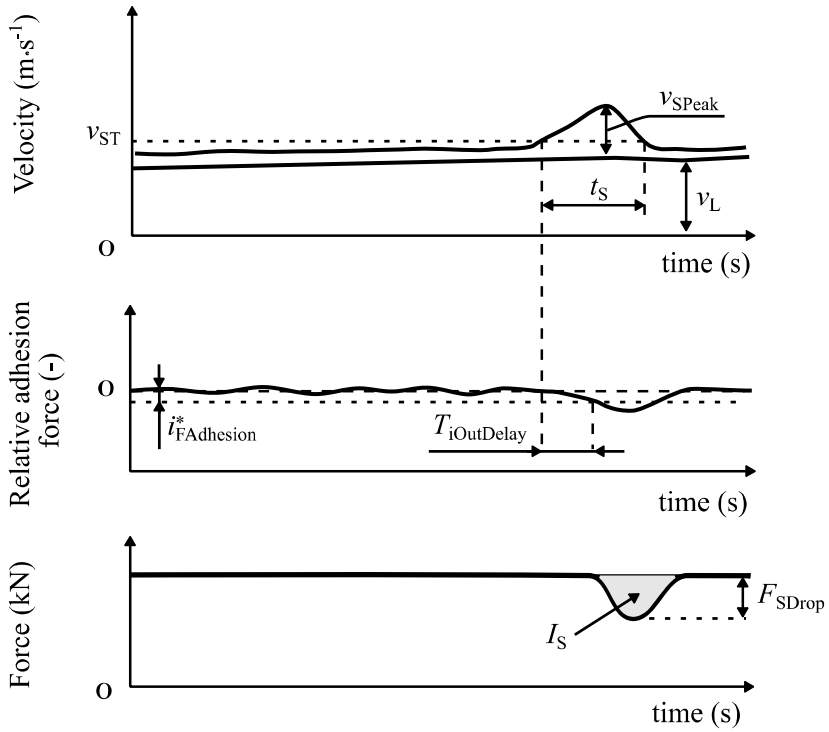

Figure 5.9 Slip controller evaluation criteria definition

5.3.1 Proposed Slip Controller Simulations on Measured Data

The proposed slip controller simulations with the UKF on measured data are made, and comparison with the KF, EKF are also made. The comparison is shown in Figure 5.10. There are compared the estimated relative adhesion force $i_{\mathrm{FAdhesion}}$ calculated by the proposed slip controller with different estimators. The comparison is made for UKF and the EKF without a nonlinear function. The EKF without nonlinear function provides the same results as the KF, and the UKF provides very similar results. The difference occurs when slippage occurs. This comparison is made to demonstrate that the filters have the same settings and are correctly set up.

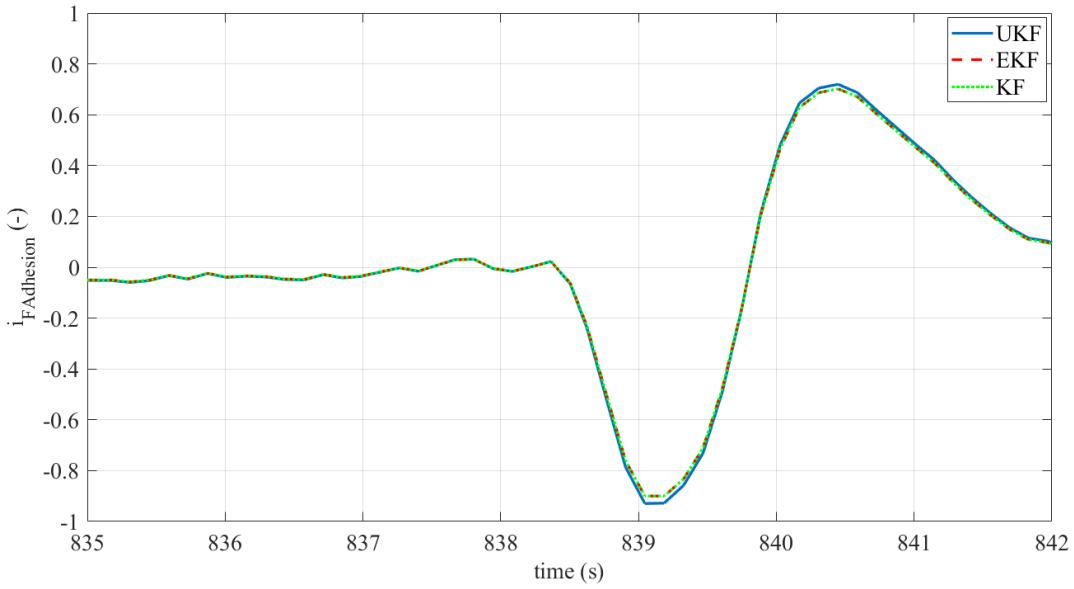

Figure 5.10 Proposed slip controller simulations with different estimators without nonlinear function

When the nonlinearity is implemented to the UKF and EKF algorithm, the estimated relative adhesion force start decreases more. The situation is depicted in Figure 5.11. The time course for the KF is the same as it is depicted in Figure 5.10 because the nonlinearity is not implemented into the KF. The UKF and EKF have similar time course. The noise level is approximately the same for all filters. However, the UKF has higher offset than the EKF and KF. Therefore, the filters have the time $t_{\text{iOutDelay}}$ the same. The proposed slip controller with different filers is summarized in Table 5.2.

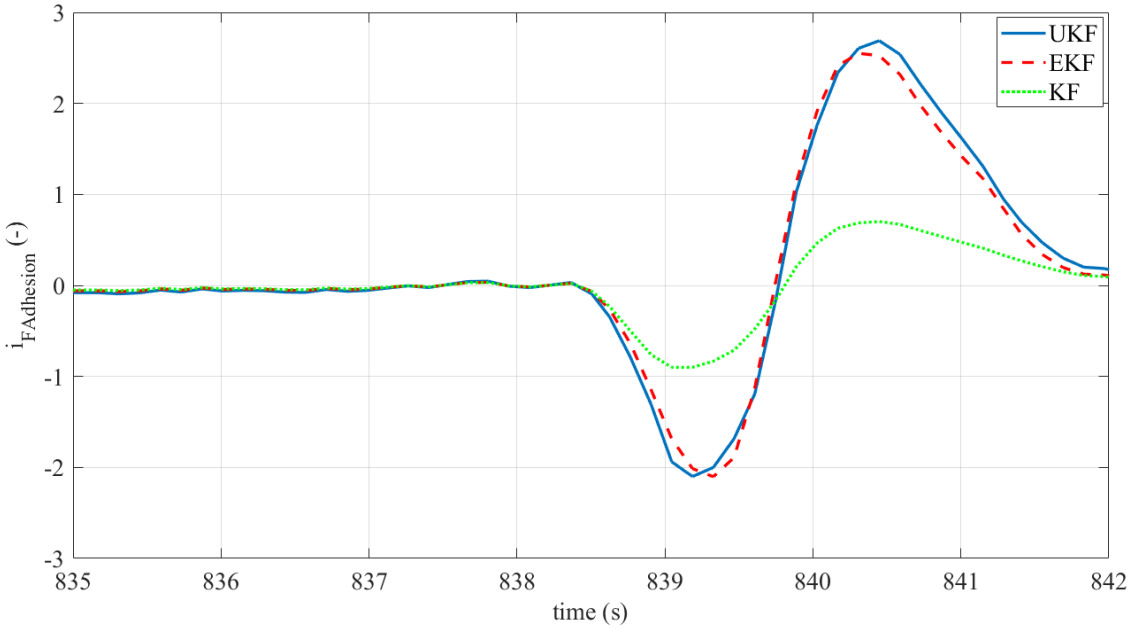

Figure 5.11 Proposed slip controller simulations with different estimators with nonlinear function

Table 5.2 Summary of the proposed slip controller performance with different filters with nonlinear function

Estimator	$t_{\text{iOutDelay}}$ (s)	$i^*_{FAdhesion}$ (-)
KF	0.02	-0.05
EKF	0.02	-0.05
UKF	0.02	-0.05

5.3.2 Proposed Slip Controller Simulations on the Mathematical Model

The simulation results for the proposed slip controller based on a UKF are depicted in Figure 5.12. The adhesion conditions are the same as for the re-adhesion controller verification. The slip controller reacts when the adhesion force starts to decrease, and the applied force does not exceed the adhesion force in the simulation. Therefore, the slippage does not occur. The increase of the slip velocity is small, and it is almost the same as the noise. Therefore, the same time course without noise is depicted in Figure 5.13. The UKF initial state vector is also depicted in the figure. The next simulations are made without noise and figures have the same scale as the Figure 5.5 and Figure 5.6 for better clarity and easier comparison. The trajectory of the operating point is depicted in Figure 5.14. The trajectories of the operating points are closer when the proposed slip-controller is used than in the re-adhesion controller case. The operating point returns to the stable area just below the actual adhesion-slip characteristic. The PI controller constants and the UKF parameters are given in Table 5.4.

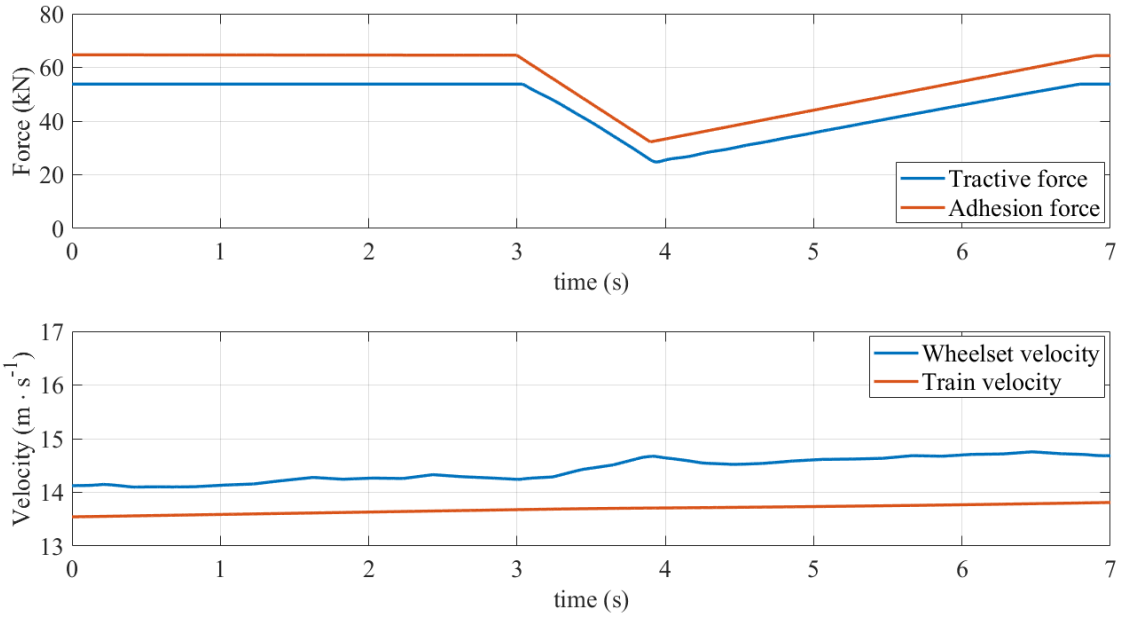

Figure 5.12 Simulation results of the proposed slip controller based on the UKF with noise on the wheel velocity

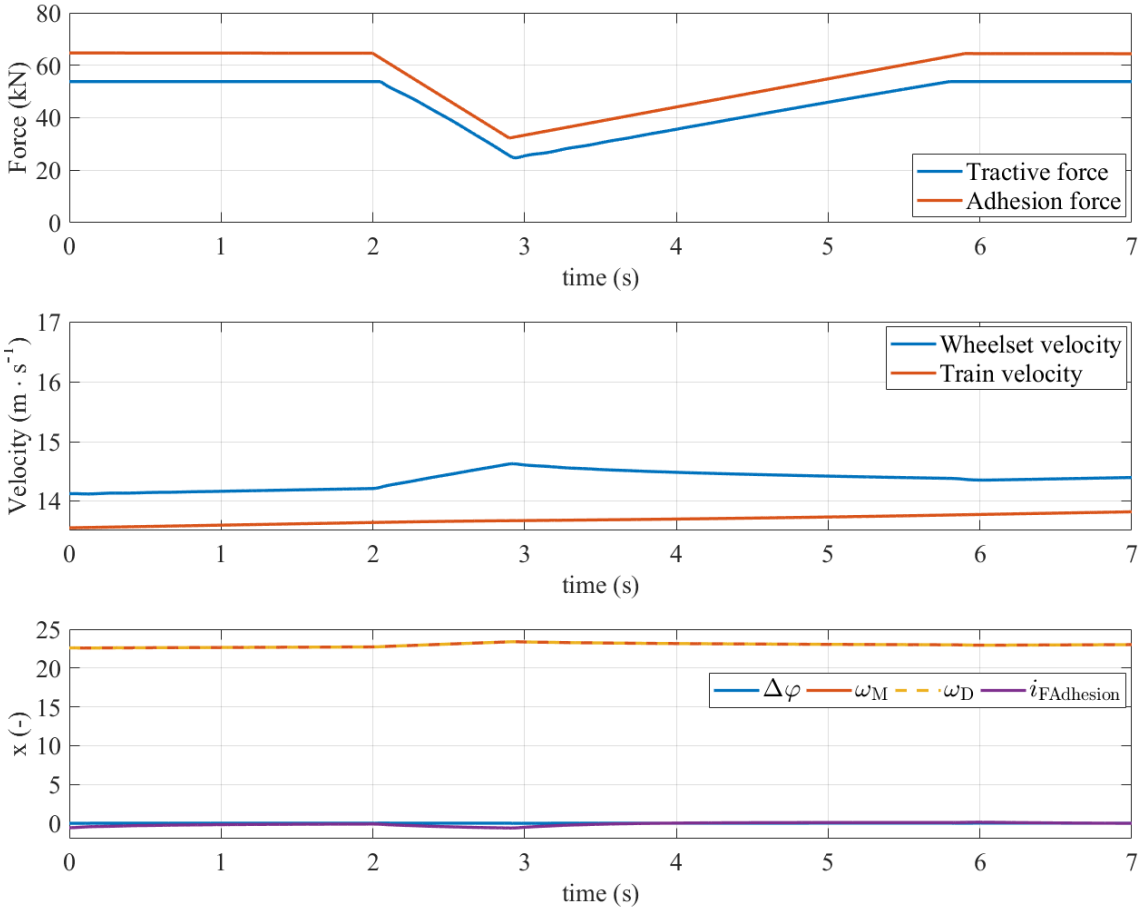

Figure 5.13 Simulation results of the proposed slip controller based on the UKF without noise

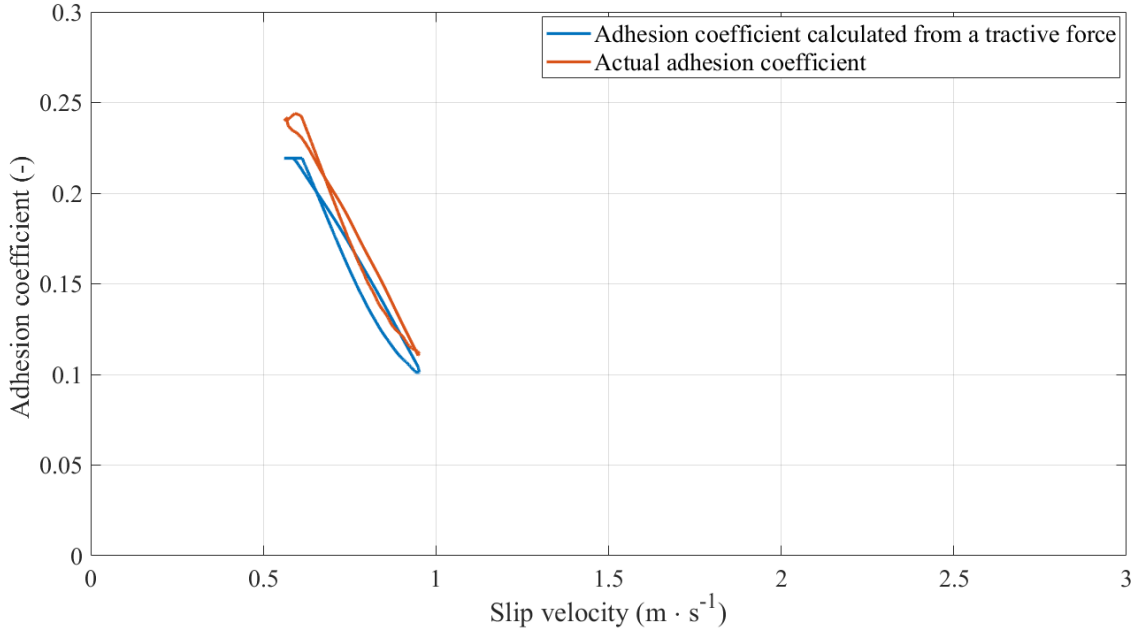

Figure 5.14 Operating point trajectory during simulation of the proposed slip controller based on the UKF

The simulation results for the EKF are depicted in Figure 5.15. The time course is only depicted because the results are very similar to the UKF because the behaviour of the filters is also very similar. Therefore, there is no difference between the proposed slip controller with the UKF and the EKF in this particular case.

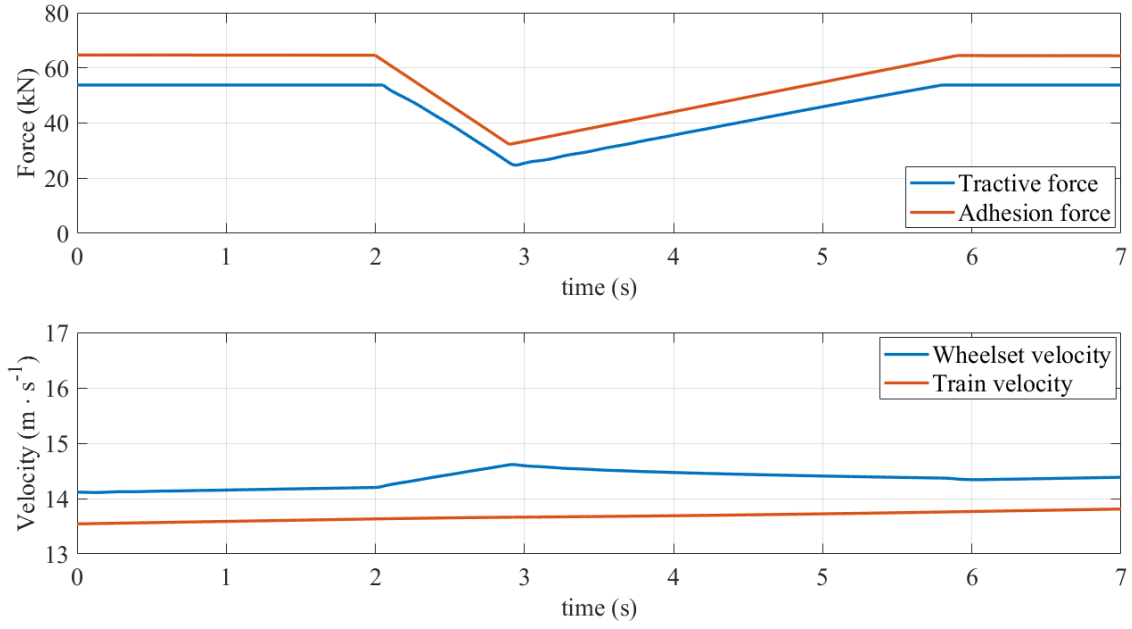

Figure 5.15 Simulation results of the proposed slip controller based on the EKF

The simulation results for the proposed slip controller with a KF are depicted in Figure 5.16 and Figure 5.17. The KF has different controller settings than the UKF and EKF because the KF starts to oscillate when the settings for the UKF are used. The different settings cause higher slip velocity because the controller reaction is delayed. The delay causes the higher power loss in

the contact area than the UKF. The adhesion utilisation is also worse because the operating point trajectory of the KF is broader than the UKF.

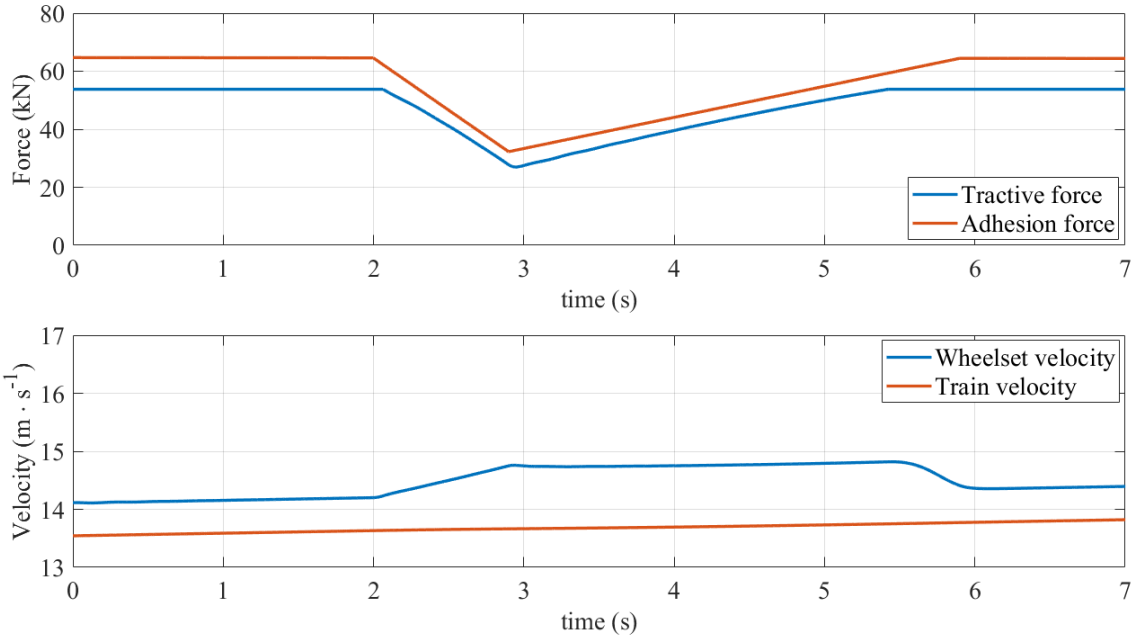

Figure 5.16 Simulation results of the proposed slip controller based on the KF

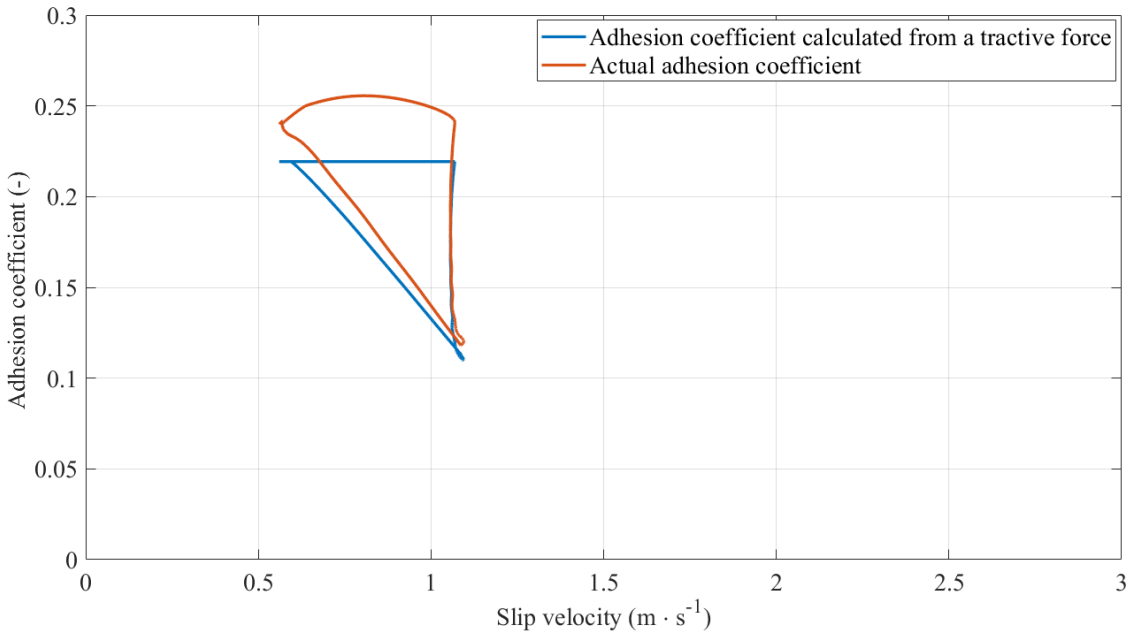

Figure 5.17 Operating point trajectory during simulation of the proposed slip controller based on the KF

5.3.3 Other Slip Controller Simulations on the Mathematical Model

The simulations of conventional slip controllers that estimates the adhesion-slip characteristic slope that are based on the DO and LO are included in this subchapter to be possible to compare the proposed slip controller performance with the widely used slip controllers. The slip controllers presented in the subchapter are conventional and they estimate the adhesion force. Therefore, the derivative calculation is required to get the adhesion-slip characteristic slope.

The simulation results for the zero-order DO are shown in Figure 5.18 and Figure 5.19. The slip controller based on the DO causes higher tractive force decrease that takes a long time, and the force does not reach the original value at the end of the simulation. The force increases gradually due to the controller different setting. The controller has to have the different setting because the slip controller causes oscillations when the controller is fast.

The simulations results for the LO are depicted in Figure 5.20 and Figure 5.21. The slip controller does not decrease the applied force so much. However, the slip velocity is high although the slippage does not occur. Moreover, the output of the LO oscillates.

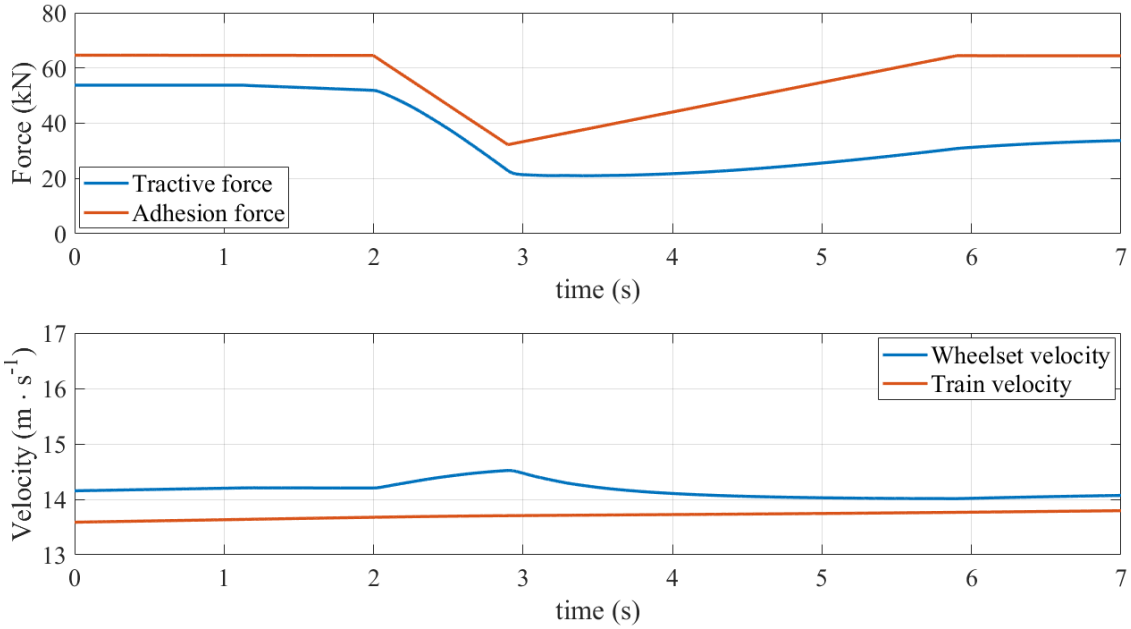

Figure 5.18 Simulation results of the proposed slip controller based on the DO

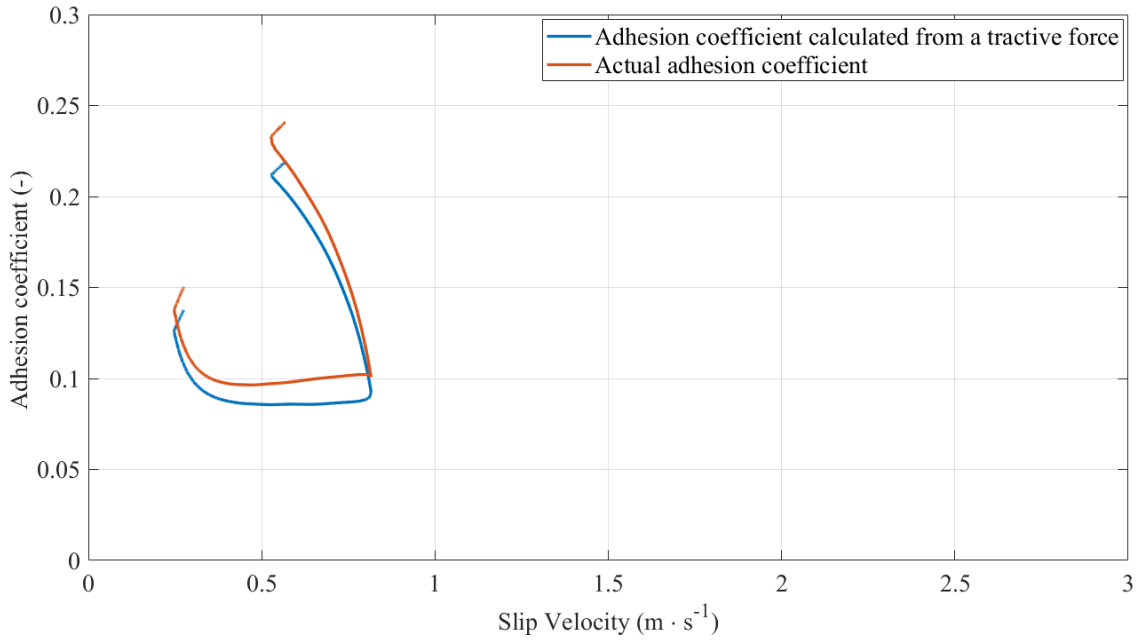

Figure 5.19 Operating point trajectory during simulation of the proposed slip controller based on the DO

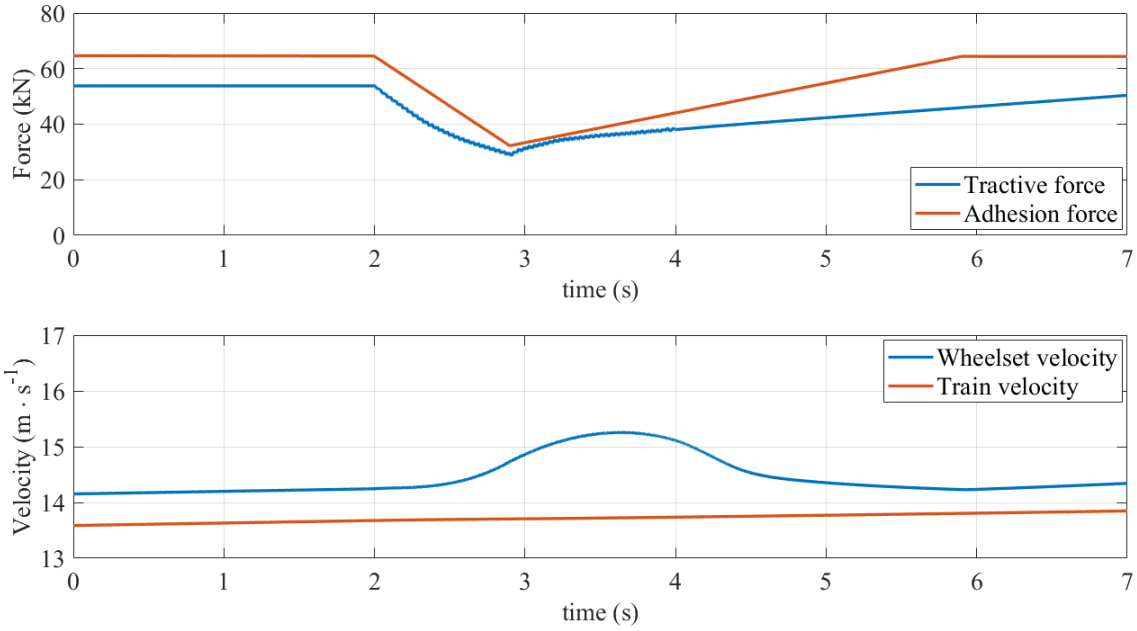

Figure 5.20 Simulation results of the proposed slip controller based on the LO

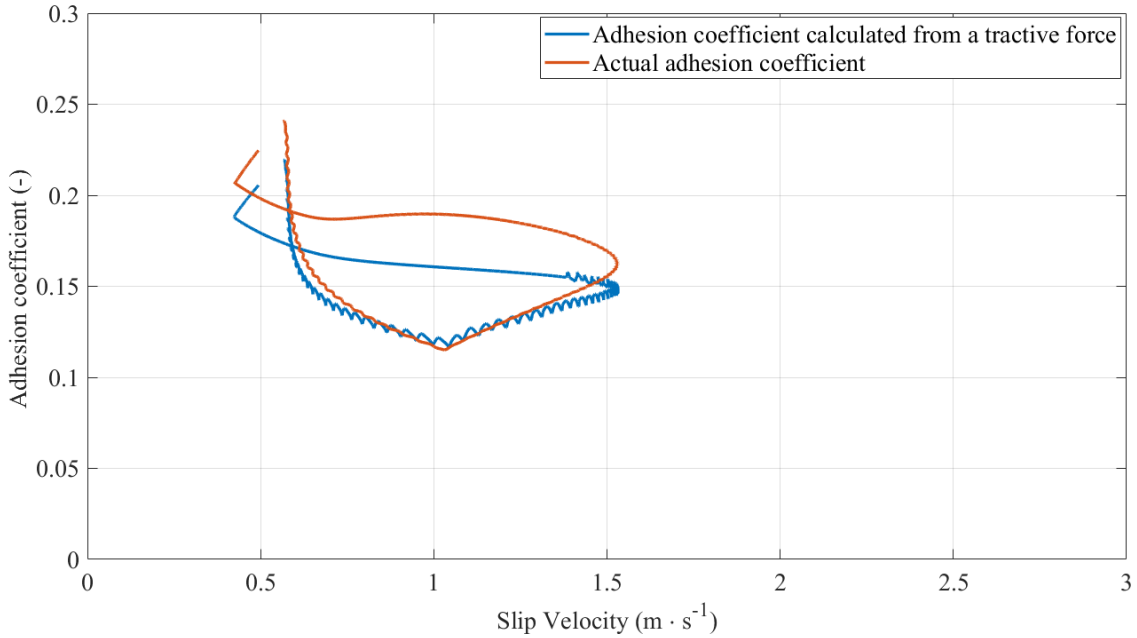

Figure 5.21 Operating point trajectory during simulation of the proposed slip controller based on the LO

5.3.4 Slip Controllers and Re-adhesion Controller Comparison

Comparisons of the proposed slip controller with different estimators, conventional slip controllers and the re-adhesion controller used in the locomotive are in Table 5.3. The slip controllers setting is summarised in Table 5.4. The comparison is made according to the defined evaluation criteria. The relative adhesion force is not available for the re-adhesion controller, and the estimator output delay cannot be defined. Therefore, the tractive force decreasing is used instead of the relative adhesion force that can be longer. The slippage does not occur when the slip controllers were used, therefore, the time duration of the slippage is not defined for the slip controllers and it is only used for the re-adhesion controller.

The shortest time of the estimator output delay have the conventional estimators. The proposed slip control method based on the UKF and EKF have slightly higher time and the KF has two times longer time delay than the UKF and EKF due to the different controller settings. The train velocity is the same for all types of used estimators in the proposed slip controller. The train velocity, when the proposed slip controller is used, is about 0.1 $m \cdot s^{-1}$ higher than the conventional slip controllers and 0.2 $m \cdot s^{-1}$ higher than the re-adhesion controller. The slip velocity peak is almost the same in the proposed slip controller and in the conventional method based on the DO. The slippage does not occur during the proposed slip controller simulations. The proposed slip controller based on the UKF and EKF have lower maximum power losses than the KF. The KF has higher power loss due to the higher slip velocity that occurs at higher adhesion coefficient value than in the UKF and EKF case. Low power loses has the conventional method based on the DO. The method based on the LO has similar power loses as the proposed slip controller based on the KF. However, the highest power loss has the re-adhesion controller.

Table 5.3 Slip controllers and re-adhesion controller comparison

Method	$t_{iOutDelay}$ (s)	$i^*_{FAdhesion}$ (-)	v_L ($m \cdot s^{-1}$)	v_{SPeak} ($m \cdot s^{-1}$)	t_s (s)	P_{SLoss} (kW)	F_{SDrop} (kN)	I_S (kN·s)
UKF	0.03	-0.1	13.9	0.4	-[2]	30	33	62
EKF	0.03	-0.1	13.9	0.4	-[2]	30	33	62
KF	0.06	-0.05	13.9	0.55	-[2]	73	31	63
DO	0.02	-0.25	13.8	0.33	-[2]	39	37	151
LO	0.02	-0.25	13.8	0.93	-[2]	70	29	47
Re-adhesion	0.35[1]	-	13.7	2.96	1.4	105	50	337[3]

[1] The relative adhesion force is not available for the re-adhesion controller. Therefore, the tractive force decreasing is used instead of the relative adhesion force.
[2] The slippage does not occur.
[3] The high value is caused by the re-adhesion controller gradual ramp, and the tractive force increase takes almost 8 seconds

Table 5.4 Slip controllers settings

Parameter	UKF	EKF	KF	DO	LO
k_I	0.002	0.002	0.01	0.004	0.002
k_P	0.5	0.5	0.5	0.05	0.5
k_C	0.004	0.004	0.02	0.08	0.004
$i^*_{FAdhesion}$	-0.1	-0.1	-0.05	-0.25	-0.25
Q	diag(10, 1, 1, 1)	diag(10, 1, 1, 1)	diag(10, 1, 1, 1)	-	-
R	0.01	0.01	0.01	-	-
α	1	-	-	-	-
β	2	-	-	-	-
κ	0	-	-	-	-
K_s	0.72	0.72	-	-	-

5.3.5 Simulations during Different Conditions of the Proposed Slip Controller

The simulations with multiple slippages were made. The simulations settings are the same as in the previous chapter, and the settings are described in Table 5.4. The multiple slippages are frequent as it is shown measured data in Figure 5.2. However, the multiple slippages in Figure

5.2 are caused by the re-adhesion controller improper work. The multiple slippages in the next figures are caused by the adhesion decrease because the proposed slip controller cannot cause the multiple slippages as the re-adhesion controller. The simulation results are shown in Figure 5.22 for the slip controller with the UKF. The slippages are eliminated in its beginning, and the true slippage does not occur. The slippages begin at different train velocity. The slip controller reaction is the same in all cases. The simulation results for the EKF are similar to the UKF. The simulation results for the KF are depicted in Figure 5.23.

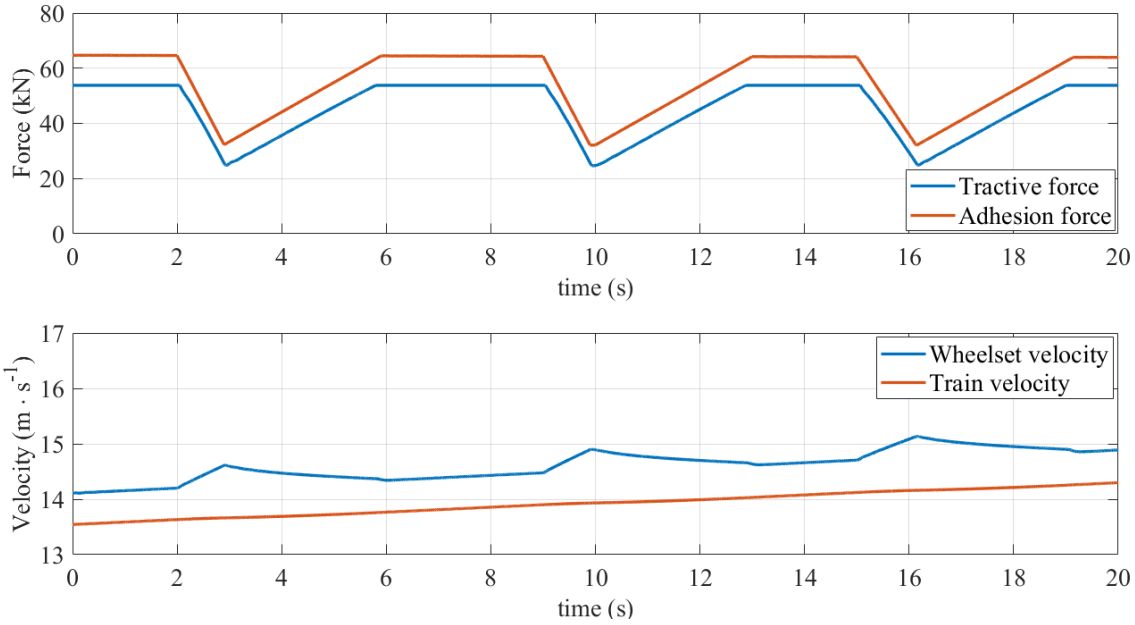

Figure 5.22 Simulation results of the proposed slip controller based on the UKF with multiple slippages

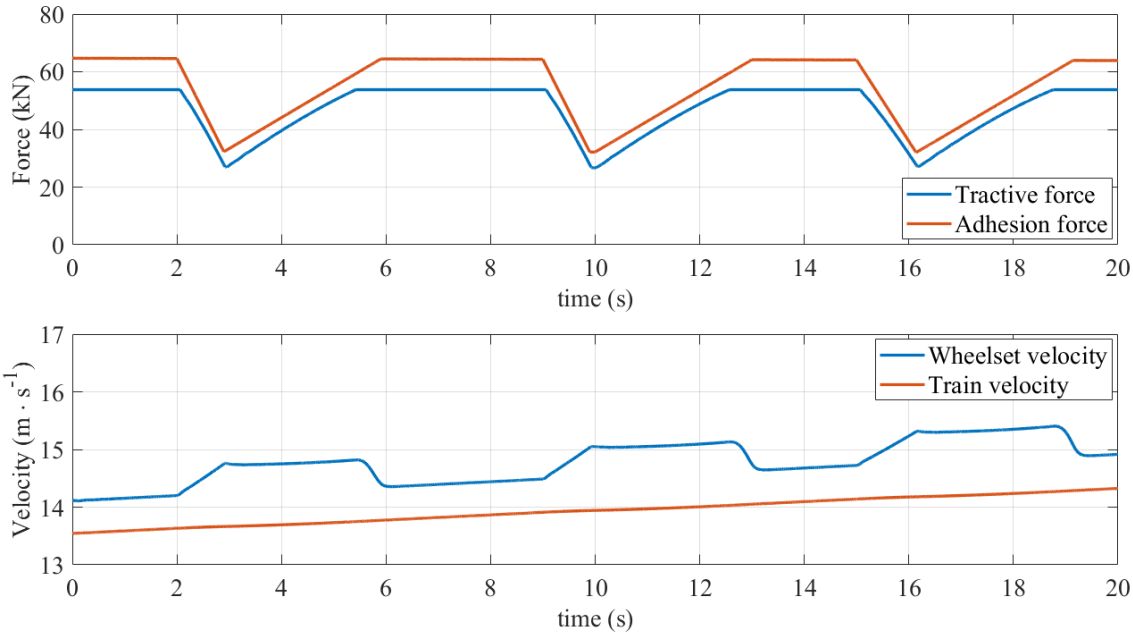

Figure 5.23 Simulation results of the proposed slip controller based on the KF with multiple slippages

The simulations results for a case when the locomotive goes from tractive mode to coasting and back to the tractive mode are shown in Figure 5.24 and Figure 5.25. The tractive force decreases and increases in a ramp function that is provided by a locomotive computer. The simulation results for the slip controller based on the UKF and EKF are the same, and the simulation result for the UKF is depicted in Figure 5.24, and for the KF in Figure 5.25. The slip controller based on the KF does not react, but the slip controller based on the UKF limits the applied force at high values. Therefore, the wheel velocity is higher when the KF is used, but the train velocity is almost the same at the end of the simulation. Therefore, the KF causes higher slip velocity.

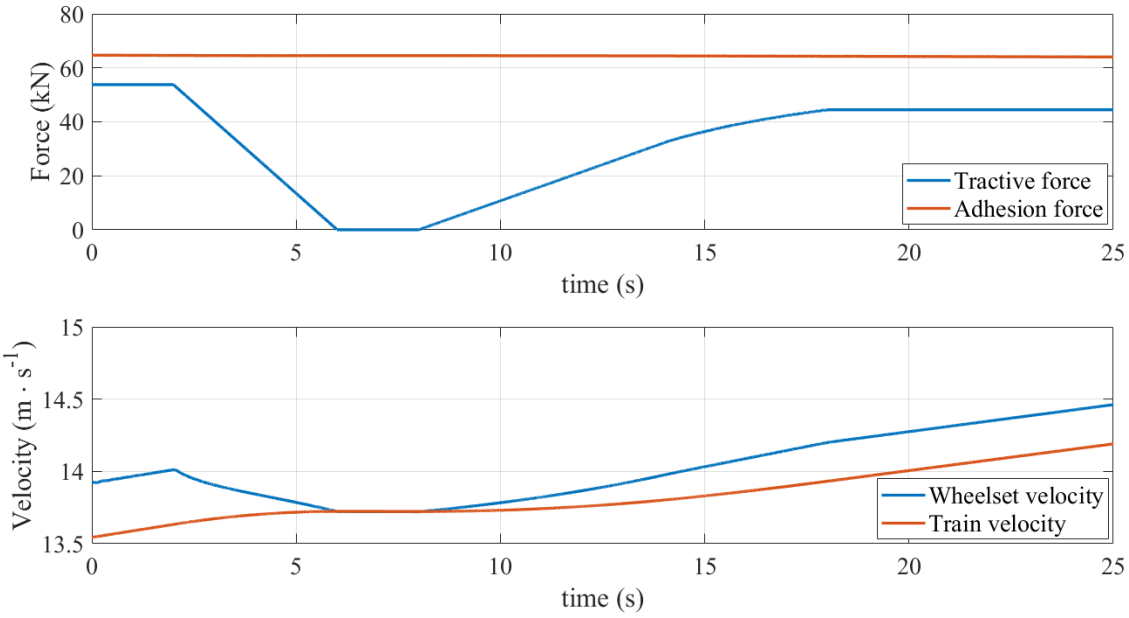

Figure 5.24 Simulation results of the proposed slip controller based on the UKF when train goes to from tractive to coasting mode and back

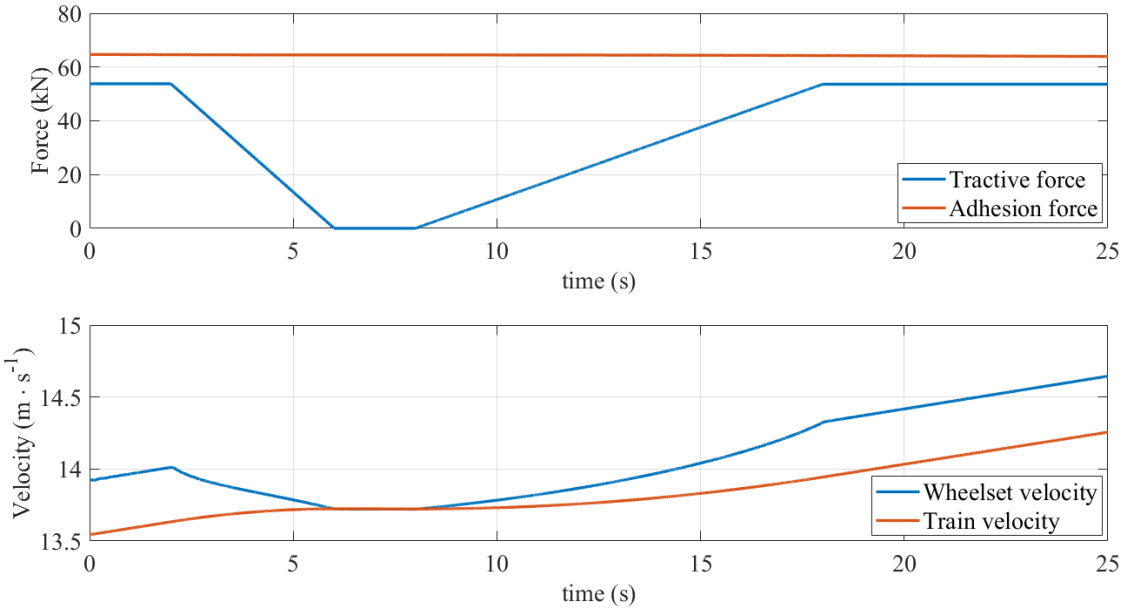

Figure 5.25 Simulation results of the proposed slip controller based on the KF when train goes from tractive to coasting mode and back

The simulation results for a case when the train goes from coasting to traction with a ramp that is steeper than the ramp depicted in previous figures is depicted in Figure 5.26 to Figure 5.28. The slip controller based on the UKF works correctly and the oscillations in the velocity time course at the beginning are damped as it is shown in Figure 5.26. The corresponding state vector time course is also depicted in Figure 5.26. The variable $i_{\mathrm{FAdhesion}}$ is negative due to the step torque function. The slip controller based on the EKF is depicted in Figure 5.27. The slip controller fails due to the EKF divergence in the case as it is shown in the state vector. The EKF has the highest train velocity at the end of simulation due to the EKF failure. The EKF divergence limits the controller setting of the slip controller and if a faster controller is used the slip controller can fail. The problem with the EKF divergence can be solved by adding limitations to the EKF computation. However, the adding of the limitations requires considering the influence to the slip controller performance. The slip controller with the KF is depicted in Figure 5.28. The slip controller works correctly, and the behaviour is similar to the UKF.

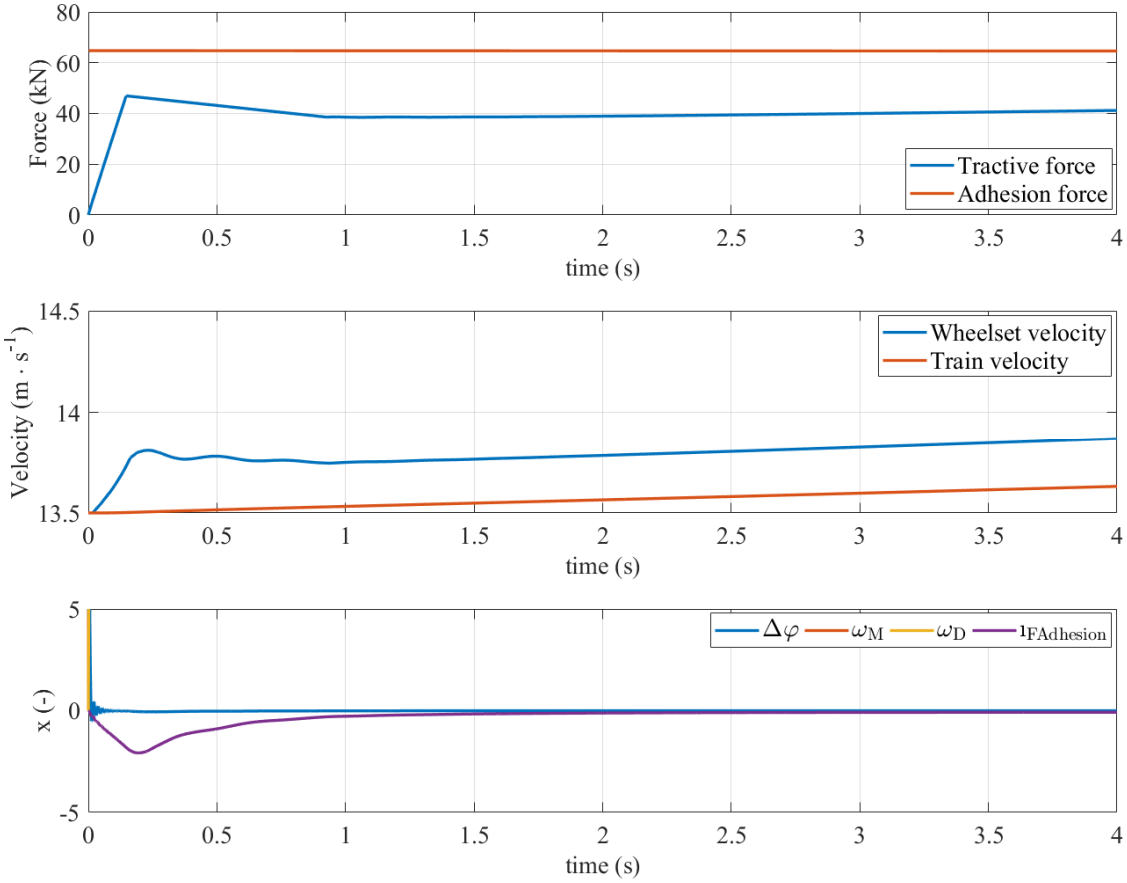

Figure 5.26 Slip controller start after reset with the UKF

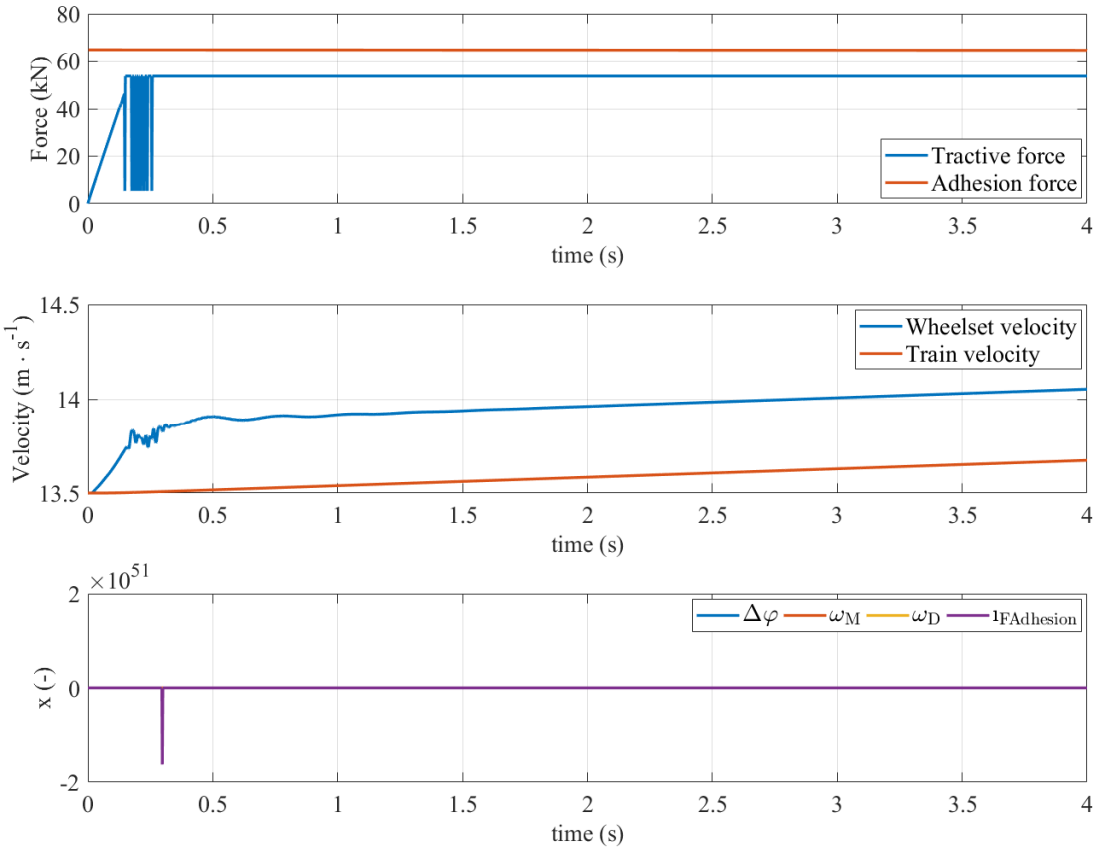

Figure 5.27 Slip controller start after reset with the EKF

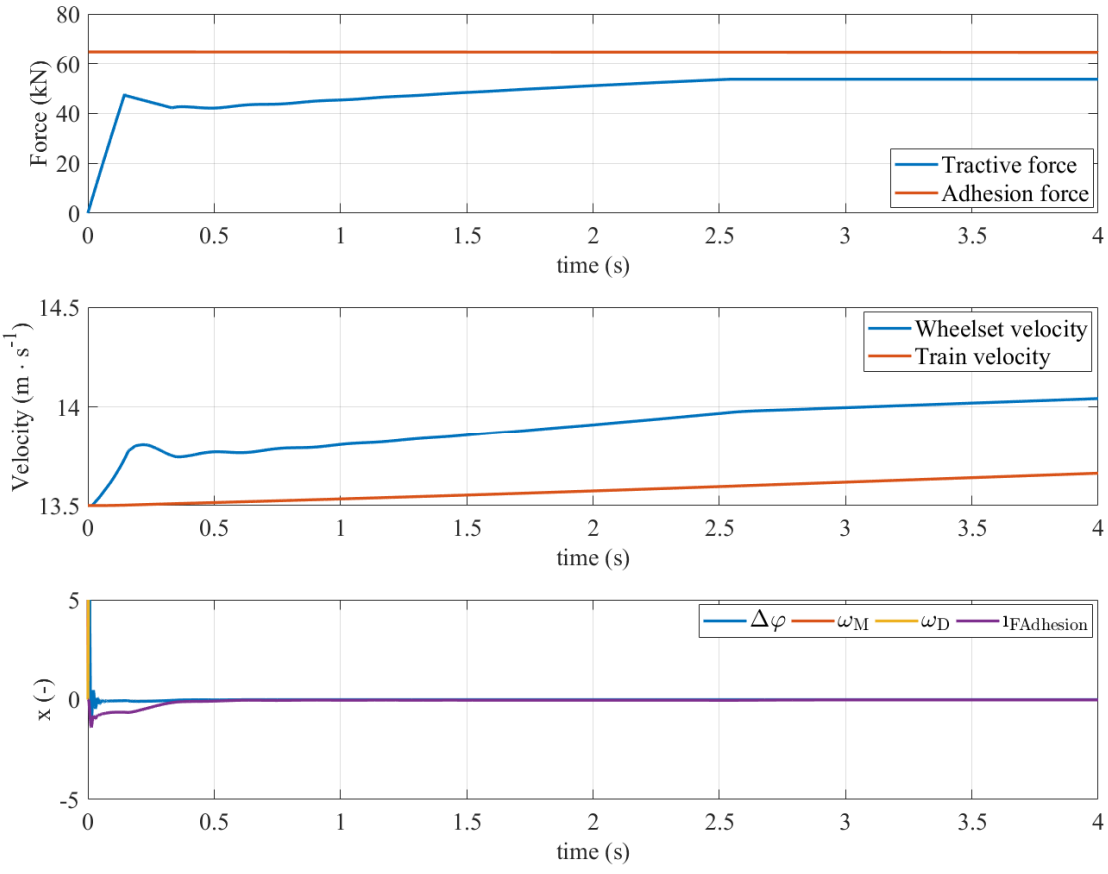

Figure 5.28 Slip controller start after reset with the KF

The locomotive starting from zero speed for the proposed slip controller based on the UKF is depicted in Figure 5.29 and Figure 5.30. The adhesion force, applied force, wheelset velocity, train velocity, measured velocity, estimated velocity and state vector are depicted in the figures. The wheelset velocity represents actual wheelset velocity and the velocity is used for the measured velocity calculation. The estimated velocity is calculated by the UKF as a part of the state vector. The adhesion conditions are good in Figure 5.29. The problem with low resolution does not occur during the starting. The stairs on the measured wheel velocity and the state vector are caused by the incremental encoder low resolution. However, the estimated wheel velocity is smoother. The stairs on the velocity causes the stairs on the state vector, but it does not affect the estimated relative adhesion force. The adhesion decreases in the case that is depicted in Figure 5.30. When the wheelset velocity starts increase, the stairs gradually disappear and their influence decreases. The slip controller reaction is delayed because the tractive force increase on a ramp and the slip controller has to decrease the tractive force faster than the ramp increases the force. This behaviour is given by the slip controller connection to the locomotive control structure where the required tractive force is limited by the slip controller output. However, the slip controller can eliminate the slippage at its beginning in the adverse case.

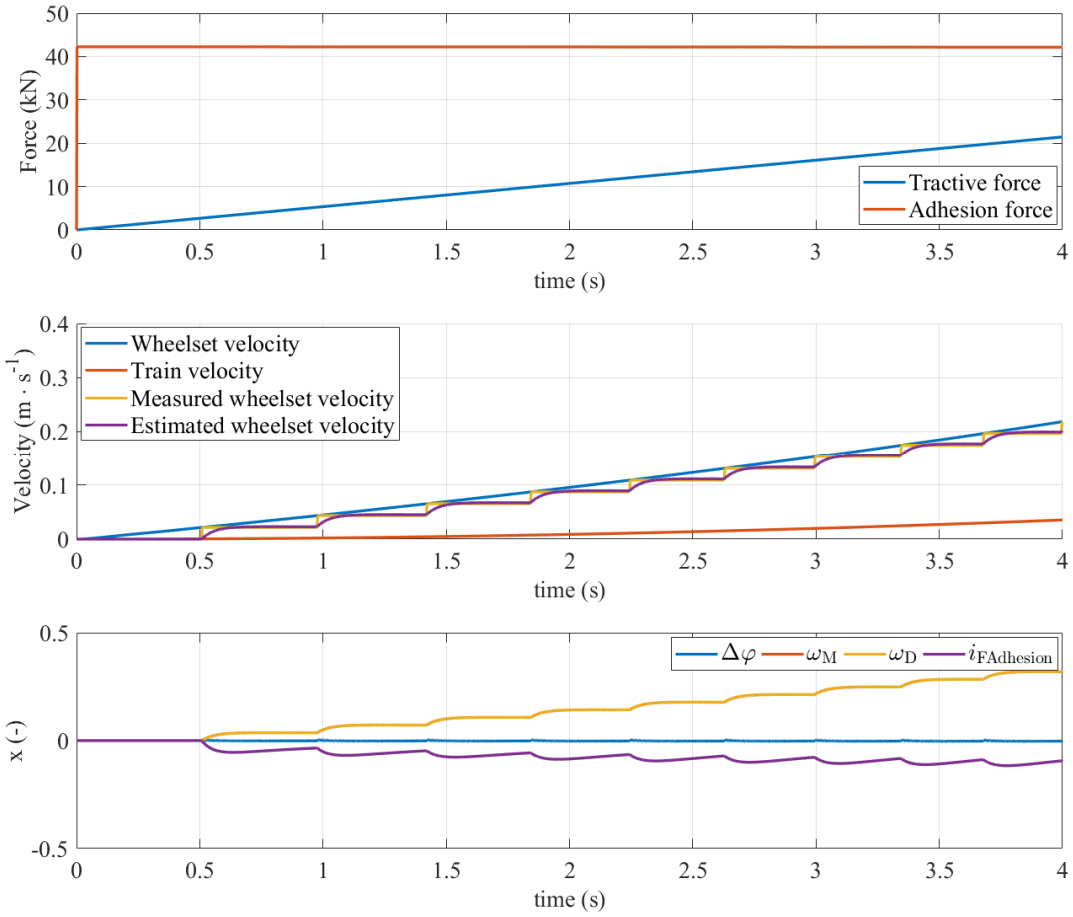

Figure 5.29 Locomotive starting with the slip controller based on the UKF

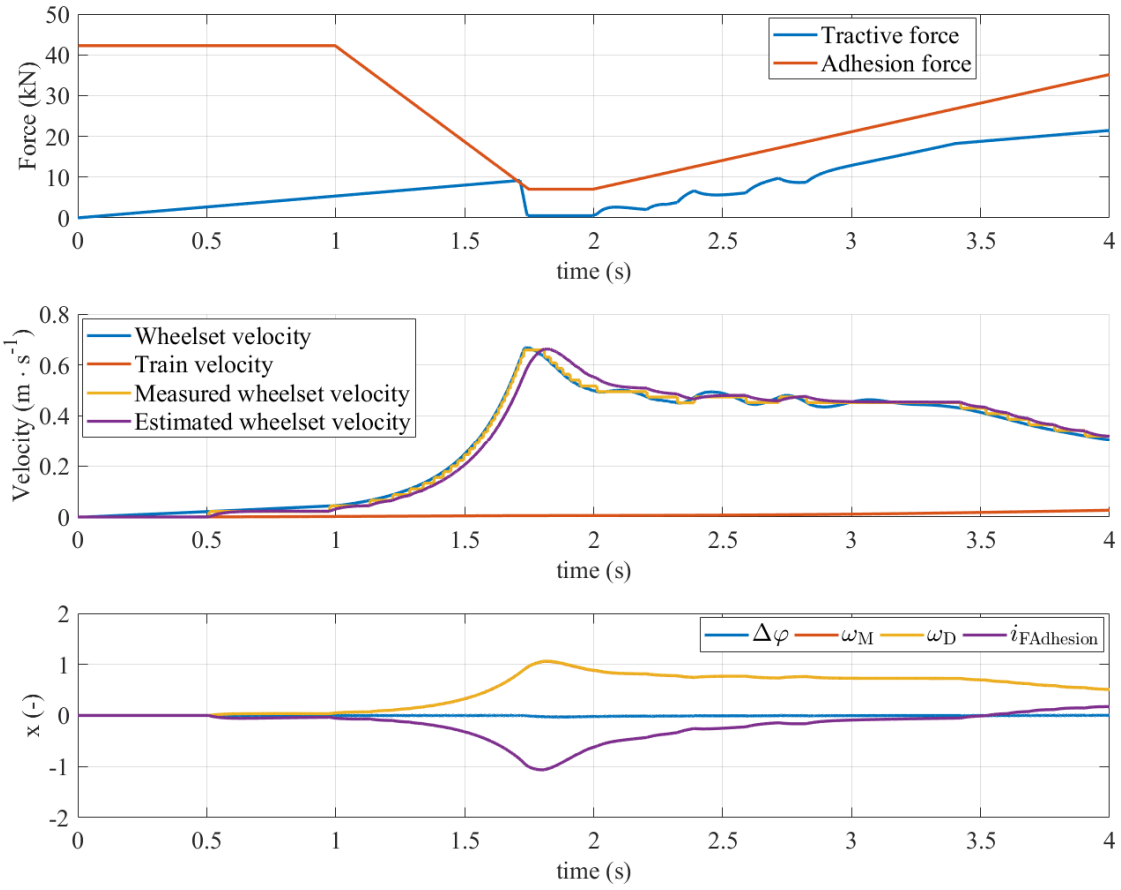

Figure 5.30 Locomotive starting with the slip controller based on the UKF with adhesion decrease

5.4 Slip Controller Implementation to the Digital Signal Processor

The implementation into a DSP was made to verify the possibility the slip controller used in a locomotive. The used DSP is TMS320F28335. The calculation period of the proposed slip controller is set up to 100 µs. The period was set with respect an electric drive controller calculation period for the electric drives. The UKF, EKF and KF were implemented into the DSP. The functionality is evaluated on measured data. The comparison of Matlab software simulations and the DSP calculations for the UKF are depicted in Figure 5.31. The results are identical, and the implementation is correct.

5.4.1 Estimators Computational Complexity

The general calculation complexities of the estimators are indicated in Table 3.1 The system, which corresponds to the proposed slip controller complexity, is described in Table 5.5. Every variable has defined its dimension and type. If the type is a general matrix or general vector, the matrix or vector consists of real numbers that have to be calculated, and its position and value cannot be predicted. Therefore, multiplications have to be done with all matrix or vector. Numbers of required mathematical operations and the number of required machine cycles for calculation are summarized in Table 5.6. There are two values in EKF a UKF in Table 5.6. The first value is the case when an EKF or UKF is calculated without nonlinear function. The second case takes the nonlinearity into account. This division is made because the nonlinear function can have a different complexity when the different description of nonlinearity is used. The EKF computational complexity is the same as the KF computational complexity when the

nonlinear function is not implemented to the EKF. The UKF requires calculation of a Cholesky factorisation calculation, which calculation is taken into account for a number of cycles.

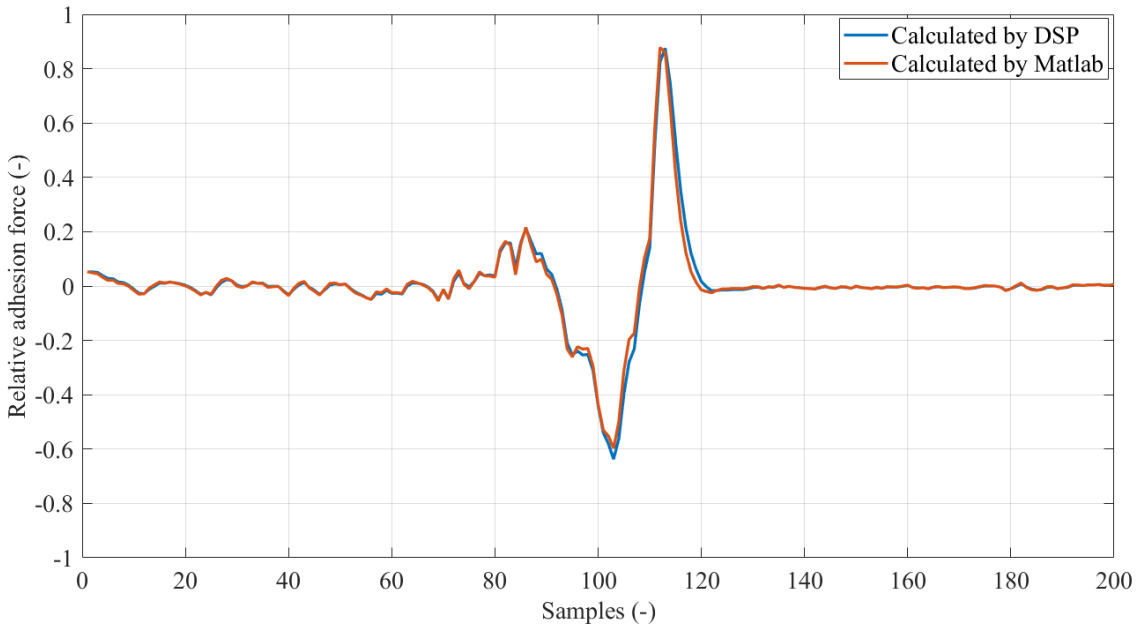

Figure 5.31 Comparison of the Matlab simulations and DSP calculations

Table 5.5 Proposed estimator parameters

Variable	Dimension	Type
A	4×4	General matrix
C	1×4	One output [0 1 0 0]
R	1×1	Real number
Q	4×4	Diagonal matrix
P	4×4	General matrix
K	4×1	General vector
x	4×1	General vector
y	1×1	Real number

The machine cycles are valid for the TMS320F28335 DSP. One machine cycle takes 6.67 ns. The presumed time consumption based on a Matlab calculation and actual required time in DSP are summarized in Table 5.7. The values of presumed time and required time in DSP are different because loops and conditionals are neglected in calculations based on Matlab calculations. The main influence of the neglected code parts is shown in the UKF. The overall computational time of the UKF is shorter than 100 µs, and the slip controller can be implemented into a locomotive computer.

Table 5.6 Computational complexity of the state estimators in number of operations and machine cycles

State estimator	KF		EKF		UKF	
	Operations	Cycles	Operations	Cycles	Operations	Cycles
Multiplications	213	1491	213 / 220	1491/ 1540	626 / 633	4382 / 4431
Divisions	4	944	4 / 6	944/ 1428	4 / 6	944 / 1428
Additions and Subtractions	193	1351	193 / 194	1351/ 1358	636 / 637	4452 / 4459
Total	-	3786	-	3786/ 4326+769	-	9778+2370 / 10318+769 + 2370
Note	-		EKF / EKF with nonlinearity, +nonlinearity require a square root and exponential function calculation		UKF / UKF with nonlinearity, +nonlinearity require a square root and exponential function calculation. +UKF requires Cholesky factorisation calculation in all cases	

Table 5.7 Computational complexity of the state estimators in required time for the worst case

State estimator	KF	EKF	UKF
Presumed time (μs)	25.2	33.9	84.6
Required time in DSP (μs)	26.6	38.3	95.3

5.5 Slip Controller Simulations Evaluation

The proposed slip controller based on the UKF, EKF and KF have the same detection time delay of an estimator output $t_{\text{iOutDelay}}$ and its output compared by the required relative adhesion force value $i^*_{FAdhesion}$ is also the same in an open loop. The slip controller based on the UKF and EKF provide very similar results in typical application cases. The difference occurs when the controller is connected. The UKF and the EKF can be substituted in the case. The KF provides worst results, and the achieved slip velocity is higher than in the UKF an EKF case. This behaviour is given by the PI controller different settings in the KF case. The PI has to be set up due to the slip controller stability when the KF is used. Therefore, the KF is less appropriate than the UKF and EKF. The main difference between the UKF and EKF occur when a step torque change is used. The slip controller based on the EKF can fail in the case. This behaviour limits the controller setting, and during the tuning of the controller it has to be the feature taken into account. If the situation occurs during the locomotive run, e.g. by computer reset, the slip controller fails.

The proposed slip controller based on the UKF, KF and EKF provides better results than applied re-adhesion controller. The comparison is summarized in Table 5.3. The comparison is made according to the defined evaluation criteria. The relative adhesion force is not available for the re-adhesion controller, and the estimator output delay cannot be defined. Therefore, the tractive force decreasing is used instead of the relative adhesion force that can be longer.

However, the estimator output delay is shorter in the proposed slip controller for all estimators than the re-adhesion controller. The KF has two times longer time delay. The train velocity is the same for all types of used estimators, and about 0.2 $m \cdot s^{-1}$ higher than for the re-adhesion controller. The slippage does not occur during the proposed slip controller simulations. The UKF and EKF have the lowest maximum power losses. The KF has higher power loss due to the higher slip velocity that occurs at higher adhesion coefficient value than in the UKF and EKF case. The operating point was almost at the adhesion-slip characteristic maximum value. The highest power loss has the re-adhesion controller. The slippage only occurs in the re-adhesion controller simulations. The proposed slip controller works without slippage. Therefore, the highest slip velocity in the stable area of the adhesion-slip characteristic only occurs. The maximum force decrease of the proposed slip controller is almost the same for all estimators, and it is lower than the re-adhesion controller. The impulse is the lowest for the proposed slip controller with the KF this lowest value is redeemed by higher slip velocity and the power loss. The time consumption of the proposed slip controller based on the UKF is the highest, but the time is not too long. Therefore, it is eventually possible to implement the proposed slip controller to the locomotive computer. Based on the simulations it can be said that the UKF provides the best results.

6 CONCLUSION

The doctoral thesis presents a novel slip controller for electric locomotives that are intended for freight trains hauling. The presented slip controller determines the adhesion-slip characteristic slope and enables to keep the operating point on the adhesion-slip characteristic that corresponds to the required characteristic slope. The adhesion-slip characteristic is variable, and changes during a train run. The adhesion conditions direct measurement is not possible during the train run. Therefore, the adhesion-slip characteristic slope has to be estimated by an estimator. The proposed slip controller uses the UKF for the estimation. The adhesion-slip characteristic contains a nonlinearity that causes problems of conventional methods, and that can cause their failure. The proposed slip controller uses the nonlinearity description to cope with the problem. Other problems of the existing slip controllers occur during the train starts and when the adhesion-slip characteristic has not expressed the maximum point. The proposed slip controller can cope with the problems. The proposed slip controller also eliminates a derivative calculation of the estimated adhesion force and does not require the train velocity value that is problematic to determine. The proposed slip controller is compared with the existing re-adhesion controller and some conventional slip control methods, and the proposed slip controller provides better results.

The design of the proposed slip controller is based on a study of the existing slip controllers that are described in the literature, and the method summarization is made in the doctoral thesis. The slip controllers can be sorted into the re-adhesion controllers and the slip controllers. The slip controllers can be further sorted with respect to the methods that are based on the adhesion-slip characteristic parameters and methods that are based on the other principles. The most perspective slip controllers are based on the adhesion-slip characteristic slope determination. Therefore, the proposed slip controller is based on the principle of the adhesion-slip characteristic. The slip controller requires the description of the nonlinear function of the adhesion-slip characteristic. Therefore, the adhesion phenomenon is also described in the doctoral thesis. The proposed slip controller principles and features are also described in the doctoral thesis. The difference between the existing methods based on the same principle is demonstrated, and the proposed slip controller advantages are also described. The proposed slip control method can stably work in different adhesion conditions without risk of failure. The output of the slip controller detection part can be directly used as the controller input. This approach eliminates the requirement of a classical method to a calculation of derivative from the estimated adhesion coefficient. The slip controller description includes a description of estimators that can be used in the controller. The estimator that is used by the proposed slip controller requires the mathematical model of the system. Therefore, the two-mass and three-mass models are described. The slip controller is developed in the Matlab software by using a measured data and simulations. The simulation processes with the simulation model are also described. Finally, the simulation results based on the measured data and simulation model are presented.

The proposed slip controller is designed as a modular that is split into the slip detection part and control part. The detection part estimates the current adhesion-slip characteristic slope. The detection part of the slip controller is based on the UKF. The UKF that is highly time-consuming. The DSP that is used on locomotives as the wheelset controllers must calculate the slip controller in time around 100 μs. The proposed slip controller meets the required conditions. However, the DSP used on older locomotives or on modern locomotives with

complicated electric drive controller can have a problem with the UKF calculation. Therefore, the slip controller is designed as modular, and the UKF can be replaced by some other type of estimator. The slip controller was also tested with the EKF and KF that is less time-consuming, but they provide worst results, and the slip controller stability is not guaranteed in all cases. The UKF can be replaced by the EKF. The implementation requires some additional protection to eliminate the EKF problem with the divergence. The controller part of the slip controller is based on a PI controller. The controller can be replaced by any proper controller type if it is suitable or required.

6.1 Suggestions for the Future Work

The slip controller development still continues, and the next work can continue in the proposed slip controller improvement or designed the new slip controller. The proposed slip controller is based on the adhesion-slip characteristic slope detection by the UKF. The KF and EKF are also described and tested as estimators in the doctoral thesis. However, different estimators can be used for the purpose, e.g. Particle filter can be used as the observer and can be used for the purpose. The proposed slip controller work with the PI controller, but another controller type can also be tested, e.g. a state controller, sliding mode controller or fuzzy controller. Other future work can be based on the tuning of the covariance matrixes that is highly time-consuming because their settings have to be made in cooperation with the controller part. The slip controller was implemented into the DSP. However, its functionality was not verified on the locomotive. Next work can try to implement the proposed method to the locomotive.

6.2 Objectives Fulfilment

The objectives are fulfilled as follows:

1. **Summarize the pieces of knowledge about slip control method principles and evaluate their requirements and effectivity**. The first objective is described in chapter 2.2. The methods strengths, weaknesses and requirements are summarized in chapter 2.5. The methods that determine an adhesion-slip characteristic slope are perspective methods, and if some weaknesses are eliminated the methods can be effective. When the methods are evaluated the slip velocity determination, and a locomotive computer throughput has to be taken into account. Therefore, the slip velocity measurement is described in chapter 2.3, and a locomotive computer influence to the slip controller is described in chapter 2.4.
2. **Summarize appropriate state estimators that can be used in the proposed slip controller and evaluate their possible using in the proposed slip controller and select a proper estimator for the slip controller.** The estimators are summarized in chapter 3.1. The selected estimator is the UKF. The KF and EKF can also be used if it is required. However, some specific behaviour of the estimators has to be considered before the implementation of the KF and the EKF. The principle of the covariance matrices settings and their influence to the filter performance and the discretisation of the matrices are also described in the chapter. The KF and EKF can be used in the proposed slip controller due to the slip controller modularity.
3. **Design a slip controller that can be used for a locomotive.** The slip controller design is described in chapters 3.2 and 3.3. The slip controller uses a nonlinearity description that describes the adhesion that is described in chapter 2.1. The proposed slip controller estimates the adhesion-slip characteristic slope and tries to set the operating point to point where the characteristic has the required slope. The slip controller background and difference against the conventional slip controllers are also described.

4. **Design a proper mathematical simulation model of a locomotive part that can be used for the slip controller design and evaluation. Design a proper mathematical model for the slip controller.** The models and complete method of evaluation are described in chapter 4. The chapter describes the five-mass mathematical simulation model and two models for the estimator. The models for the estimators are the three-mass and two-mass models. The models are compared among themselves, and its eigenvalues are compared with measurement. The simulation principles are also described in the chapter. The model comparison with the measured data is made in chapter 5.2.
5. **Verify the designed slip controller performance with the help of a mathematical model and measured data as well as the slip controller execution time in a digital signal processor.** This point is described in chapter 5. The slip controller verification based on simulations and measurement is described in chapter 5.3. The execution time in the DSP is described in chapter 5.4. The method can work correctly according to the simulation, and the implementation of the DSP is also possible. The overall slip controller evaluation is made in chapter 5.5.

Based on that I consider all objectives of my doctoral thesis are completed.

REFERENCES

[1] I. Hussain, T. X. Mei and M. Mirzapour, "Real time estimation of the wheel-rail contact condtions using multi-Kalman filtering and fuzzy logic," *Proceedings of 2012 UKACC International Conference on Control*, Cardiff, 2012, pp. 691-696.

[2] W. Liao, H. Chen, W. Cai and Y. Song, "A novel active adhesion control design for high speed trains without vehicle speed measurement," *Proceedings of the 33rd Chinese Control Conference*, Nanjing, 2014, pp. 221-226.

[3] C. Jenks "Improved Methods for Increasing Wheel/Rail Adhesion in the Presence of Natural Contaminants, "*Transit Co-operative Research Program, Research Results Diges*, no 17, 1997.

[4] H. Chen, "Factors that infuence the adhesion coefficieent between wheel and rail," Railway Technology Avalanche, no. 40, pp. 6, 2012.

[5] I. Hussain, T. X. Mei, and R. T. Ritchings, "Estimation of wheel–rail contact conditions and adhesion using the multiple model approach", *Vehicle System Dynamics*, vol. 51, no. 1, pp. 32–53, Jan. 2013.

[6] X. Cao *et al.*, "The effect of alumina particle on improving adhesion and wear damage of wheel/rail under wet conditions", *Wear*, vol. 348–349, pp. 98–115, Feb. 2016.

[7] K. Kondo, "Anti-slip control technologies for the railway vehicle traction," *2012 IEEE Vehicle Power and Propulsion Conference*, Seoul, 2012, pp. 1306-1311.

[8] L. Wenli, Z. Leiting, and D. Kan, "Performance Analysis of Re-adhesion Optimization Control Based On Full-dimension State Observer", *Procedia Engineering*, vol. 23, pp. 531–536, Jan. 2011.

[9] R. Lewis, U. Olofsson, *Wheel-rail interface handbook.* CRC Press, Boca Raton, 2009.

[10] K. Xu, G. Xu, and C. Zheng, 'Novel determination of Wheel-Rail adhesion stability for electric locomotives', *Int. J. Precis. Eng. Manuf.*, vol. 16, no. 4, pp. 653–660, Apr. 2015.

[11] B. Picasso, D. Caporale and P. Colaneri, "Braking Control in Railway Vehicles: A Distributed Preview Approach," in *IEEE Transactions on Automatic Control*, vol. 63, no. 1, pp. 189-195, Jan. 2018.

[12] H. Chen, T. Ban, M. Ishida, T. Nakahara, "Experimental instigation of influential factors on adhesion between wheel and rail under wet conditions", *Wear*, vol. 265, no 9-10, 2008, pp. 1504-1511.

[13] D. Kun, L. Kaijun and X. Qunsheng, "Application of Unscented Kalman Filter for the State Estimation of Anti-lock Braking System", IEEE International Conference on Vehicular Electronics and Safety, 2006, pp. 130-133.

[14] A. Rezaeian *et al.*, "Novel Tire Force Estimation Strategy for Real-Time Implementation on Vehicle Applications," in *IEEE Transactions on Vehicular Technology*, vol. 64, no. 6, June 2015, pp. 2231-2241.

[15] B. R. Liang and W. S. Lin, "A new slip ratio observer and its application in electric vehicle wheel slip control," *2012 IEEE International Conference on Systems, Man, and Cybernetics (SMC)*, Seoul, 2012, pp. 41-46.

[16] M. Wielitzka, M. Dagen and T. Ortmaier, "State and maximum friction coefficient estimation in vehicle dynamics using UKF," *2017 American Control Conference (ACC)*, Seattle, WA, 2017, pp. 4322-4327.

[17] A. Sakai, Y. Tamura and Y. Kuroda, "An efficient solution to 6DOF localization using Unscented Kalman Filter for planetary rovers", IEEE/RSJ International Conference on Intelligent Robots and Systems, 2009, pp. 4154-4159.

[18] R. Wang and J. Wang, 'Tire–road friction coefficient and tire cornering stiffness estimation based on longitudinal tire force difference generation', *Control Engineering Practice*, vol. 21, no. 1, pp. 65–75, Jan. 2013.

[19] J. Zdenek, "System Design and Software Architecture of Traction Vehicle Control Computer," *2006 12th International Power Electronics and Motion Control Conference*, Portoroz, 2006, pp. 1205-1210.

[20] J. Zdenek, "Traction vehicle distributed control computer system architecture with auto reconfiguration features and extended DMA support," *2008 13th International Power Electronics and Motion Control Conference*, Poznan, 2008, pp. 1638-1645.

[21] J. Zdenek, "Distributed control computer backbone communication channel of electric locomotive with effective DMA support," *Proceedings of 14th International Power Electronics and Motion Control Conference EPE-PEMC 2010*, Ohrid, 2010, pp. T6-27-T6-34.

[22] K. Ohishi, Y. Ogawa, I. Miyashita and S. Yasukawa, "Anti-slip re-adhesion control of electric motor coach based on force control using disturbance observer," *Conference Record of the 2000 IEEE Industry Applications Conference. Thirty-Fifth IAS Annual Meeting and World Conference on Industrial Applications of Electrical Energy (Cat. No.00CH37129)*, Rome, 2000, pp. 1001-1007 vol.2.

[23] K. Ohishi, Y. Ogawa, I. Miyashita and S. Yasukawa, "Adhesion control of electric motor coach based on force control using disturbance observer," *6th International Workshop on Advanced Motion Control. Proceedings*, Nagoya, Japan, 2000, pp. 323-328.

[24] T. Hata, H. Hirose, S. Kadowaki, K. Ohishi, N. Iida, M. Takagi, S. Yasukawa "Anti-slip re-adhesion control based on speed sensor-less vector control and disturbance observer for electric multiple units, series 205-5000 of East Japan Railway Company," *IEEE International Conference on Industrial Technology, 2003*, 2003, pp. 772-777 Vol.2.

[25] Y. Ishikawa and A. Kawamura, "Maximum adhesive force control in super high speed train," *Power Conversion Conference - Nagaoka 1997., Proceedings of the*, Nagaoka, 1997, pp. 951-954 vol.2.

[26] Y. Takaoka and A. Kawamura, "Disturbance observer based adhesion control for Shinkansen," *6th International Workshop on Advanced Motion Control. Proceedings*, Nagoya, Japan, 2000, pp. 169-174.

[27] A. Kawamura, T. Furuya, K. Takeuchi, Y. Takaoka, K. Yoshimoto and Meifen Cao, "Maximum adhesion control for Shinkansen using the tractive force tester," *IEEE 2002 28th Annual Conference of the Industrial Electronics Society. IECON 02*, vol.1, 2002, pp. 567-572

[28] W. Lin, Z. Liu, L. Diao, G. Zhang, D. Chen and Z. Li, "Maximum Adhesion Force Control Simulated Model of Electric Locomotive," *2007 IEEE International Conference on Automation and Logistics*, Jinan, 2007, pp. 1704-1708.

[29] Y. Shimizu, K. Ohishi, T. Sano, S. Yasukawa and T. Koseki, "Anti-slip re-adhesion control based on disturbance observer considering bogie vibration," *2007 European Conference on Power Electronics and Applications*, Aalborg, 2007, pp. 1-10.

[30] P. Pichik and J. Zdenek, "Adhesion Force Detection Method Based on the Kalman Filter for Slip Control Purpose", *Automatika*, vol. 57, no. 2, pp. 405–415, 2016.

[31] S. Wang, J. Xiao, J. Huang, and H. Sheng, "Locomotive wheel slip detection based on multi-rate state identification of motor load torque, " *Journal of the Franklin Institute*, vol. 353, no. 2, 2016, pp. 521–540.

[32] P. Pichlík, J. Zděnek, "Extended Kalman Filter Utilization for a Railway Traction Vehicle Slip Control*" In: Optimization of Electrical and Electronic Equipment (OPTIM) & 2017 Intl Aegean Conference on Electrical Machines and Power Electronics (ACEMP), 2017 International Conference on. IEEE*, 2017. pp. 869-874

[33] R. Schreiber, P. Kögel, P. Häse, and P. Hildenbrand, "Regelung zur optimalen Kraftschlußausnutzung bei Drehstromlokomotiven auf der Basis der Steigung der Kraftschlußkennlinie," (in German), *EB*, vol. 93, no. 5, p. 157-173, 1995

[34] R. Schreiber and P. Kögel "Identifikationsmethode zur Bestimmung der Adhäsion zwischen Rad und Schiene," (in German), *ZEV GA*. vol. 120, no. 2, p. 48-54, 1996

[35] T. X, Mei, J. H. Yu and D. A. Wilson, "A Mechatronic Approach for Anti-slip Control in Railway Traction", *Proceedings of the 17th World Congress*, *The International Federation of Automatic Control*, Seoul, Korea, July 2008

[36] T. X. Mei and I. Hussain, "Detection of wheel-rail conditions for improved traction control," *IET Conference on Railway Traction Systems (RTS 2010)*, Birmingham, 2010, pp. 1-6.

[37] R. Palm, and K. Storjohann, "Torque Optimization for a Locomotive using Fuzzy Logic, " *ACM*; 1994. p. 105-109

[38] M. Buscher, R. Pfeiffer and H. J. Schwartz, "Radschlupfregelung für Drehstromlokomotiven," (in German), *EB*. vol. 91, no. 5, p. 163-178 1993

[39] R. Stock, L. Stanlake, C. Hardwick, M. Yu, D. Eadie, R. Lewis, "Material concepts for top of rail friction management – Classification, characterisation and application“ Wear, vol. 366-367, 2016, pp. 225-232.

[40] M. Spiryagin, K. S. Lee and H. H. Yoo, "Control system for maximum use of adhesive forces of a railway vehicle in a tractive mode“, *Mechanical Systems and Signal Processing*, vol. 22, no. 3, 2008, pp. 709-720.

[41] M. Spiryagin, K. S. Lee and H. H. Yoo, “Study on using noise for adhesion control system of railway vehicle,” *14th International Congers on Sound & Vibration, ICSV14*, Cairns, Australia, July 2007

[42] J. Huang, J. Xiao, D. Zhao and S. Wang, "A wheel slip detection method of electric locomotive based on time-frequency analysis," *17th International IEEE Conference on Intelligent Transportation Systems (ITSC)*, Qingdao, 2014, pp. 1221-1225.

[43] J.n Huang, J. Xiao and H. Weiss, "Simulation study on adhesion control of electric locomotives based on multidisciplinary virtual prototyping," *2008 IEEE International Conference on Industrial Technology*, Chengdu, 2008, pp. 1-4.

[44] L. Diao, L. Zhao, Z. Jin, L. Wang and S. M. Sharkh, "Taking Traction Control to Task: High-Adhesion-Point Tracking Based on a Disturbance Observer in Railway Vehicles," in *IEEE Industrial Electronics Magazine*, vol. 11, no. 1, pp. 51-62, March 2017.

[45] M. Lehtla and H. Hoimoja, "Slip control upgrades for light-rail electric traction drives," *2008 13th International Power Electronics and Motion Control Conference*, Poznan, 2008, pp. 1581-1584.

[46] E. Saumweber and G. Winkle, "Eine neue Gleitschutzgeneration für die Eisenbahn unter Vervendung von Mikroprozessoren, " (in German), *EB*; 1981. vol. 79, no. 9, p. 331-336.

[47] W. Lang, G. Roth, "Optimale Kraftschlussaustutzung bei Hochleistungs-Schienenfahzeugen, " (in German) *ETR* vol. 42, no. 1-2 pp. 61-66, 1993

[48] D. Y. Park, M. S. Kim, D. H. Hwang, J. H. Lee and Y. J. Kim, "Hybrid re-adhesion control method for traction system of high-speed railway," *Electrical Machines and Systems, 2001. ICEMS 2001. Proceedings of the Fifth International Conference on*, Shenyang, 2001, pp. 739-742 vol.2.

[49] O. Polach, “Influence of Locomotive Tractive Effort on the Forces Between Wheel and Rail, “ *Vehicle System Dynamics*, vol. 35, pp. 7-22, 2001.

[50] A. K. Kumar,"Method and system of limiting the application of sand to a railroad rail", U.S. Patent 7,290,870B2, Nov. 6, 2007.

[51] R., I. Popovici "Friction in Wheel - Rail Contacts," Ph.D. dissertation, Univ. of Twente, Enschede, The Netherlands, 2010.

[52] S. H. Park, J. Kim, J. J.Choi and H. Yamazaki, "Modeling and control of adhesion force in railway rolling stocks," *Control Systems, IEEE* , vol.28, no.5, pp.44-58, October 2008

[53] J. Izer, *Klejové vozy, dodatek*, 1 st ed. (in Czech) Bratislava, Alfa, 1998

[54] D. Frylmark and S. Johnsson., "Automatic Slip Control for Railway Vehicles," M.S. thesis, Dept. of Elect. Eng., Linkopings univ., Linkopings, Sweeden, 2003.

[55] O. Polach, Creep forces in simulations of traction vehicles running on adhesion limit, *Wear*, Volume 258, Issues 7–8, 2005, Pages 992-1000

[56] J.J. Kalker, "Wheel-rail rolling contact theory", *Wear*, Volume 144, Issues 1–2, 1991, Pages 243-261

[57] H. Wang, J. Zeng, R. Luo, "Study on wheel/rail adhesion force and its control of high-speed trains considering aerodynamic loads and track excitations", *Wear*, vol. 314 no. 1-2, 2014, pp. 299-304.

[58] M. Yamashita and T. Soeda, 'Development of Re-adhesion Control Method Considering Axle-weight Transfer of Electric Locomotive', *QR of RTRI*, vol. 52, no. 1, pp. 7–12, 2011.

[59] M. Lata, J. Čáp and P. Voltr "New Practical Results about Adhesion Limites Obtained from Experimental Stan Testing," *Scientific Papers of the University of Pardubice Series B - The Jan Perner Transport Faculty*; 2009.

[60] J. Liu, Q. Peng, Z. Huang, H. Li, D. Wang, Y. Chen, F. LinZhou, "A novel estimator for adhesion force of railway vehicles braking systems and reference speed calculation," *2017 29th Chinese Control And Decision Conference (CCDC)*, Chongqing, 2017, pp. 7606-7611.

[61] M. Danzer. (2008), *Elektrická trakce 7. Adheze.* (In Czech) [online], Available: http://www.kves.uniza.sk/kvesnew/dokumenty/et/ET%20skripta%20Danzer/ETR700.pdf

[62] J. He, B. Dou, C. Zhang, L. Liu and X. Yin, "Anti-slip strategy of locomotives using improved adhesion characteristic curve slope method," *2017 Chinese Automation Congress (CAC)*, Jinan, China, 2017, pp. 855-860.

[63] T. Watanabe and M. Yamashita, "Basic study of anti-slip control without speed sensor for multiple motor drive of electric railway vehicles," *Proceedings of the Power Conversion Conference-Osaka 2002*, Osaka, 2002, pp. 1026-1032 vol.3.

[64] M. Yamashita and T. Watanbe, "A readhesion control method without speed sensor for electric railway vehicles," *Electric Machines and Drives Conference, 2003. IEMDC'03. IEEE International* , vol.1, no., pp. 291- 296 vol.1, 1-4 June 2003

[65] T. Watanabe, 'Anti-slip Readhesion Control with Presumed Adhesion Force - Method of Presuming Adhesion Force and Running Test Results of High-speed Shinkansen Train -', *Quarterly Report of RTRI*, vol. 41, no. 1, pp. 32–36, 2000.

[66] M. Yamashita and T. Soeda, "Anti-slip re-adhesion control method for increasing the tractive force of locomotives through the early detection of wheel slip convergence," *2015 17th European Conference on Power Electronics and Applications (EPE'15 ECCE-Europe)*, Geneva, 2015, pp. 1-10.

[67] D. H. Hwang, M. S. Kim, D. Y. Park, Y. J. Kim and D. H.Kim, "Re-adhesion control for high-speed electric railway with parallel motor control system," *ISIE 2001. 2001 IEEE International Symposium on Industrial Electronics Proceedings*, Pusan, 2001, pp. 1124-1129 vol.2.

[68] A. D. Cheok and S. Shiomi, "A fuzzy logic based anti-skid control system for railway applications," *Knowledge-Based Intelligent Electronic Systems, 1998. Proceedings KES '98. 1998 Second International Conference on*, Adelaide, SA, 1998, pp. 195-201 vol.1.

[69] A. D. Cheok and S. Shiomi, "Combined heuristic knowledge and limited measurement based fuzzy logic antiskid control for railway applications," in *IEEE Transactions on Systems, Man, and Cybernetics, Part C (Applications and Reviews)*, vol. 30, no. 4, pp. 557-568, Nov 2000.

[70] M. Yamashita, T. Watanabe, "Readhesion Control Method without Speed Sensors for Electric Railway Vehicles, " *QR of RTRI*;. vol. 46, no. 2, 2005p. 85-89

[71] T. Watanabe and M. Yamashita, "A novel anti-slip control without speed sensor for electric railway vehicles," *Industrial Electronics Society, 2001. IECON '01. The 27th Annual Conference of the IEEE*, Denver, CO, 2001, pp. 1382-1387 vol.2.

[72] N. H. Jo, C. Jeon and H. Shim, "Noise Reduction Disturbance Observer for Disturbance Attenuation and Noise Suppression," in *IEEE Transactions on Industrial Electronics*, vol. 64, no. 2, pp. 1381-1391, Feb. 2017.

[73] X. Hong, R. Zhang, L. Wu, Y. Li and K. Wang, "Simulation of adhesion control method based on phase-shift," *2013 International Conference on Electrical Machines and Systems (ICEMS)*, Busan, 2013, pp. 2077-2080.

[74] Z. Huang, Z. Xu, B. Chen, R. Zhang, Y. Chen and Q. Peng, "Sliding mode control for urban railway anti-slip system based on optimal slip ratio estimation with forgetting factor recursive least-squares," *2017 36th Chinese Control Conference (CCC)*, Dalian, 2017, pp. 9502-9507.

[75] Q. Peng, J. Liu, Z. Huang, W. Liu and H. Li, "Sliding model control based on estimation of optimal slip ratio for railway wheel slide protection using extremum seeking," *2016 IEEE Energy Conversion Congress and Exposition (ECCE)*, Milwaukee, WI, 2016, pp. 1-6.

[76] K. Xu, G.-Q. Xu, and C.-H. Zheng, 'Analysis of torque transmitting behavior and wheel slip prevention control during regenerative braking for high speed EMU trains', *Acta Mechanica Sinica*, vol. 32, no. 2, pp. 244–251, Apr. 2016.

[77] J. S. Kim, S. H. Park, J. J. Choi and H. Yamazaki, "Adaptive Sliding Mode Control of Adhesion Force in Railway Rolling Stocks" in *Sliding Mode Control*, InTech, 2011

[78] R. Schreiber, P. Kögel, and P. Hildenbrand "Verfahren zur Steuerung und Regelung eines elektrischen Antriebs eines Fahrzeugs", (in German), European Patent 0621156 A2, 1993.

[79] R. Schreiber and P. Kögel "Verfahren und Anordnung zur Bestimmung der Phasenverschiebung zweier korrelierter Signale," (in German), European Patent 0826549B1, 2001.

[80] J. Liu, H. Zhao, and W. Zhai, 'Mechanism of self-excited torsional vibration of locomotive driving system', *Front. Mech. Eng. China*, vol. 5, no. 4, pp. 465–469, Dec. 2010

[81] P. Pichlik and J. Zdenek, "Overview of slip control methods used in locomotives", *Transaction on Electrical Engineering*, Vol.3, No.2, 2014.

[82] S. Sadr, D. A. Khaburi and J. Rodríguez, "Predictive Slip Control for Electrical Trains," in *IEEE Transactions on Industrial Electronics*, vol. 63, no. 6, pp. 3446-3457, June 2016.

[83] K. Lu, Y. Song and W. Cai, "Robust adaptive re-adhesion control for high speed trains," *17th International IEEE Conference on Intelligent Transportation Systems (ITSC)*, Qingdao, 2014, pp. 1215-1220.

[84] H. Yamazaki, Y. Karino, T. Kamada, M. Nagai, T. Kimura, "Effect of Wheel-Slip Prevention Control Using Nonlinear Robust Control Theory", *Quarterly Report of RTRI*, vol. 48, no. 1, pp 22,29, Feb. 2007.

[85] B. Engel, H. P. Beck and J. Alders, "Verschleißreduzierte Radschlupfregelung mit hoher Kraftslußausnutzung", (in German), *EB*. vol. 96, no. 6, 1998, p. 201-209

[86] P. Pichlik and J. Zdenek, "Locomotive velocity estimation for a slip control purpose by an unscented Kalman filter," *2017 18th International Scientific Conference on Electric Power Engineering (EPE)*, Kouty nad Desnou, 2017, pp. 1-5.

[87] F. Jiang and Z. Gao, "An adaptive nonlinear filter approach to the vehicle velocity estimation for ABS," *Proceedings of the 2000. IEEE International Conference on Control Applications. Conference Proceedings*, Anchorage, AK, 2000, pp. 490-495.

[88] M. Amiri and B. Moaveni, "Vehicle velocity estimation based on data fusion by Kalman filtering for ABS," *20th Iranian Conference on Electrical Engineering (ICEE2012)*, Tehran, 2012, pp. 1495-1500.

[89] P. Pichlík, "Locomotive Longitudinal Velocity Estimation" *Poster 2015. Prague: CTU in Prague*, 2015.

[90] P. Pichlík and J. Zděnek, "Train Velocity Estimation Method Based on an Adaptive Filter with Fuzzy Logic", *Journal of Electrical Engineering*. 2017, 2(68), 125-131.

[91] Pichlík, P.; Zoubek, O.; Zděnek, J.; Lettl, J. "Railway Traction Vehicle Longitudinal Velocity Estimation by Kalman Filter", *Proceedings of PIERS 2015 in Prague. Cambridge: Electromagnetics Academy*, 2015, pp. 2518-2521

[92] P. Pichlík and J. Zděnek, "Train velocity estimation by extended Kalman filter," *2016 8th International Conference on Electronics, Computers and Artificial Intelligence (ECAI)*, Ploiesti, 2016, pp. 1-4.

[93] T. Ishrat, G. Ledwich, M. Vilathgamuwa and P. Borghesani, "Wheel slip control based on traction force estimaton of electric locomotives," *2016 Australasian Universities Power Engineering Conference (AUPEC)*, Brisbane, QLD, 2016, pp. 1-6.

[94] K. Kim, S. H. Kong and S. Y. Jeon, "Slip and Slide Detection and Adaptive Information Sharing Algorithms for High-Speed Train Navigation Systems," in *IEEE Transactions on Intelligent Transportation Systems*, vol. 16, no. 6, pp. 3193-3203, Dec. 2015.

[95] R. Mazl and L. Preucil, "Sensor data fusion for inertial navigation of trains in GPS-dark areas," *IEEE IV2003 Intelligent Vehicles Symposium. Proceedings (Cat. No.03TH8683)*, 2003, pp. 345-350.

[96] B. Allotta, P. D'Adamio, M. Malvezzi, L. Pugi, A. Ridolfi and G. Vettori, "A localization algorithm for railway vehicles," *2015 IEEE International Instrumentation and Measurement Technology Conference (I2MTC) Proceedings*, Pisa, 2015, pp. 681-686.

[97] B. Lv, "Design of velocity radar for railway," *2010 International Conference on Microwave and Millimeter Wave Technology*, Chengdu, 2010, pp. 1637-1639.

[98] L. Yuan, W. Zhao, C. Li and D. Zhou, "Error correction method for train speed measurement using Doppler radar in train control system," *2013 IEEE Eleventh International Symposium on Autonomous Decentralized Systems (ISADS)*, Mexico City, Mexico, 2013, pp. 1-4.

[99] A. Mirabadi, N. Mort and F. Schmid, "Application of sensor fusion to railway systems," *1996 IEEE/SICE/RSJ International Conference on Multisensor Fusion and Integration for Intelligent Systems*, Washington, DC, 1996, pp. 185-192.

[100] M. Malvezzi, B. Allotta, M. Rinchi, B. Bruzzo and P. Bernardi, "Odometric Estimation for Automatic Train Protection and Control Systems, " *8th Word Congress on Railway Research*, Korea, 2008.

[101] B. Picasso, D. Caporale, and P. Colaneri, 'A distributed braking control algorithm with preview action for railroad vehicles', *IFAC Proceedings Volumes*, vol. 47, no. 3, pp. 7330–7335, Jan. 2014.

[102] M. Yamashita and T. Soeda, "A novel slip control method considering axle-weight transfer for electric locomotive," *2010 IEEE Vehicle Power and Propulsion Conference*, Lille, 2010, pp. 1-6.

[103] A. Radke and Zhiqiang Gao, "A survey of state and disturbance observers for practitioners," *2006 American Control Conference*, Minneapolis, MN, 2006, pp. 6

[104] A. F. Taha, J. Qi, J. Wang and J. H. Panchal, *Dynamic state estimation under cyber attacks: A comparative study of kalman filters and observers*, 2015, [online] Available: http://arxiv.org/abs/1508.07252.

[105] Y. Zhang, Z. Zhao, T. Lu, L. Yuan, W. Xu and J. Zhu, "A comparative study of Luenberger observer, sliding mode observer and extended Kalman filter for sensorless vector control of induction motor drives," *2009 IEEE Energy Conversion Congress and Exposition*, San Jose, CA, 2009, pp. 2466-2473.

[106] M. Cuibus, V. Bostan, S. Ambrosii, C. Ilas and R. Magureanu, "Luenberger, Kalman and neural network observers for sensorless induction motor control," *Proceedings IPEMC 2000. Third International Power Electronics and Motion Control Conference*, Beijing, 2000, pp. 1256-1261 vol.3.

[107] V. E. Kumar, J. Jerome and S. Ayyappan, "Comparison of four state observer design algorithms for MIMO system," *Archives of Control Sciences Vol. 23, 2013 No. 2, pages 131–144*

[108] K.R. Muske, T. F. Edgar, *Nonlinear process control*, Prentice-Hall, Inc., Upper Saddle River, NJ, 1997

[109] R. Faragher, "Understanding the Basis of the Kalman Filter Via a Simple and Intuitive Derivation [Lecture Notes]," in *IEEE Signal Processing Magazine*, vol. 29, no. 5, pp. 128-132, Sept. 2012.

[110] S. J. Julier, J. K. Uhlmann and H. F. Durrant-Whyte, "A new approach for filtering nonlinear systems," *American Control Conference, Proceedings of the 1995*, Seattle, WA, 1995, pp. 1628-1632 vol.3.

[111] S. J. Julier and J. K. Uhlmann,"A New Extension of the Kalman Filter to Nonlinear Systems," *Proc. SPIE*, vol. 3068, Feb. 1997.

[112] S. Julier, J. Uhlmann and H. F. Durrant-Whyte, "A new method for the nonlinear transformation of means and covariances in filters and estimators," in *IEEE Transactions on Automatic Control*, vol. 45, no. 3, pp. 477-482, Mar 2000.

[113] E. A. Wan and R. van der Merwe, "The Unscented Kalman Filter", in *Kalman Filtering and Neural Networks*. John Wiley & Sons, Inc., 2002, pp. 221–280.

[114] P. Kim, *Kalman Filter for Beginners with MATLAB examples*. A-Jin Publishing Company 2011.

[115] E. A. Wan and R. Van Der Merwe, "The unscented Kalman filter for nonlinear estimation," *Proceedings of the IEEE 2000 Adaptive Systems for Signal Processing, Communications, and Control Symposium*, Lake Louise, Alta., 2000, pp. 153-158.

[116] M. S. Grewal, A. P. Andrews, *Kalman Filtering Theory and Practice Using MATLAB*. 3rd edition, Wiley, New York 2008.

[117] J. Chen, J. Song, L. Li, G. Jia, X. Ran and C. Yang, "UKF-based adaptive variable structure observer for vehicle sideslip with dynamic correction," in *IET Control Theory & Applications*, vol. 10, no. 14, pp. 1641-1652, 9 19 2016.

[118] K. Kyslan, V. Šlapák, V. Fedák, F. Ďurovský and K. Horváth, "Design of load torque and mechanical speed estimator of PMSM with unscented Kalman filter — An

engineering guide," *2017 19th International Conference on Electrical Drives and Power Electronics (EDPE)*, Dubrovnik, 2017, pp. 297-302.

[119] J. Musić, M. Cecić, V. Zanchy, "Real-Time Body Orientation Estimation Based on Two-Layer Stochastic Filter Architecture," *Automatika*, vol.51, no.5, pp.264,274, 2010.

[120] P. Pichlík, J. Zděnek, "Dependence of locomotive adhesion force estimation by a Kalman filter on the filter settings*" In: TRANSCOM 2017, 12th International Scientific Conference Of Young Scientists On Sustainable, Modern and Safe Transport. Linz: Elsevier BV*, 2017. pp. 695-700

[121] C. Van Loan, "Computing integrals involving the matrix exponential," in *IEEE Transactions on Automatic Control*, vol. 23, no. 3, pp. 395-404, Jun 1978.

[122] P. Pichlík and J. Zděnek, "Comparison of a Locomotive Adhesion Force Estimation Methods for a Wheel Slip Control Purpose," *2017 9th International Conference on Electronics, Computers and Artificial Intelligence (ECAI)*, 2017, pp. 1-4.

[123] P. Pichlík. "Comparison of Different Kalman Filters Types Performance for a Locomotive Slip Control Purposes" *Poster 2017. Prague: CTU in Prague*, 2017

[124] P. Pichlík and J. Zděnek, "Locomotive Wheel Slip Control Method Based on an Unscented Kalman Filter", *IEEE Transactions on Vehicular Technology*, 2018, (*in press*)

[125] C. Bernsteiner, G. Muller, A. Meierhofer, K. Six, D. Kunstner and P. Dietmaier, "Development of white etching layers on rails: simulations and experiments", *Wear*, vol. 366-367, 2016, pp. 116-122.

[126] D. Ross and J. Theys *Using the dsPIC30F / dsPIC33F for Vector Control of an ACIM*. [Online]. Available: http://www.microchip.com/wwwAppNotes/AppNotes.aspx?appnote=en019806

[127] O. Polach, "Experience with use of a time saving method for wheel-rail forces calculation", *Scientific papers of the University of Pardubice. Series B, The Jan Perner Transport Faculty*, pp. 5-18, 2000

[128] S. Senini, F. Flinders and W. Oghanna, "Dynamic simulation of wheel-rail interaction for locomotive traction studies," *Proceedings of the 1993 IEEE/ASME Joint Railroad Conference*, Pittsburgh, PA, 1993, pp. 27-34.

[129] J. Guzinski, H. Abu-Rub, M. Diguet, Z. Krzeminski and A. Lewicki, "Speed and Load Torque Observer Application in High-Speed Train Electric Drive," in *IEEE Transactions on Industrial Electronics*, vol. 57, no. 2, pp. 565-574, Feb. 2010.

[130] M. Fleischer, "Reduced model identification for traction drive-trains," *Fourtieth IAS Annual Meeting. Conference Record of the 2005 Industry Applications Conference,* 2005, pp. 2873-2879 Vol. 4.

[131] P. Pichlik, "Locomotive Model for Slip Control Simulation", *18th International Student Conference on Electrical Engineering*, May 2014.

[132] B. Engel, *Verschleißmindernde Kraftschlussregelung mit Zustandsregler für elektrische Traktionsantriebe*. (in German) Diss. TU Clausthal; 1996

[133] H. S. Hansen, M. U. Nawaz, and N. Olsson, 'Using operational data to estimate the running resistance of trains. Estimation of the resistance in a set of Norwegian tunnels', *Journal of Rail Transport Planning & Management*, vol. 7, no. 1, pp. 62–76, Jun. 2017.

[134] O. Zoubek, P. Pichlik, J. Zděnek, and J. Lettl, "Locomotive wheel speed measurement under wheel slip conditions", Proceedings of PIERS 2015 in Prague. Cambridge: Electromagnetics Academy, 2015, pp. 2528–2533.

LIST OF AUTHOR'S PUBLICATIONS RELATED TO THE DOCTORAL THESIS

Publications in Journals with Impact Factor

P. Pichlík and J. Zděnek, "Train Velocity Estimation Method Based on an Adaptive Filter with Fuzzy Logic", *Journal of Electrical Engineering.* 2017, 2(68), 125-131. Contribution 50%.

- Journal impact factor (2016): 0.483

P. Pichlík and J. Zděnek, "Adhesion Force Detection Method Based on the Kalman Filter for Slip Control Purpose", *Automatika*, vol. 57, no. 2, pp. 405–415, 2016. Contribution 50%.

- Journal impact factor (2016): 0.38
- Number of citations in WoS: 1
    - K. Kyslan, V. Šlapák, V. Fedák, F. Ďurovský and K. Horváth, "Design of load torque and mechanical speed estimator of PMSM with unscented Kalman filter — An engineering guide," *2017 19th International Conference on Electrical Drives and Power Electronics*, Dubrovnik, 2017, pp. 297-302.

P. Pichlík and J. Zděnek, "Locomotive Wheel Slip Control Method Based on an Unscented Kalman Filter", *IEEE Transactions on Vehicular Technology*, 2018, (*in press*). Contribution 50%

- Journal impact factor (2016): 4.066

Publications in Reviewed Journals

-

Patents

Co-authorship of two pending patents with 12% share and 10% share respectively.

Publications Excerpted in Web of Science

P. Pichlík, J. Zděnek, "Dependence of locomotive adhesion force estimation by a Kalman filter on the filter settings" *In: TRANSCOM 2017, 12th International Scientific Conference Of Young Scientists On Sustainable, Modern and Safe Transport. Linz: Elsevier BV*, 2017. pp. 695-700. Contribution 50%.

P. Pichlík and J. Zděnek, "Train velocity estimation by extended Kalman filter," *2016 8th International Conference on Electronics, Computers and Artificial Intelligence (ECAI)*, Ploiesti, 2016, pp. 1-4. Contribution 50%.

P. Pichlík, O. Zoubek and J. Zděnek, "Measuring device for measurement of train dynamic motion during wheel slip," *2014 International Conference on Applied Electronics*, Pilsen, 2014, pp. 247-250. Contribution 33%.

- Number of citations in WoS: 2
    - C. Zhang, X. Cheng, J. He, and G. Liu, "Automatic Recognition of Adhesion States Using an Extreme Learning Machine", *Int. J. Robot. Autom.*, vol. 32, no. 2, pp. 194–200, 2017.
        - Journal impact factor (2016): 0.674

- M. Novák and Ž. Ferková, "Analysis of tram DC traction motors pairing," *2016 IEEE International Power Electronics and Motion Control Conference (PEMC)*, Varna, 2016, pp. 631-636.

P. Pichlík and J. Zděnek, "Locomotive velocity estimation for a slip control purpose by an unscented Kalman filter," *2017 18th International Scientific Conference on Electric Power Engineering (EPE)*, Kouty nad Desnou, 2017, pp. 34-38. Contribution 50%.

Other Publications

P. Pichlík and J. Zděnek, "Extended Kalman filter utilization for a railway traction vehicle slip control," *2017 International Conference on Optimization of Electrical and Electronic Equipment (OPTIM) & 2017 Intl Aegean Conference on Electrical Machines and Power Electronics (ACEMP)*, Brasov, 2017, pp. 869-874. Contribution 50%.

P. Pichlík and J. Zděnek, "Comparison of a Locomotive Adhesion Force Estimation Methods for a Wheel Slip Control Purpose," *2017 9th International Conference on Electronics, Computers and Artificial Intelligence (ECAI)*, 2017, pp. 1-4. Contribution 50%.

P. Pichlík "Comparison of Different Kalman Filters Types Performance for a Locomotive Slip Control Purposes" *Poster 2017. Prague: CTU in Prague*, 2017. Contribution 100%.

P. Pichlík Zoubek, O.; Zděnek, J.; Lettl, J. "Railway Traction Vehicle Longitudinal Velocity Estimation by Kalman Filter", *Proceedings of PIERS 2015 in Prague. Cambridge: Electromagnetics Academy*, 2015, pp. 2518-2521. Contribution 25%.

O. Zoubek, P. Pichlík, J. Zděnek, and J. Lettl, "Locomotive wheel speed measurement under wheel slip conditions", *Proceedings of PIERS 2015 in Prague. Cambridge: Electromagnetics Academy*, 2015, pp. 2528–2533. Contribution 25%.

P. Pichlík, "Locomotive Longitudinal Velocity Estimation" *Poster 2015. Prague: CTU in Prague*, 2015. Contribution 100%.

P. Pichlík and J. Zděnek, "Overview of slip control methods used in locomotives", *Transaction on Electrical Engineering*, Vol.3, No.2, 2014. Contribution 50%.

P. Pichlík "Locomotive Model for Slip Control Simulation", *18th International Student Conference on Electrical Engineering*, May 2014. Contribution 100%.

P. Pichlík "Hybrid Slip Control Method for Railway Traction," *18th International Student Conference on Electrical Engineering*, 2013. Contribution 100%.

P. Pichlík "Basic study of Slip Control Methods for Railway Traction Vehicles," *XX. International Symposium on Electric Machinery In Prague*. Praha: ČVUT FEL, 2013, pp. 45-49. Contribution 100%.

LIST OF AUTHOR'S OTHER PUBLICATIONS

Publications in Journals with Impact Factor

-

Publications in Reviewed Journals

-

Patents

-

Publications Excerpted in Web of Science

P. Pichlík and J. Zděnek, "Converter regulation of stand-alone photovoltaic system at low solar radiation," *2012 International Conference on Applied Electronics*, Pilsen, 2012, pp. 207-210. Contribution 50%.

- Number of citations in WoS: 3
  - J. R. Vazquez and A. D. Martin, "Backstepping Control of a Buck-Boost Converter in an Experimental PV-System', *J. Power Electron.*, vol. 15, no. 6, pp. 1584–1592, Nov. 2015.
    Journal impact factor (2016): 1.047
  - Mike Ranjram, Gregor Simeonov and Peter W. Lehn, "A high step-up transformerless DC/DC converter with flat efficiency", *Industrial Electronics Society IECON 2014 - 40th Annual Conference of the IEEE*, pp. 1034-1040, 2014.
  - M. Madaci, D. Kerdoun, A. Boumassata and N. Cherfia, "Power active filter system implimentation for photovoltaic generation system (PVGS) used in standing alone zones", *Environment and Electrical Engineering (EEEIC) 2013 13th International Conference on*, pp. 74-79, 2013.

Other Publications

P. Pichlík and J. Zděnek, "Application of DC-DC Converters for Increasing of Power Production from Partially Shaded Photovoltaic String," *ELEN 2012*. Prague, 2012. Contribution 50%.

P. Pichlík, "Design of isolated DC-DC photovoltaic microconverter,". *Poster 2012. Prague: CTU in Prague*, 2012. Contribution 100%.

P. Pichlík and M. Lev, "Simulation and Implementation of Photovoltaic DC-DC Converter," *XIX. International Symposium On Electric Machinery In Prague*, 2011, pp. 84-89. Contribution 50%.

P. Pichlík and J. Zděnek, "Implementation of DC-DC Converter Power Supply and Control For Photovoltaic," *XIX. International Symposium On Electric Machinery In Prague*, 2011, pp. 90-96. Contribution 50%.

J. Bauer, J. Lettl, P. Pichlík and J. Zděnek, "Low Power Photovoltaic Converter Control and Development" *Transaction on Electrical Engineering*, Vol. 1, No 3, 2012. Contribution 25%.